

POLITECNICO DI TORINO

I Facoltà di Ingegneria

Corso di Laurea Magistrale in Ingegneria Meccanica

Tesi di Laurea Magistrale

**Numerical modelling of a floating wave
energy converter using U-Tank technology**



Relatori:

Prof. Giovanni Bracco

Prof.ssa Giuliana Mattiazzo

Candidato:

Ilaria Muolo

Ottobre 2020

[dedica]

Abstract

In the last years, the issue of renewable energies has been taking on a great importance. There are many forms of renewable energy, among these, wave energy has a great importance thanks to his great potential.

The purpose of this thesis is to model a floating wave energy converter using the U-Tank technology and also, to define the gross power produced in different marine conditions (regular and irregular waves).

The system consists of a floater with an interior U-Tank partially filled with water. The device is moored at the seabed with a mooring system, the floater is designed to be multi-directional; therefore, the device is able to align itself with the incoming wave direction. The inclusion of the U-Tank technology into a floating wave energy converter allows the slow tuning of the device. The dynamics characteristics of the U-Tank are functions of the amount of air into the two lateral reservoirs. The advantage of this concept is that the floater is totally closed from the external environment and it has no parts in motion.

In the U-Tank technology two lateral reservoirs of the U-Tank are connected by an air duct. The motion of the U-shaped oscillating water column (induced by the rolling of the floater), forces the air through the duct where an accumulator and a turbine are installed to extract power from the wave motion.

The numerical model is used to analyze the U-Tank in a frequency and time domain, to analyze the effect of the changing parameters on the system efficiency; the whole study aims to verify the gross power produced by U-Tank in different sea state.

Contents

LIST OF FIGURES	VII
LIST OF TABLES	X
1. INTRODUCTION	- 1 -
1.1 CLASSIFICATION OF WAVE ENERGY CONVERTERS.....	- 2 -
1.2 TANK TECHNOLOGY IN WECS	- 3 -
1.3 STATE OF THE ART.....	- 4 -
2. EQUATION OF THE U-TANK DYNAMICS MODEL	- 6 -
3. DAMPING PTO WITHOUT AIR DYNAMICS	- 10 -
3.1 TRENDS USING PITCH ANGLE OF 1 [DEG].....	- 11 -
3.2 TRENDS USING PITCH ANGLE OF 5 [DEG].....	- 13 -
3.3 MEAN POWER ABSORPTION.....	- 15 -
4. AIR DYNAMICS	- 18 -
4.1 PRESSURE DROP THROUGH A RESISTANCE.....	- 18 -
4.2 EVALUATION OF THE AIR INFLUENCE ON THE WHOLE SYSTEM	- 25 -
4.3 ANALYSIS USING OTHER R_v VALUES.....	- 29 -
4.4 INITIAL VOLUME VARIATION.....	- 34 -
5. TIME DOMAIN	- 37 -
5.1 BLOCK DIAGRAMS.....	- 40 -
5.1.1 Dynamics of the U-Tank	- 40 -
5.1.2 Volume variation block of the left air chamber.....	- 42 -
5.1.3 Volume variation block of the right air chamber.....	- 44 -
5.1.4 Control on the charge and discharge process of the air chamber	- 45 -
5.1.5 Fixed volume V_c block diagram.....	- 47 -
5.2 ANALYSIS USING DIFFERENT AMPLITUDE AND PERIOD VALUES	- 49 -
5.2.1 Amplitude 5 [deg].....	- 49 -
5.2.2 Amplitude 10 [deg].....	- 53 -
5.2.3 Amplitude 20 [deg].....	- 57 -
5.3 AIR INFLUENCE COMPARING LINEAR AND NON-LINEAR SYSTEM	- 61 -
6. POWER EXTRACTION	- 66 -
6.1 MEAN POWER EXTRACTION	- 68 -
6.2 VARIATION OF THE INITIAL AIR VOLUME	- 72 -
6.2.1 $V_0= 125 [m^3]$	- 73 -
6.2.2 $V_0= 250 [m^3]$	- 76 -
6.2.3 $V_0= 500 [m^3]$	- 78 -
7. CONCLUSIONS	- 81 -
7.1 FURTHER WORK	- 85 -
BIBLIOGRAPHY	- 86 -

List of Figures

Figure 1.1: Wave energy resource potential [1]	- 1 -
Figure 1.2: Classification of wave energy converters based on their location [8]	- 2 -
Figure 1.3: UGEN wave energy converter concept [7]	- 4 -
Figure 2.1: Geometrical features of the U-Tank	- 6 -
Figure 2.2: Acceleration forces working on the U-Tank	- 7 -
Figure 3.1: Magnitude by varying BPTO using $\delta=1$ [deg]	- 11 -
Figure 3.2: Phase by varying BPTO using $\delta=1$ [deg]	- 12 -
Figure 3.3: Torque by varying BPTO using $\delta=1$ [deg]	- 13 -
Figure 3.4: Magnitude by varying BPTO using	- 14 -
Figure 3.5: Phase by varying BPTO using	- 14 -
Figure 3.6: Torque by varying BPTO using	- 15 -
Figure 3.7: Mean Power Absorption by varying BPTO using	- 16 -
Figure 3.8: Mean Power Absorption by varying BPTO using	- 17 -
Figure 4.1: Schematization of the system used to evaluate the pressure drop through a resistance	- 18 -
Figure 4.2: Bode Diagram of the pressure drop through a resistance transfer function	- 23 -
Figure 4.3: Magnitude by varying R_V	- 23 -
Figure 4.4: Phase by varying R_V	- 24 -
Figure 4.5: Bode Diagram of the global system transfer function	- 26 -
Figure 4.6: Magnitude of the global system by varying R_V	- 27 -
Figure 4.7: Phase of the global system transfer function by varying R_V	- 27 -
Figure 4.8: Power extracted from resistance	- 29 -
Figure 4.9: Bode Diagram of the pressure drop through a resistance transfer function using new R_V values	- 30 -
Figure 4.10: Magnitude of the pressure drop through a resistance transfer function using new R_V values	- 30 -
Figure 4.11: Phase of the pressure drop through a resistance transfer function using new R_V values	- 31 -
Figure 4.12: Bode Diagram of the global system transfer function using new R_V values	- 32 -
Figure 4.13: : Magnitude of the global system transfer function using new R_V values	- 32 -
Figure 4.14: : Phase of the global system transfer function using new R_V values	- 33 -
Figure 4.15: Power extracted from resistance using new R_V values	- 33 -
Figure 4.16: Magnitude by varying R_V and V_0	- 34 -
Figure 4.17: Power extracted by varying R_V and V_0	- 35 -
Figure 4.18: Mass flow by varying R_V and V_0	- 35 -
Figure 4.19: Pressure variation by varying R_V and V_0	- 36 -
Figure 5.1: Scheme of the analyzed system	- 37 -
Figure 5.2: U-Tank dynamics block	- 41 -
Figure 5.3: Detail of the dynamics U-Tank block diagram	- 41 -
Figure 5.4: Volume variation block of the left air chamber	- 42 -
Figure 5.5: Detail of the Volume variation block of the left air chamber	- 42 -
Figure 5.6: Detail of the C1 block diagram left air chamber	- 43 -

Figure 5.7: Detail of the C2 block diagram left air chamber	- 43 -
Figure 5.8: Volume variation block of the right air chamber	- 44 -
Figure 5.9: Detail of the Volume variation block of the right air chamber	- 44 -
Figure 5.10: Control on the charge and discharge process on the left air chamber	- 45 -
Figure 5.11: Control on the charge and discharge process on the right air chamber	- 46 -
Figure 5.12: Switch control on the mass flow to the fixed volume as a velocity function	- 47 -
Figure 5.13: Dynamic filling block of the central fixed volume VC	- 47 -
Figure 5.14: Detail of the dynamic filling block of the central fixed volume VC	- 48 -
Figure 5.15: Detail of the C2 block diagram into the central fixed volume VC block	- 48 -
Figure 5.16: δ, τ and pressures trends using $A=5$ [deg] e $T=7$ [s]	- 49 -
Figure 5.17: Detail of the pressure's trends using pitch angle with Amplitude=5 [deg] and Period=7 [s]	- 50 -
Figure 5.18: Trends of the inlet mass flow to the fixed volume V_c using $A=5$ [deg] and $T=7$ [s]	- 50 -
Figure 5.19: δ, τ and pressures trends using $A=5$ [deg] e T of resonance	- 51 -
Figure 5.20: Trends of the inlet mass flow to the fixed volume V_c using $A=5$ [deg] and T of resonance	- 51 -
Figure 5.21: : δ, τ and pressures trends using $A=5$ [deg] e $T=11$ [s]	- 52 -
Figure 5.22: Trends of the inlet mass flow to the fixed volume V_c using $A=5$ [deg] and $T=11$ [s]	- 52 -
Figure 5.23: δ, τ and pressures trends using $A=10$ [deg] e $T=7$ [s]	- 53 -
Figure 5.24: Detail of the pressure's trends using pitch angle with Amplitude=10 [deg] and Period=7 [s]	- 54 -
Figure 5.25: Trends of the inlet mass flow to the fixed volume V_c using $A=10$ [deg] and $T=7$ [s]	- 54 -
Figure 5.26: δ, τ and pressures trends using $A=10$ [deg] e T of resonance	- 55 -
Figure 5.27: Trends of the inlet mass flow to the fixed volume V_c using $A=10$ [deg] and T of resonance	- 55 -
Figure 5.28: δ, τ and pressures trends using $A=10$ [deg] e $T=11$ [s]	- 56 -
Figure 5.29: Trends of the inlet mass flow to the fixed volume V_c using $A=10$ [deg] and $T=11$ [s]	- 56 -
Figure 5.30: δ, τ and pressures trends using $A=20$ [deg] e $T=7$ [s]	- 57 -
Figure 5.31: Detail of the pressure's trends using pitch angle with Amplitude=20 [deg] and Period=7 [s]	- 58 -
Figure 5.32: Trends of the inlet mass flow to the fixed volume V_c using $A=20$ [deg] and $T=7$ [s]	- 58 -
Figure 5.33: δ, τ and pressures trends using $A=20$ [deg] e T of resonance	- 59 -
Figure 5.34: Trends of the inlet mass flow to the fixed volume V_c using $A=20$ [deg] and T of resonance	- 59 -
Figure 5.35: δ, τ and pressures trends using $A=20$ [deg] e $T=11$ [s]	- 60 -
Figure 5.36: Trends of the inlet mass flow to the fixed volume V_c using $A=20$ [deg] and $T=11$ [s]	- 60 -
Figure 5.37: influence of air on the linear and non-linear system	- 62 -
Figure 5.38: Pressure trend in V_c in non-linear system using different amplitude of the pitch angle	- 63 -

Figure 5.39: influence of air on the linear and non-linear system by varying V_0 value	- 64 -
Figure 5.40: Pressure trend in V_c in non-linear system using different V_0 values	- 65 -
Figure 6.1: The PTO pneumatic system modelled	- 66 -
Figure 6.2: Flow rate disposal block of the generator unit	- 67 -
Figure 6.3: Mean gross power for different period and different mass flow values	- 69 -
Figure 6.4: τ , mean pressure value, mean mass flow in frequency domain of the PTO pneumatic system	- 70 -
Figure 6.5: τ , pressure inside the accumulator, mass flow extracted and gross power in time domain of the PTO pneumatic system at resonance frequency	- 71 -
Figure 6.6: Mean gross power for different period and different mass flow values and $V_0=125$ [m^3]	- 73 -
Figure 6.7: τ , mean pressure value, mean mass flow in frequency domain of the PTO pneumatic system for $V_0=125$ [m^3]	- 74 -
Figure 6.8: τ , pressure inside the accumulator, mass flow extracted and gross power in time domain of the PTO pneumatic system at resonance frequency for $V_0=125$ [m^3]	- 75 -
Figure 6.9: Mean gross power for different period and different mass flow values and $V_0=250$ [m^3]	- 76 -
Figure 6.10: τ , mean pressure value, mean mass flow in frequency domain of the PTO pneumatic system for $V_0=250$ [m^3]	- 77 -
Figure 6.11: τ , pressure inside the accumulator, mass flow extracted and gross power in time domain of the PTO pneumatic system at resonance frequency for $V_0=250$ [m^3]	- 78 -
Figure 6.12: Mean gross power for different period and different mass flow values and $V_0=500$ [m^3]	- 78 -
Figure 6.13: τ , mean pressure value, mean mass flow in frequency domain of the PTO pneumatic system for $V_0=500$ [m^3]	- 79 -
Figure 6.14: τ , pressure inside the accumulator, mass flow extracted and gross power in time domain of the PTO pneumatic system at resonance frequency for $V_0=500$ [m^3]	- 80 -

List of Tables

Table 2-1: Values of the geometrical features of the U-Tank	- 6 -
Table 3-1: Coefficients value of the U-Tank	- 10 -
Table 5-1: Values quantities used for the calculation of resistance R	- 39 -

1. Introduction

In the last few years has grown the attention towards renewable energy sources in a fullness commercial state like wind, geothermal and solar. Another renewable energy which is still not completely exploited are the ocean waves. This type of renewable energy is accessible worldwide [1]. In these last years have been studied and strengthened various technology solutions to collect ocean wave energy [2]. Wave energy is in full growth and for this reason the cost of energy is not as competitive as the other renewable energy [3]. The main problems related to the commercialization of the wave energy technology are the high corrosion due to the marine saltwater and the high loads due to the severe marine conditions.

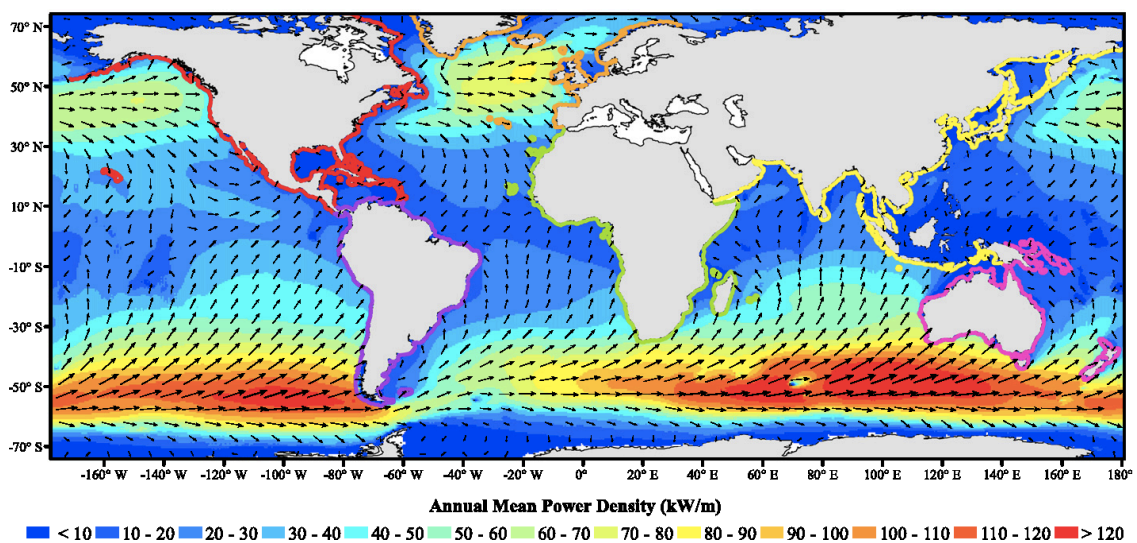


Figure 1.1: Wave energy resource potential [1]

The objective is the test of full-scale device in order to verify the performance of the device in different sea state.

1.1 Classification of wave energy converters

Wave Energy Converter (WEC) concepts can be classified in relation to the site location [4]. There are three type of devices: shoreline, nearshore and offshore.

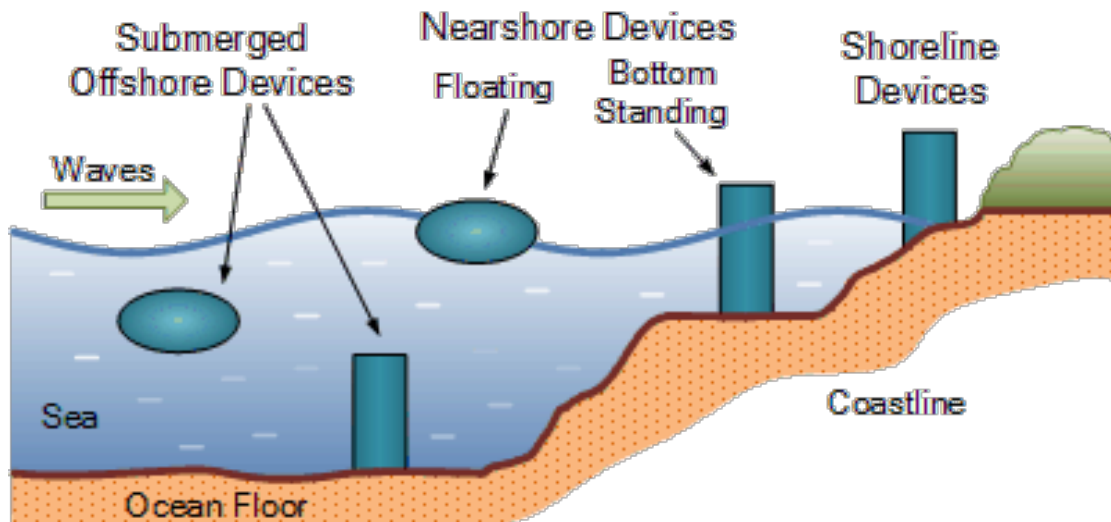


Figure 1.2: Classification of wave energy converters based on their location [8]

- Shoreline devices: are fixed structures integrate into the shoreline, harbor or breakwaters. These types of devices are based on the oscillating water column technology (OWC). The OWC is a structure where water waves can oscillate; the air is caught through a turbine adopted to collect wave energy. The main advantage of this device is the proximity to the end-users and the consequent maintenance cost reduction. On the other hand, OWC requires high costs of construction.
- Nearshore devices: are installed in shallow water and avoid the use of mooring system. The main advantage is the proximity to the shoreline and, since they are installed in open sea, the wave energy resource is higher. In case of floating devices, the mooring cost are lower than the offshore devices. The main drawback of these WECs is their proximity to the shoreline, which can cause environmental and social effects.
- Offshore devices: are installed in deep water. These types of devices have a higher source of energy compared to shoreline and nearshore devices. These devices can be floating or submerged structures moored to the seabed; moreover, because of

their distance from the shore, they produce less environmental and social impact than the near shore devices.

It's also possible to classify WECs according to their size and working direction. There are three cases: point absorber, attenuators and terminators [9].

- Point absorbers are smaller in comparison with the incident wavelength. This structure provides a mooring system. Point absorbers are usually installed in arrays because of their small dimension.
- Attenuators are a multi-body structures with a slack-moored at the seabed. In this case, the total length of the structures is longer than the incident wavelength. Attenuators are made of several hinged structures.
- Terminators are usually perpendicular to the incoming dominant wave direction.

1.2 Tank technology in WECs

Tuned Liquid Dampers (TLD) are a water sloshing tank which are a special type of tuned mass dampers; these are usually used to reduce oscillation in tall buildings and to reduce the roll motion of the ships. [10] On ships they are usually positioned above the COG (Center of Gravity) and consists in a rectangular tank filled with water. The shifting water give a roll moment out of phase with the excitation force exerted by the wave [5]. According to the roll movement there is a decrease of the roll amplitude.

The floating wave energy converter contains a floating body with an interior U-shaped tank partially filled with water [6]. The U-shaped tanks are used to overwhelm the problem which affect free-surface tanks, such as the unpredictable and high impulsive loads due to the sloshing and breaking waves phenomena inside the rectangular tank. The U-Tank is made-up by two reservoirs connected by a base duct; the whole structure is partially filled with water.

Over the years, the idea of obtaining energy from the water motion has also been developed. In the last decade, a U-Tank for generation of electricity from the wave (UGEN) has been developed by Falcão et al. [7]. In this particular case of U-Tank, there is an

additional air duct (see in Figure (1.3)). During the water sloshing, the air into the reservoirs is pressurized causing an air flow. In the air duct there is a turbine that collect energy, this system constitutes the Power Take Off (PTO). The main excitation motion of the water inside the U-Tank is the pitch and roll motion of the floater [13].

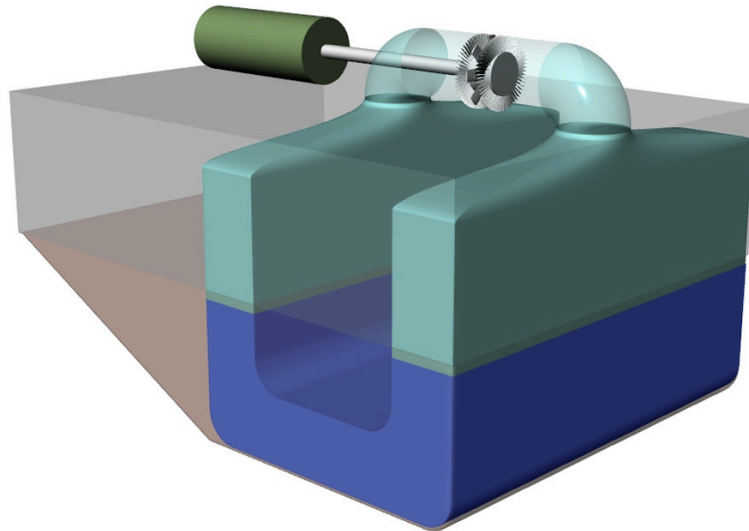


Figure 1.3: UGEN wave energy converter concept [7]

The U-Tank technology is used to adjust the resonance frequency of the WECs in a dynamic way. The resonance frequency of the entire floating system plus U-Tank can be adjusted by controlling the dynamics of the movement of the water inside the tank [14].

1.3 State of the Art

The ISWEC (Inertial Sea Wave Energy Converter) device is an offshore floating wave energy converter outlined for the Mediterranean Sea wave [11]. The operating principles on which it's based is the precession motion of a gyroscope inside the hull due to the pitching motion of the device. The electrical PTO converts the mechanical energy harvested. The floater is capable of adapting to the incident wave direction thanks to a slack mooring system [15], [16]. Different tests were carried out at the Università di Napoli Federico II to evaluate the dynamics and loads according to the conditions of the sea state and the resistance to the atmospheric agents of the new mooring system coupled with the floater.

The first test of the ISWEC idea was carried out in the wave tank at the University of Edinburgh in 2007 [17]. A first numerical model and the first experimental test was carried out on a 1:8 scale model at INSEAN in Rome (Italy) in 2012 [18]. The first 1:1 scale model was positioned off the coast of the island of Pantelleria in the end of 2015, in order to validate the technological solutions and the survival capacity of the device [19], [20].

Following a collaboration between the academic spin-off Wave-for-Energy and the Eni company, a new ISWEC 1:2 scale model was created in 2016. This last model was positioned off the coast of Ravenna (Italy) in the Adriatic Sea [21].

In the next few years it's expected to use ISWEC not only in the Mediterranean Sea but also in the oceans; thanks to the huge wave power density of the oceans. The sea state of the oceans is more complex because of the contemporary presence of local wind waves and swells caused by distant storm; but also, the wave period and height of the ocean waves are various [12]. The ISWEC device works in a specific class of wave frequencies. To achieve the goal, it's necessary to develop a solution to tune the resonance condition with the incoming wave; it's possible to create a single device capable of adapting to the site where it's installed. The system is the IOwec (Inertial Ocean Wave Energy Converter) technology, that has been developed from a Renewable Energies Group of Politecnico di Torino and the MIT i-Ship Lab.

It's possible to integrate the U-Tank technology into the ISWEC device for oceans, to allow the "slow-tuning" of the device with the incoming sea-state [5]. In this case it's possible to extend the performance bandwidth.

The intent of this thesis is to analyze the gross power extraction of the U-Tank technology installed inside an already know IOwec device for a different sea-state conditions (regular and irregular waves) in frequency and time domain.

2. Equation of the U-Tank dynamics model

In this chapter the numerical model, which describes the U-Tank and its coupling with the float, is developed.

In the following figure and table are shown all the geometrical features of the U-Tank, where x_t represents the width of the U-Tank system.

The U-Tank device consist of two lateral rectangular reservoirs connected by a central base duct.

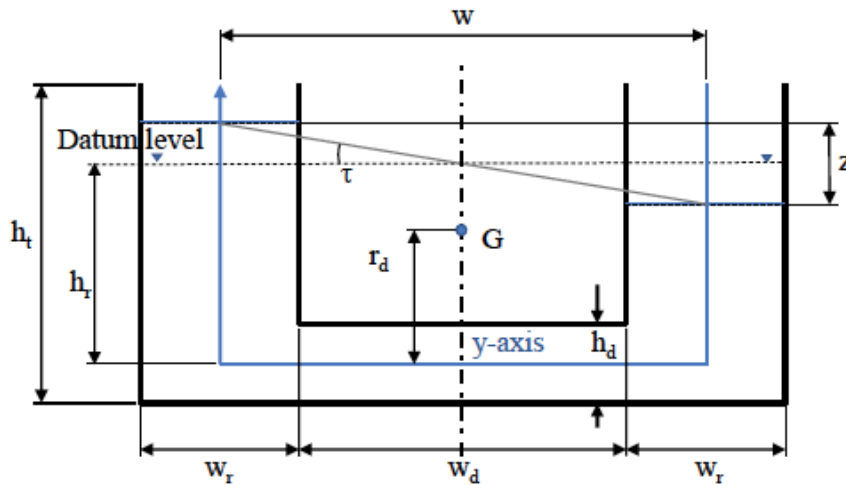


Figure 2.1: Geometrical features of the U-Tank

x_t	19.7	[m]
h_d	0.85	[m]
w_d	9.52	[m]
w_r	2.94	[m]
h_r	2.39	[m]
r_D	1.67	[m]
$w=w_d+w_r$	12.46	[m]

Table 2-1: Values of the geometrical features of the U-Tank

Through the Euler equation, it's possible to represent the water flow inside the U-Tank.

$$\frac{dv}{dt} = Y - \frac{1}{\rho} \frac{dP}{dy} \quad (2.1)$$

Where v represents the fluid velocity, P is the pressure over the y axis, in Y are represented the whole external forces influencing the fluid. It's possible to make the following assumptions:

- One-dimensional motion of the water inside the U-Tank;
- Absence of the velocity gradient along the y axis;
- Linear response of the system;
- Only the coupling of the U-Tank with the pitch DoF of the floater is accounted.

Thanks to the U-shaped geometry, it's possible to express velocity as a τ function, where τ is the angle between the water level of the two lateral tanks and is considered to be small.

$$v = \frac{w}{2} \dot{\tau} \quad (2.2)$$

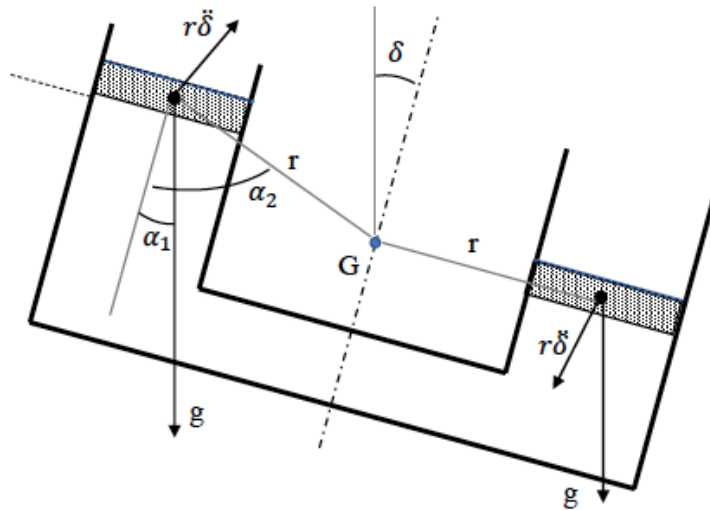


Figure 2.2: Acceleration forces working on the U-Tank

The external forces per unit mass acting on the fluid are due to different inputs. With the reference to Figure (2.2), it's possible to write the following equation for the external forces:

- Force of gravity

$$Y_g = -g \cos\alpha_1 \quad (2.3)$$

- Acceleration due to the floater motion

$$Y_\delta = -r\ddot{\delta} \sin\alpha_2 \quad (2.4)$$

- Frictional forces due to spread and localized losses

$$Y_d = -\frac{qv}{n} \quad (2.5)$$

(q is a resistance coefficient evaluated through CFD analysis and n is the U-Tank width along the perpendicular to y-axis).

Replacing the previous equations into the Equation (2.1) , it becomes:

$$\frac{w_r w \ddot{t}}{2n} + \frac{q w_r w \dot{t}}{2n^2} + g \cos\alpha_1 + r \ddot{\delta} \sin\alpha_2 = -\frac{1}{\rho} \frac{dP}{dy} \quad (2.6)$$

Integrating the Equation (2.1) along the y axis, we get:

$$\frac{\rho w_r w I_1 \ddot{t}}{2} + \frac{\rho q w_r w I_2 \dot{t}}{2} + \rho g I_3 + \rho \ddot{\delta} I_4 = P_{stern} - P_{bow} \quad (2.7)$$

$$I_1 = \frac{w}{h_d} + \frac{2h_r}{w_r} \quad (2.8)$$

$$I_2 = \frac{w}{h_d^2} + \frac{2h_r}{w_r^2} \quad (2.9)$$

$$I_3 = w\delta \quad (2.10)$$

$$I_4 = w(r_d + h_r) \quad (2.11)$$

$$P_{stern} - P_{bow} = -\rho g w \tau \quad (2.12)$$

$$Q_r = \frac{w w_r x_t}{2} \quad (2.13)$$

Equation (2.13) represents the motion of the fluid like a function of the moment of the area applied to the tank. It's now possible to write the Equation (2.7) in a clearer form.

$$a_{\tau\tau}\ddot{\tau} + b_{\tau\tau}\dot{\tau} + c_{\tau\tau}\tau = a_{\tau5}\ddot{\delta} + c_{\tau5}\delta \quad (2.14)$$

$$Q_t = \frac{\rho w_r w^2 x_t}{2} \quad (2.15)$$

Equation (2.15) represents a 1 DoF lumped parameter model of the second order; this model is dynamically joint with the floater oscillation and the pitch acceleration.

It's possible to write the hydrodynamic coefficients of the Equation (2.14) in the following way:

$$a_{\tau\tau} = Q_t w_r \left(\frac{w}{2h_d} + \frac{h_r}{w_r} \right) \quad (2.16)$$

$$c_{\tau\tau} = c_{\tau5} = Q_t g \quad (2.17)$$

$$a_{\tau5} = Q_t (r_d + h_r) \quad (2.18)$$

$$b_{\tau\tau} = 2\omega_n a_{\tau\tau} \xi \quad (2.19)$$

$$\omega_n = \sqrt{\frac{c_{\tau\tau}}{a_{\tau\tau}}} \quad (2.20)$$

In this case ξ represents the damping ratio, already estimated and set at 0.0087. Equation (2.20) represents the resonance frequency of the sloshing water inside the U-Tank and is function of the geometrical properties of the device.

Since the oscillation input δ is known, it's possible to evaluate the angle τ , through the following transfer function of the U-Tank.

$$\frac{\bar{\tau}}{\bar{\delta}} = \frac{a_{\tau5}s^2 + c_{\tau5}}{a_{\tau\tau}s^2 + b_{\tau\tau}s + c_{\tau\tau}} \quad (2.21)$$

It's also possible to write the torque (M_{U-Tank}) transfer function of the U-Tank, which is equal to:

$$\frac{\overline{M_{U-tank}}}{\bar{\delta}} = \frac{(a_{\tau5}s^2 + c_{\tau5})^2}{a_{\tau\tau}s^2 + b_{\tau\tau}s + c_{\tau\tau}} \quad (2.22)$$

3. Damping PTO without air dynamics

A first study is carried out in frequency domain on the influence of damping PTO on the regular wave system, without considering air dynamics.

Pointing out with δ the pitching motion, while τ is the vertical movement of the water in the U-Tank tanks, has been obtained the amplitude, phase and torque trends of the damping PTO system without air dynamics. This study was performed for two different pitch angles δ equal to 1 and 5 deg.

Setting the values of $\xi = 0.0087$, $\rho = 1000 \text{ kg/m}^3$ and $g = 9.81 \text{ m/s}^2$, it's possible to calculate the value of the Equations from (2.15) to (2.20). The results are shown in Table (3-1).

Q_t	$4.4959 \cdot 10^6$	[kg m]
$a_{\tau\tau}$	$1.0763 \cdot 10^8$	[kg m ²]
$c_{\tau\tau} = c_{\tau5}$	$4.4105 \cdot 10^7$	[kg m ² /s ²]
$a_{\tau5}$	$1.8253 \cdot 10^7$	[kg m ²]
ω_n	0.6402	[rad/s]
$b_{\tau\tau}$	$1.1988 \cdot 10^6$	[kg m ² /s]

Table 3-1: Coefficients value of the U-Tank

To evaluate the influence of the damping PTO, the transfer function shown in Equation (2.21) was modified as follow.

$$\frac{\bar{\tau}}{\bar{\delta}} = \frac{a_{\tau5}s^2 + c_{\tau5}}{a_{\tau\tau}s^2 + (b_{\tau\tau} + B_{PTO})s + c_{\tau\tau}} \quad (3.1)$$

Where:

$$B_{PTO} = n \cdot b_{\tau\tau} \quad (3.2)$$

In Equation (3.2), n represents a multiplicative coefficient that assumes the values of 0, 3.25, 5.5, 7.75 and 10.

The trends obtained for the two different values of the input are shown in the following paragraphs.

3.1 Trends using pitch angle of 1 [deg]

In the following figures are shown the magnitude and phase trends using the Equation (3.1) and a pitch angle equal to 1 [deg].

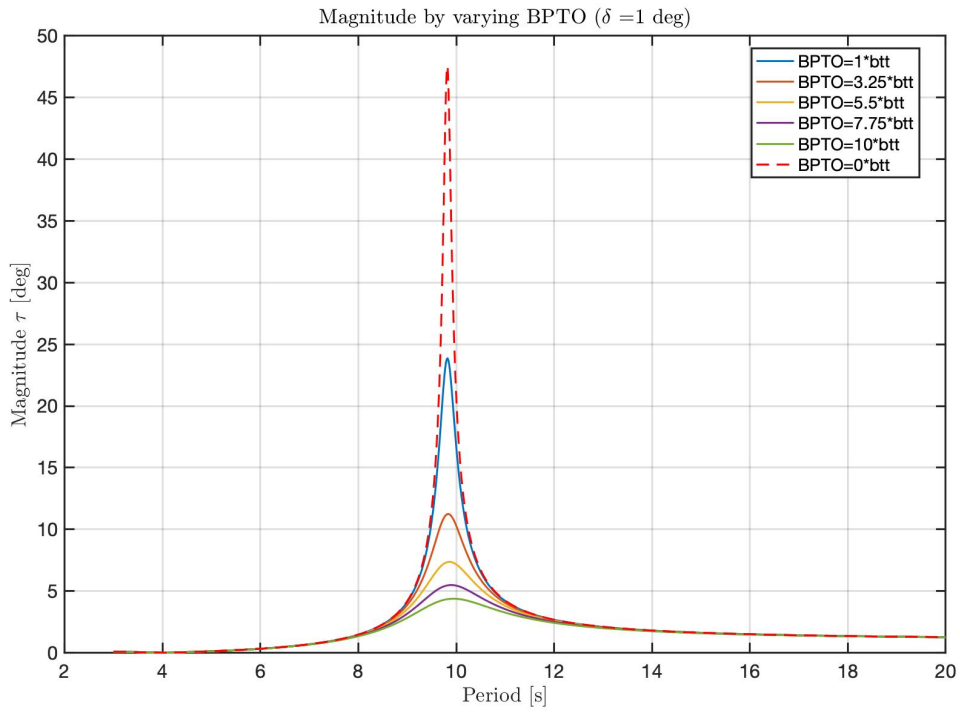


Figure 3.1: Magnitude by varying BPTO using $\delta=1$ [deg]

The Figure (3.1) shows that by increasing the damping B_{PTO} value, there is a significant decrease of the magnitude value.

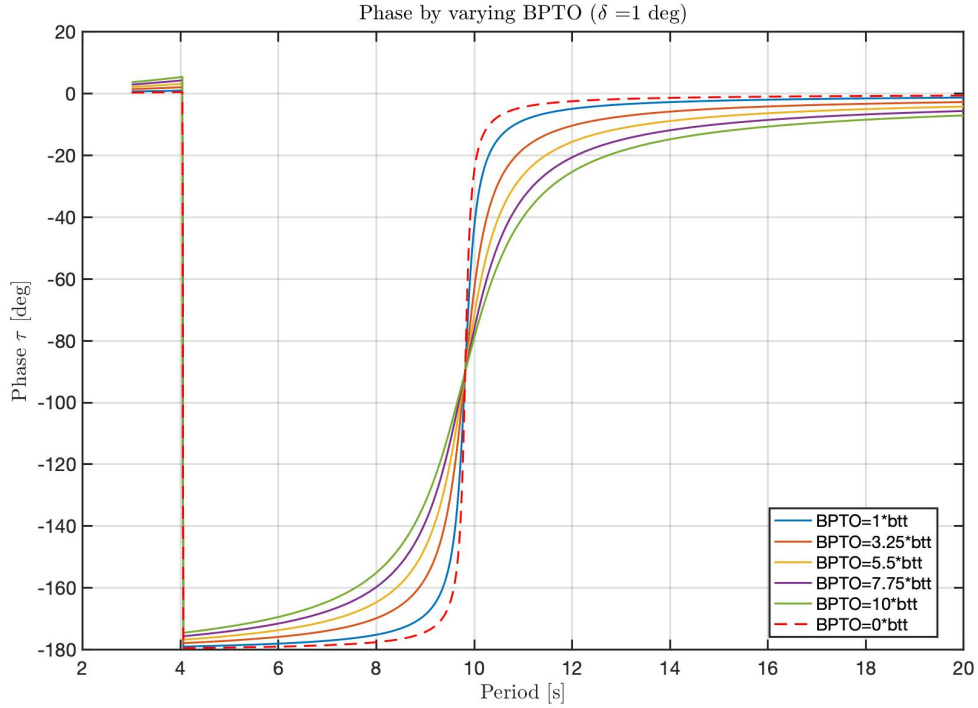


Figure 3.2: Phase by varying BPTO using $\delta=1$ [deg]

From the Equation (3.1) is possible to notice that the transfer function has 2 zeros at the numerator and 2 poles at the denominator; therefore, the phase has a trend that starts from -180° and reaches 0° passing through the point of inflection with a vertical tangent at a frequency equal to the one where there is the maximum value of magnitude.

Furthermore, the torque trend (shown in the Figure (3.3)) was evaluated according to the following equation:

$$\frac{\overline{M_{U-tank}}}{\bar{\delta}} = \frac{(a_{\tau 5} s^2 + c_{\tau 5})^2}{a_{\tau \tau} s^2 + (b_{\tau \tau} + B_{PTO})s + c_{\tau \tau}} \quad (3.3)$$

Also in this case, increasing the B_{PTO} damping value, there is a significant decrease in the maximum values reached.

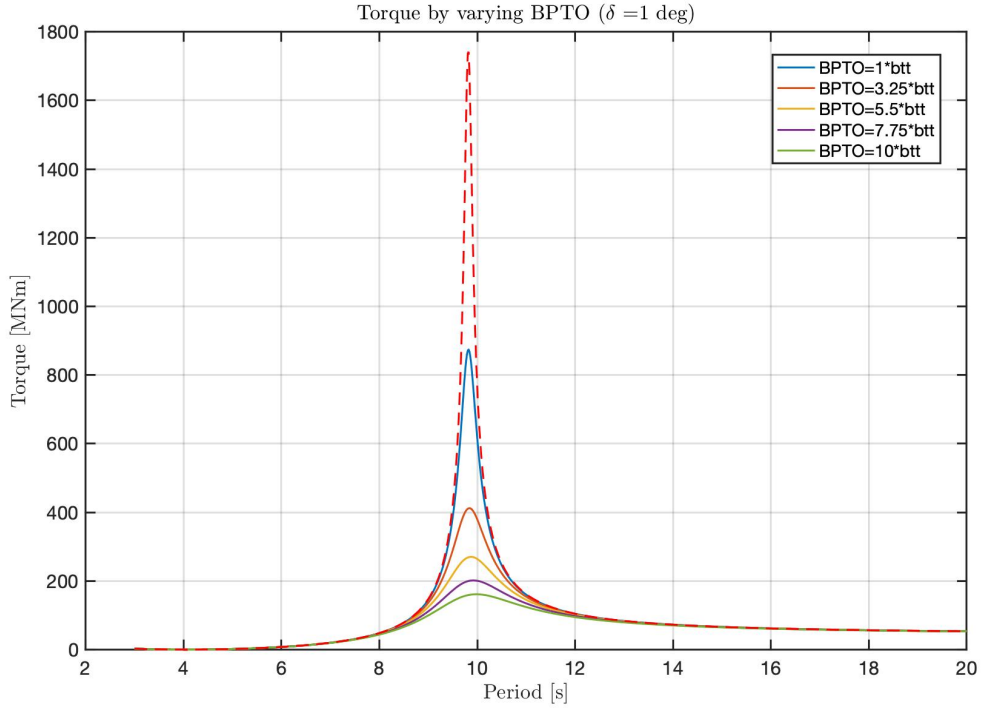


Figure 3.3: Torque by varying BPTO using $\delta=1$ [deg]

3.2 Trends using pitch angle of 5 [deg]

Later on, the pitch angle value is changed. Using $\delta = 5^\circ$ and Equations (3.1) and (3.3), we obtained the trends shown in the following figures.

In this case it's possible to make the same considerations of the previous paragraph, namely increasing the B_{PTO} damping value, there is a significant decrease in the maximum values reached.

Also, it's possible to note that, compared to the case with a pitch angle of 1 deg, there is a considerable increase in the maximum values reached both in magnitude and in torque.

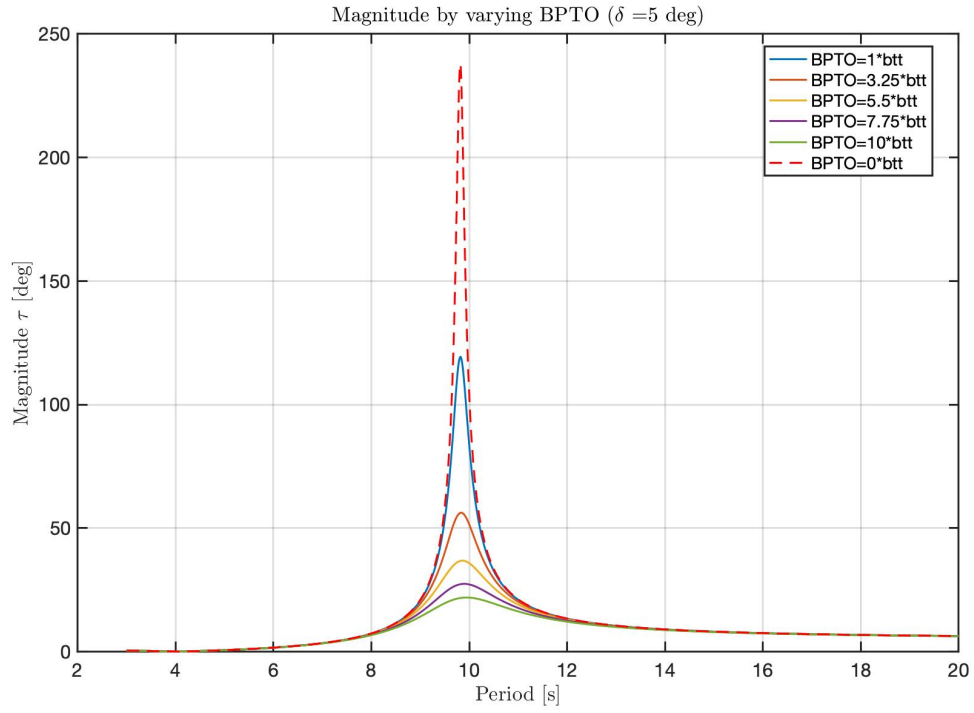


Figure 3.4: Magnitude by varying BPTO using

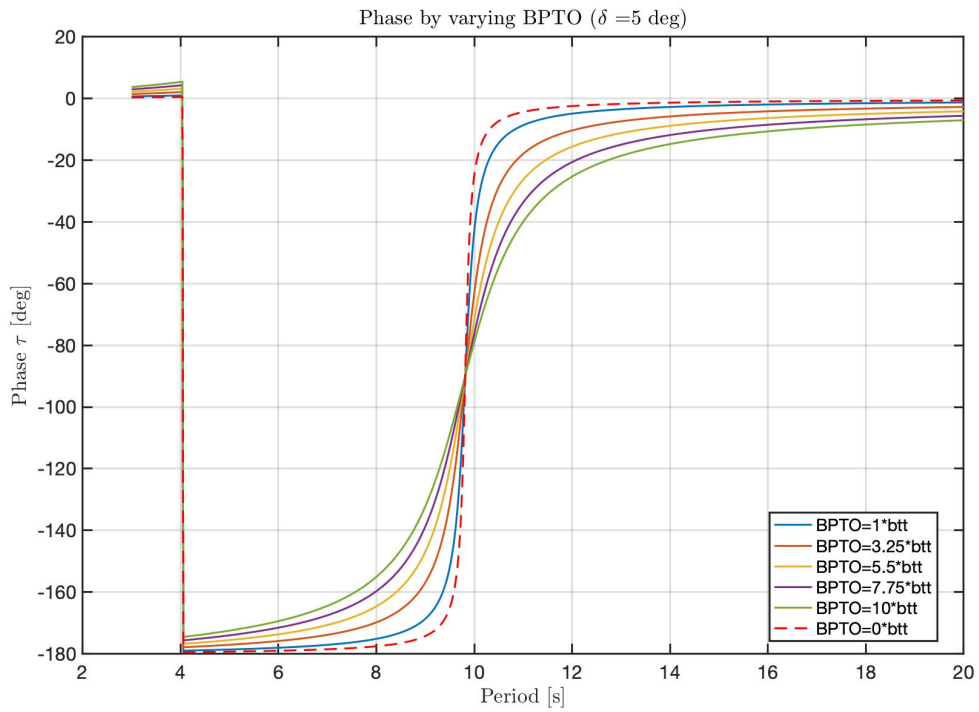


Figure 3.5: Phase by varying BPTO using

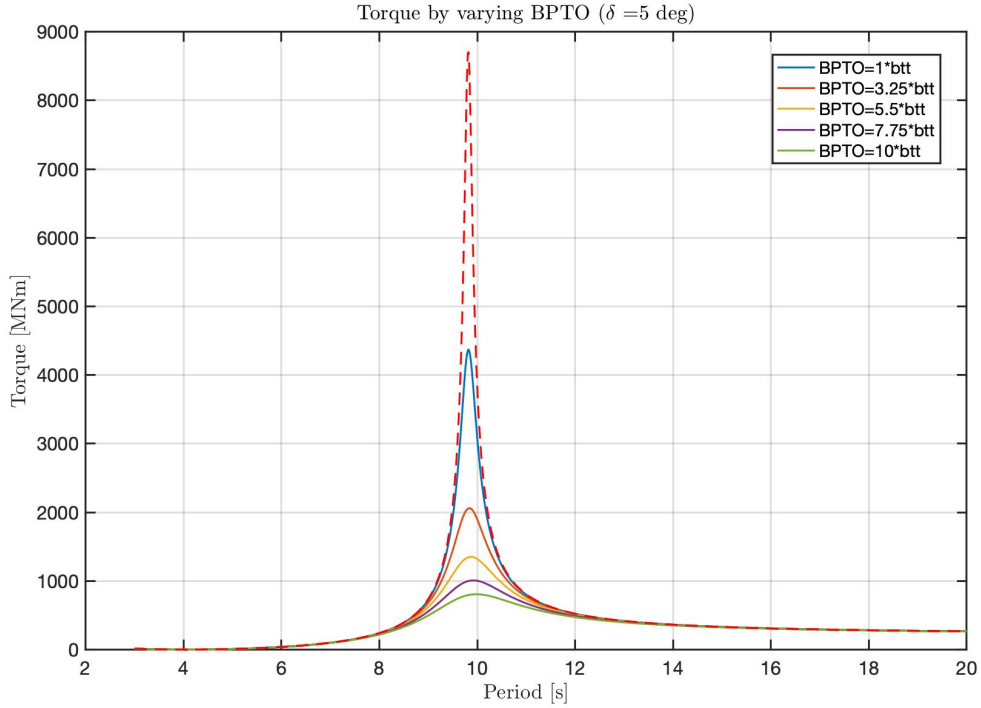


Figure 3.6: Torque by varying BPTO using

3.3 Mean Power Absorption

In this paragraph are presented the parameters to evaluate the power captured by Wave Energy Converters (WECs). The PTO have to maximize the energy extracted from the waves and have to tune the device so as to make it resonant with the incoming waves [4].

In this case, as mean power absorbed is identified the average power wasted by the PTO mechanical damper during a wave period. To obtain the mean power absorption, it is supposed that the waves are sinusoids and integrating over a wave period we obtain the following equation:

$$\bar{P} = \frac{1}{T} \int_0^T B_{PTO} u^2 dt = \frac{B_{PTO} (\omega \tau_0)^2}{2} \quad (3.3)$$

Where u is the velocity of τ , B_{PTO} is the damping PTO coefficient, T is the wave period and τ_0 is the magnitude obtained in the previous analysis for different pitch angle δ .

In the following figures it's possible to see the trend of the mean power absorption for different B_{PTO} and delta input values.

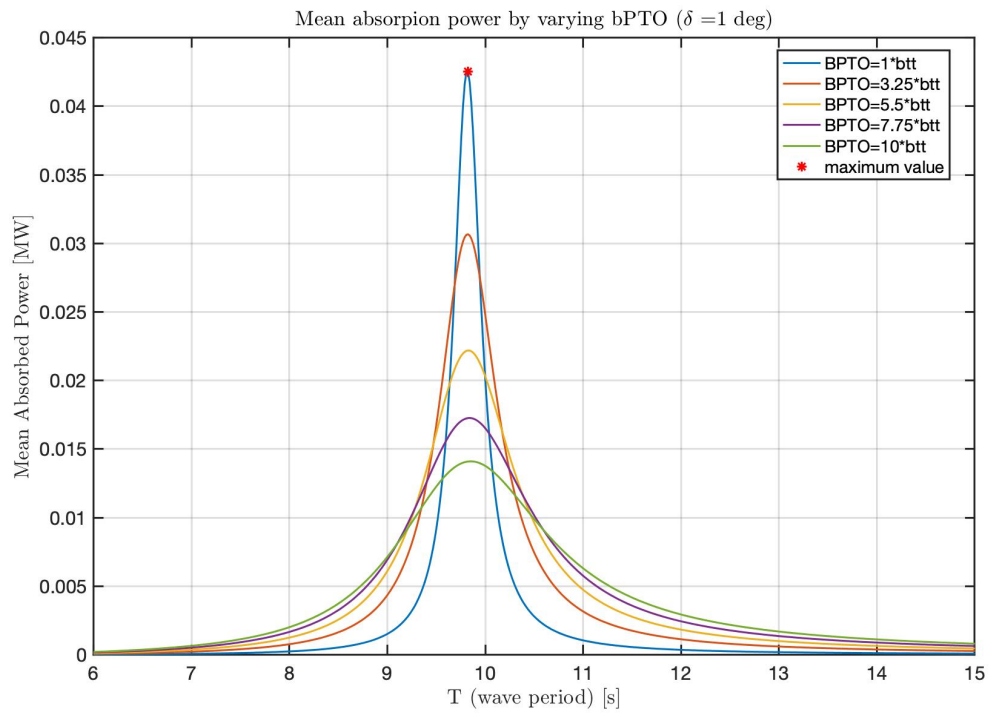


Figure 3.7: Mean Power Absorption by varying BPTO using

For a pitch angle equal to $\delta = 1$ [deg], the maximum value of mean power absorption is equal to:

$$\bar{P} = 0.0425 \text{ MW}$$

$$B_{PTO} = 1.1988 * 10^6 \text{ kg m}^2 / \text{s}$$

$$\omega = 0,6396 \text{ rad/s}$$

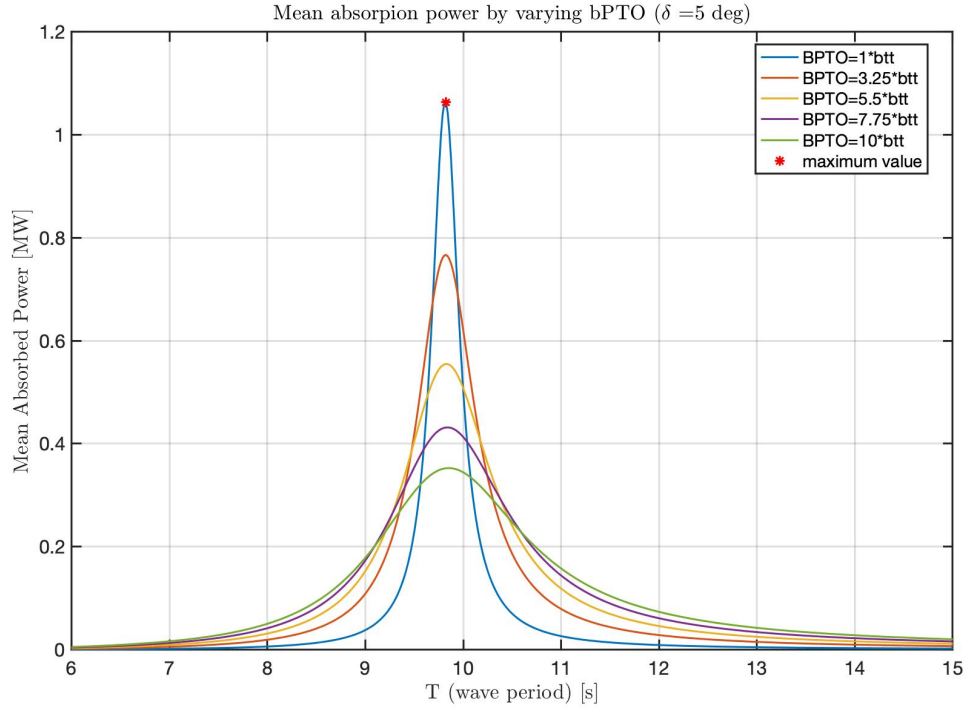


Figure3.8: Mean Power Absorption by varying BPTO using

For a pitch angle equal to $\delta = 5 [deg]$, the maximum value of mean power absorption is equal to:

$$\bar{P} = 1,063 \text{ MW}$$

$$B_{PTO} = 1.1988 * 10^6 \text{ kg m}^2 / \text{s}$$

$$\omega = 0,6396 \text{ rad/s}$$

It's possible to notice that, in both cases, the frequency of the maximum value of mean power absorption is close to the frequency of resonance. From the trend in the Figures (3.7) and (3.8), it's possible to see how for different values of frequency, there are different B_{PTO} values that maximizes the mean power absorption.

4. Air dynamics

In this part of the work, is evaluated the influence of air on the entire system. The analysis is conducted in the frequency domain. The work is divided into two phases:

- the first in which the pressure drop through a resistance (located in the air-side duct) is evaluated according to the kinematics of the U-Tank ;
- the second in which is evaluated the influence of air on the whole system (U-Tank coupled with the air resistance). Furthermore, the relative power extracted through the resistance is evaluated.

Everything was evaluated by setting $\delta = 1$ [deg] and assuming an isothermal transformation.

4.1 Pressure drop through a resistance

In this first case, the system is schematized as two air pistons (which simulate the motion of the water in the U-Tank) and an air duct which connects the two air pistons. R_V is a resistance that can represent the behavior of a valve or air turbine. It causes a pressure drop between the two U-Tank air reservoirs, influencing the dynamics of the U-Tank. In the following Figure (4.1) is represented the schematization of the system used to evaluate the pressure through a resistance (R_V).

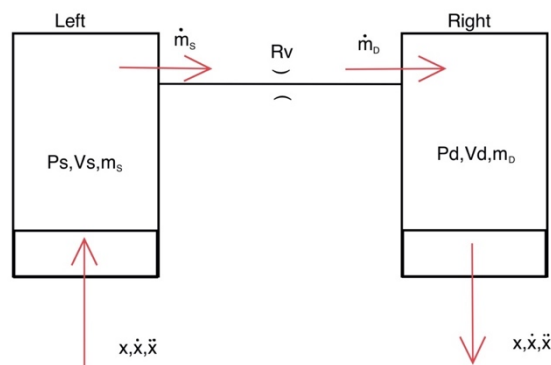


Figure 4.1: Schematization of the system used to evaluate the pressure drop through a resistance

To evaluate the pressure drop (ΔP) on the resistance as a consequence of the variation of the R_V value, are used the following equations:

$$\begin{cases} V_S = V_0 - Ax \\ V_D = V_0 + Ax \end{cases} \quad (4.1)$$

$$\Delta P = P_S - P_D = R_V \dot{m} \quad (4.2)$$

$$m_S = \frac{P_S V_S}{RT_0} \quad (4.3)$$

$$m_D = \frac{P_D V_D}{RT_0} \quad (4.4)$$

Where in Equations (4.1) V_0 is the initial volume of the air inside the piston, A is the area of the piston and x is the movement made by the water inside the U-Tank, which is positive upwards in the left chamber and positive downwards in the right chamber.

The pressure drop in Equation (4.2) is the pressure difference between the two air chambers, which can also be written as the mass flow through the resistance multiplied by the resistance value.

In Equations (4.3) and (4.4) are evaluated the mass of the air inside the air chamber where: P_S and P_D are the pressures inside the right and left chamber, V_S and V_D are the volumes of the right and left air chamber (which change as the value of x increases or decreases), $R = 8,3145 \frac{J}{mol K}$ is the gas constant and $T_0 = 293,15 K$ is the initial air temperature.

By deriving the Equations (4.3) and (4.4) respect to time, we obtain the mass flow with two values that are varying over time (pressure and volume).

$$\begin{aligned} \dot{m}_S &= \frac{1}{RT_0} (\dot{P}_S V_S + P_S \dot{V}_S) = \frac{1}{RT_0} (\dot{P}_S V_0 - P_0 A \dot{x}) \\ \dot{m}_D &= \frac{1}{RT_0} (\dot{P}_D V_D + P_D \dot{V}_D) = \frac{1}{RT_0} (\dot{P}_D V_0 + P_0 A \dot{x}) \end{aligned} \quad (4.5)$$

As shown in Figure (4.1), the flow rate \dot{m}_S comes out of the left chamber and is therefore negative; while the flow \dot{m}_D enters the right chamber and is positive. At this point it's possible to write that:

$$\dot{m}_D = -\dot{m}_S \quad (4.6)$$

Substituting the Equation (4.5) into the Equation (4.6), we obtain:

$$\frac{1}{RT_0} (\dot{P}_D V_0 + P_0 A \dot{x}) = -\frac{1}{RT_0} (\dot{P}_S V_0 - P_0 A \dot{x})$$

$$\dot{P}_D V_0 + P_0 A \dot{x} = -\dot{P}_S V_0 + P_0 A \dot{x}$$

By carrying out the appropriate simplifications, we obtain:

$$\dot{P}_D = -\dot{P}_S \quad (4.7)$$

The pressure increases in the left chamber due to the compression of the air carried out by the positive movement of the water in the U-Tank; while there is a pressure variation in the opposite direction in the right-hand chamber as there is an expansion of the volume of air.

Substituting the Equation (4.7) into the Equation (4.2) derived respect to time we obtain:

$$\Delta \dot{P} = \dot{P}_S - \dot{P}_D$$

$$\Delta \dot{P} = 2\dot{P}_S = -2\dot{P}_D \quad (4.8)$$

While substituting (4.5) in (4.2) we obtain:

$$\frac{\Delta P}{R_V} = \dot{m}_D = \frac{1}{RT_0} (\dot{P}_D V_0 - P_0 A \dot{x}) \quad (4.9)$$

From Equation (4.8) it's possible to write $\dot{P}_D = -\Delta \dot{P} / 2$, at this point it's possible to insert this value in the Equation (4.9) obtaining:

$$\frac{\Delta P}{R_V} = \frac{1}{RT_0} \left(-\frac{\Delta \dot{P}}{2} V_0 + P_0 A \dot{x} \right) = -\left(\frac{V_0}{2RT_0} \right) \Delta \dot{P} + \left(\frac{P_0 A}{RT_0} \right) \dot{x} \quad (4.10)$$

$$\left(\frac{V_0}{2RT_0} \right) \Delta \dot{P} = -\frac{\Delta P}{R_V} + \left(\frac{P_0 A}{RT_0} \right) \dot{x}$$

Assuming small variations of τ , it's possible to write that $x \cong \frac{w}{2} \tau$; the derivative respect to time of x is equal to $\dot{x} = \frac{w}{2} \dot{\tau}$. Substituting the value of \dot{x} in the previous equation, we obtain:

$$\begin{aligned} \left(\frac{V_0}{2RT_0} \right) \Delta \dot{P} &= -\frac{\Delta P}{R_V} + \left(\frac{P_0 A w}{2RT_0} \right) \dot{\tau} \\ \Delta \dot{P} &= -\left(\frac{2RT_0}{R_V V_0} \right) \Delta P + \left(\frac{P_0 A w}{V_0} \right) \dot{\tau} \end{aligned} \quad (4.11)$$

At this point, the pressure variation into the chambers is linked with the kinematics of the U-Tank; therefore, it's now possible to apply the Laplace transform to the Equation (4.11).

$$\begin{aligned} \overline{\Delta P} s &= -\overline{\Delta P} \left(\frac{2RT_0}{R_V V_0} \right) + \bar{\tau} s \left(\frac{P_0 A w}{V_0} \right) \\ \overline{\Delta P} \left[s + \left(\frac{2RT_0}{R_V V_0} \right) \right] &= \bar{\tau} s \left(\frac{P_0 A w}{V_0} \right) \end{aligned} \quad (4.12)$$

$$\begin{cases} G_0 = \left(\frac{P_0 A w}{V_0} \right) \\ H_0 = \left(\frac{2RT_0}{R_V V_0} \right) \end{cases} \quad (4.13)$$

Substituting the Equation (4.13) into the Equation (4.12), we obtain:

$$\frac{\overline{\Delta P}}{\bar{\tau}} = \frac{s G_0}{s + H_0} = \frac{s \frac{G_0}{H_0}}{\frac{s}{H_0} + 1} \quad (4.14)$$

$$\begin{cases} G = \frac{G_0}{H_0} = \frac{P_0 A w R_V}{2RT_0} \\ \alpha = \frac{1}{H_0} = \frac{V_0 R_V}{2RT_0} \end{cases} \quad (4.15)$$

At this point, substituting the Equation (4.15) in (4.14), we obtain the transfer function of the system.

$$\frac{\overline{\Delta P}}{\bar{\tau}} = \frac{sG}{\alpha s + 1} \quad (4.16)$$

Where G is the static gain and α is the time constant.

The Equation (4.16) represents the transfer function combine the input $\bar{\tau}$ (which represents the kinematics of the U-Tank) and the output $\overline{\Delta P}$ (which represents the pressure variation between the two air chambers).

In this transfer function, it's possible to notice that there is a zero at the numerator and a first order at the denominator. Furthermore, everything that is a function of the U-Tank is fixed, while the value of the resistance R_V influences the transfer function. Therefore, it's possible to perform a study of the influence of the resistance value (R_V) on the transfer function.

In a first approximation, have been chosen arbitrary values of R_V equal to 0.1, 0.3, 0.5, 0.6, 0.8, 1, 1.5.

Below there is the trend of the amplitude and phase of the transfer function by varying R_V . It's possible to notice that by increasing the resistance value, the amplitude diagram moves upwards, resulting in a decrease in the cutoff frequency.

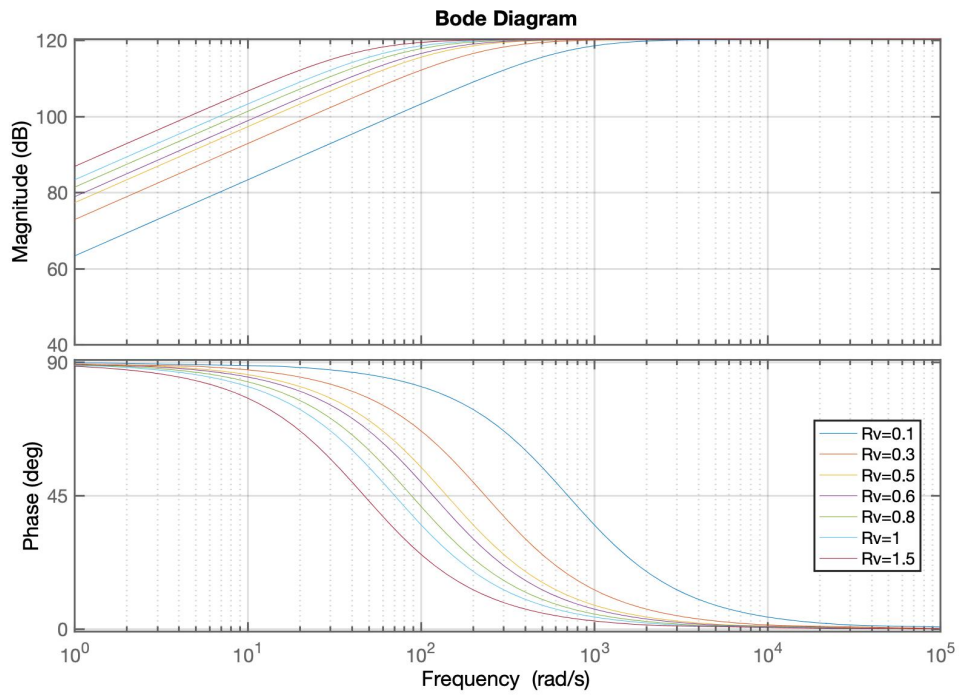


Figure 4.2: Bode Diagram of the pressure drop through a resistance transfer function

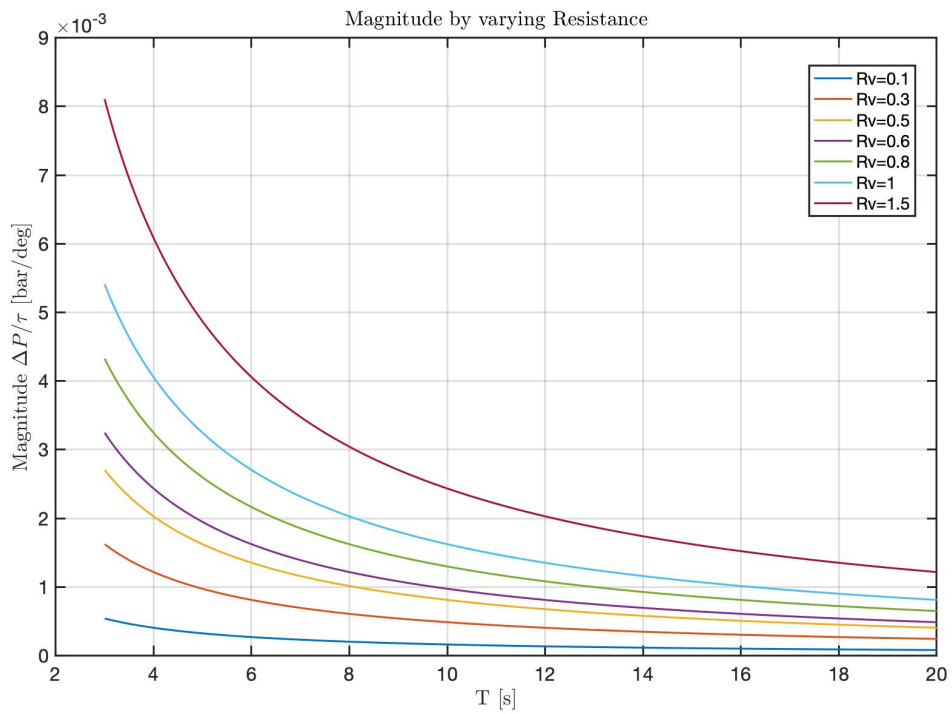


Figure 4.3: Magnitude by varying R_v

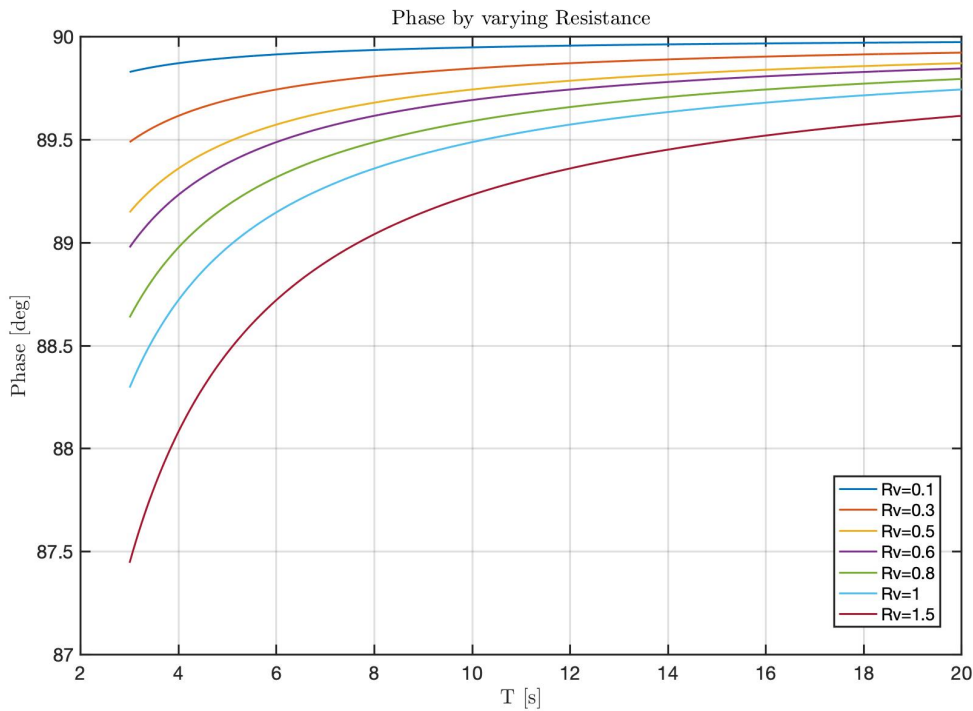


Figure 4.4: Phase by varying R_v

To get the Figure (4.2), we used the following script:

```

for i=1:length(Res.Rv)
    G(i)=((Res.P0*Res.A*Par.W*Res.Rv(i))/(2*Res.R*Res.T0));
    alpha(i)=((Res.V0*Res.Rv(i))/(2*Res.R*Res.T0));

    s = tf('s');
    sys = (G(i)*s)/(alpha(i)*s+1);
    bode(sys);
end

```

While to obtain the Figures (4.3) and (4.4), we used the following script:

```

for i=1:length(Res.Rv)
    G(i)=((Res.P0*Res.A*Par.W*Res.Rv(i))/(2*Res.R*Res.T0));
    alpha(i)=((Res.V0*Res.Rv(i))/(2*Res.R*Res.T0));

    s = tf('s');
    sys = (G(i)*s)/(alpha(i)*s+1);
    [mag,phase]=bode(sys,Wave.frequency);
end

```

In this case was executed only the plot of “*squeeze(mag)*” and “*squeeze(phase)*”, in order to obtain the magnitude value not in dB but in the unit of measurement of our interest.

4.2 Evaluation of the air influence on the whole system

After calculating the pressure drop on the resistance as a function of the kinematics of the U-Tank, it's possible to evaluate the transfer function of the global system (made up by the U-Tank and the resistance), in which is estimated the influence of air on the entire system.

Starting from the following equation that represents the dynamics of the sloshing water inside the U-Tank:

$$a_{\tau\tau}\ddot{\tau} + b_{\tau\tau}\dot{\tau} + c_{\tau\tau}\tau = [a_{\tau5}\ddot{\delta} + c_{\tau5}\delta] \quad (4.17)$$

It's now possible to add the effect of the pressure variation as a function of the kinematics of the U-Tank, to apply the Laplace transform in order to obtain the transfer function of the global system of the coupled U-Tank system and the air passage through the resistance (below).

$$[a_{\tau\tau}s^2 + b_{\tau\tau}s + c_{\tau\tau}]\bar{\tau} = [a_{\tau5}s^2 + c_{\tau5}]\bar{\delta} - \overline{\Delta P}Q_r \quad (4.18)$$

By substituting in the Equation (4.18) the transfer function obtained in the previous paragraph (see Equation (4.16)), we obtain:

$$[a_{\tau\tau}s^2 + b_{\tau\tau}s + c_{\tau\tau}]\bar{\tau} = [a_{\tau5}s^2 + c_{\tau5}]\bar{\delta} - \left(\frac{sG}{\alpha s + 1}Q_r\right)\bar{\tau} \quad (4.19)$$

$$\left[a_{\tau\tau}s^2 + b_{\tau\tau}s + c_{\tau\tau} + \left(\frac{sG}{\alpha s + 1}Q_r\right)\right]\bar{\tau} = [a_{\tau5}s^2 + c_{\tau5}]\bar{\delta}$$

$$\frac{\bar{\tau}}{\bar{\delta}} = \frac{a_{\tau5}s^2 + c_{\tau5}}{a_{\tau\tau}s^2 + b_{\tau\tau}s + c_{\tau\tau} + \left(\frac{sG}{\alpha s + 1}Q_r\right)} \quad (4.20)$$

Where Q_r represents the motion of the fluid like a function of the moment of the area applied to the tank, G is the static gain and α is the time constant (see Equation (4.15)).

In this case the pressure variation provides a furthermore damping effect to the system, which is added to the damping already given in the U-tank system by the term $b_{\tau\tau}$.

Also in this case the value of the resistance R_V influences the transfer function, the magnitude and phase trends of the global system transfer function are shown below.

In a first approximation, have been chosen arbitrary values of R_V equal to 0.1, 0.3, 0.5, 0.6, 0.8, 1, 1.5.

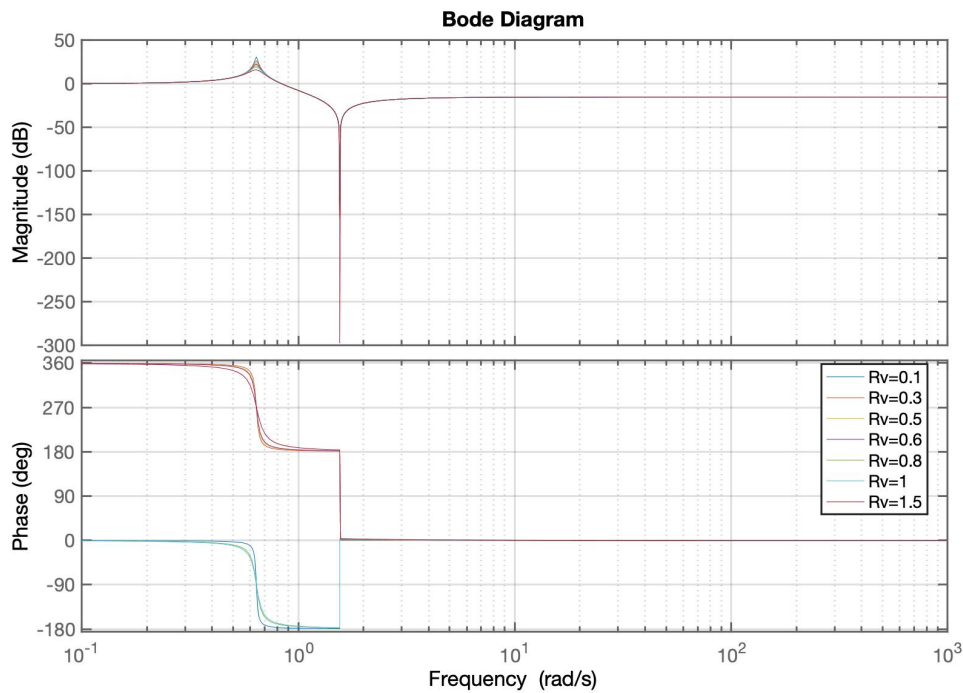


Figure 4.5: Bode Diagram of the global system transfer function

From Figures (4.5) and (4.6) it's possible to see that increasing the resistance value (R_V), there is a decrease of the magnitude value. Therefore, it can be seen that increasing the resistance value increases the damping effect given by the air on the coupled system made up by the U-Tank system and the air passage through the resistance.

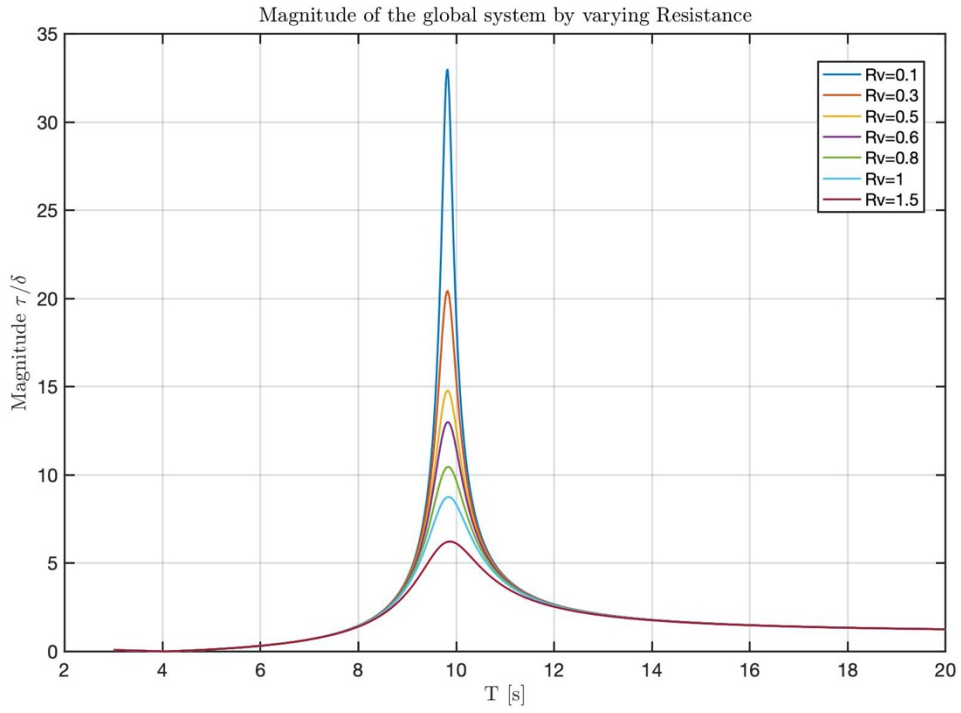


Figure 4.6: Magnitude of the global system by varying R_v

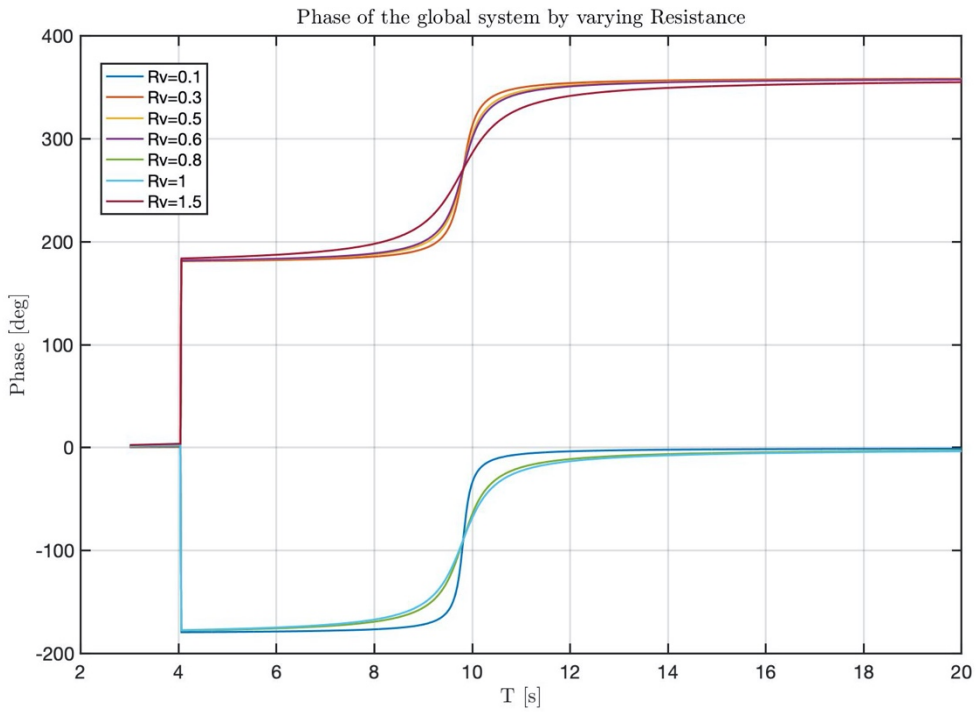


Figure 4.7: Phase of the global system transfer function by varying R_v

The value of the power extracted from the resistance is also calculated according to the following equation:

$$Pot = \Delta p \cdot \dot{m} \quad (4.21)$$

Starting from the Equation (4.16) and substituting $\bar{\tau}$ with the Equation (4.20), we obtain the value of the pressure variation of the global system.

$$\overline{\Delta P} = \frac{sG}{\alpha_S + 1} \frac{a_{\tau 5} s^2 + c_{\tau 5}}{a_{\tau \tau} s^2 + b_{\tau \tau} s + c_{\tau \tau} + \left(\frac{sG}{\alpha_S + 1} Q_r \right)} \bar{\delta} \quad (4.22)$$

From the Equation (4.2) it's possible to write:

$$\frac{\Delta P}{R_V} = \dot{m} \quad (4.23)$$

Replacing the Equations (4.22) and (4.23) into the Equation (4.21), it's possible to write the power extracted from the resistor with the following equation:

$$Pot = \Delta p \cdot \dot{m} = \frac{\left(\frac{sG}{\alpha_S + 1} \frac{a_{\tau 5} s^2 + c_{\tau 5}}{a_{\tau \tau} s^2 + b_{\tau \tau} s + c_{\tau \tau} + \left(\frac{sG}{\alpha_S + 1} Q_r \right)} \delta_0 \right)^2}{R_V} \quad (4.24)$$

Where δ_0 represents the pitch angle in radians.

From the Figure (4.8), it's possible to see that increasing the resistance value, there is a decrease of the power extracted. The maximum value of the extracted power is reached at the resonance frequency.

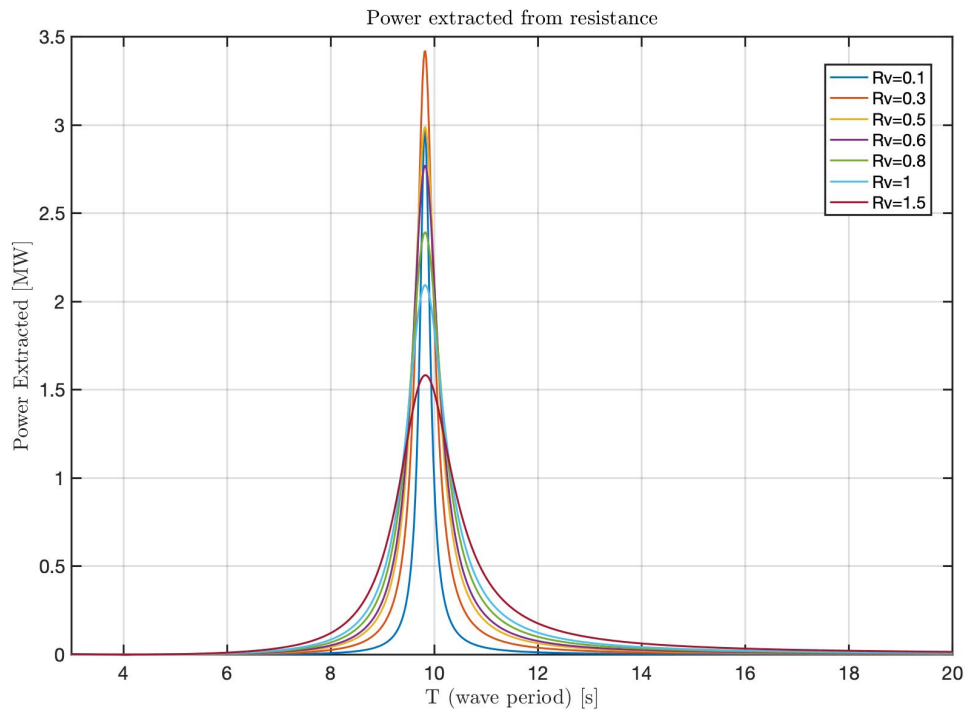


Figure 4.8: Power extracted from resistance

4.3 Analysis using other R_v values

In this paragraph the results obtained by varying the resistance values are analyzed. The following values are attributed to R_v : 0, 0.1, 1, 10, 100, 1000, 10000.

In this section both cases have been analyzed, the first case about the pressure drop on the resistance influenced by the kinematics of the U-Tank, and the second one about the influence of air on the global system.

In the first case analyzed are obtained the results shown in the following figures.

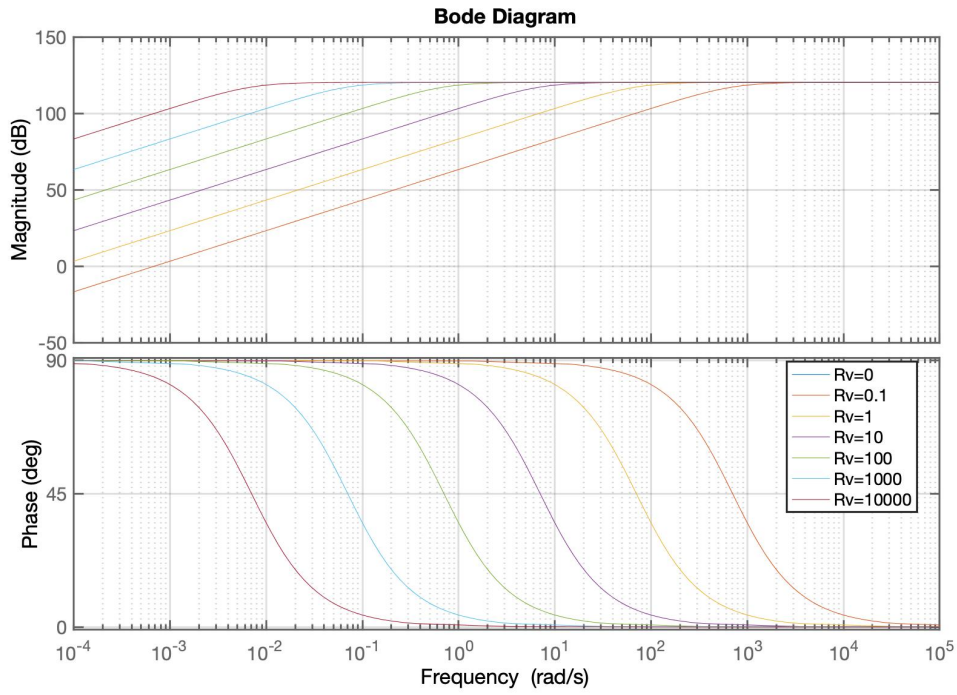


Figure 4.9: Bode Diagram of the pressure drop through a resistance transfer function using new R_V values

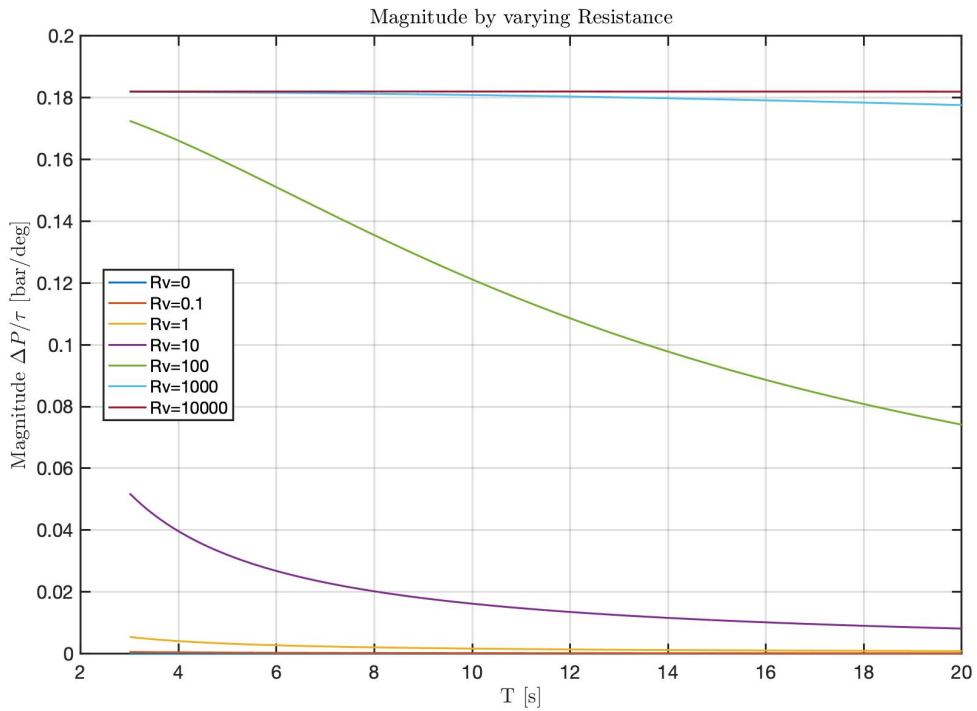


Figure 4.10: Magnitude of the pressure drop through a resistance transfer function using new R_V values

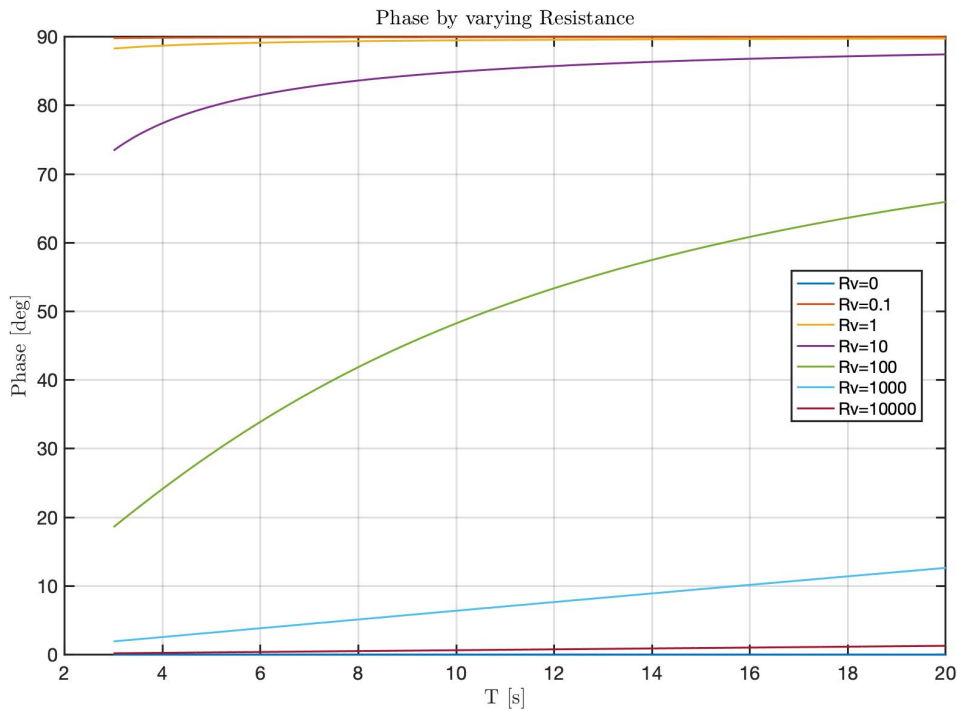


Figure 4.11: Phase of the pressure drop through a resistance transfer function using new R_V values

From Figure (4.11) is possible to notice that when the valve is completely open ($R_V=0$), the phase is equal to 90 [deg] with the position. While, when the valve is closed (for high values of R_V) the phase is equal to 0 [deg] with the position. In this last case (high values of R_V) the air can expand or collapse only in the U-Tank air chamber, so it has the same effect of a spring.

In the second case analyzed are obtained the results shown in the following figures.

Also in this second study the considerations just mentioned regarding R_V resistance and its effects are valid. For high values of R_V , the phase tends to be 0 [deg] with the position, the system behaves like a spring and for the global system (given by the coupling of the U-Tank system and the air passage through the resistance) we note the shift of the resonance peak to higher frequencies.

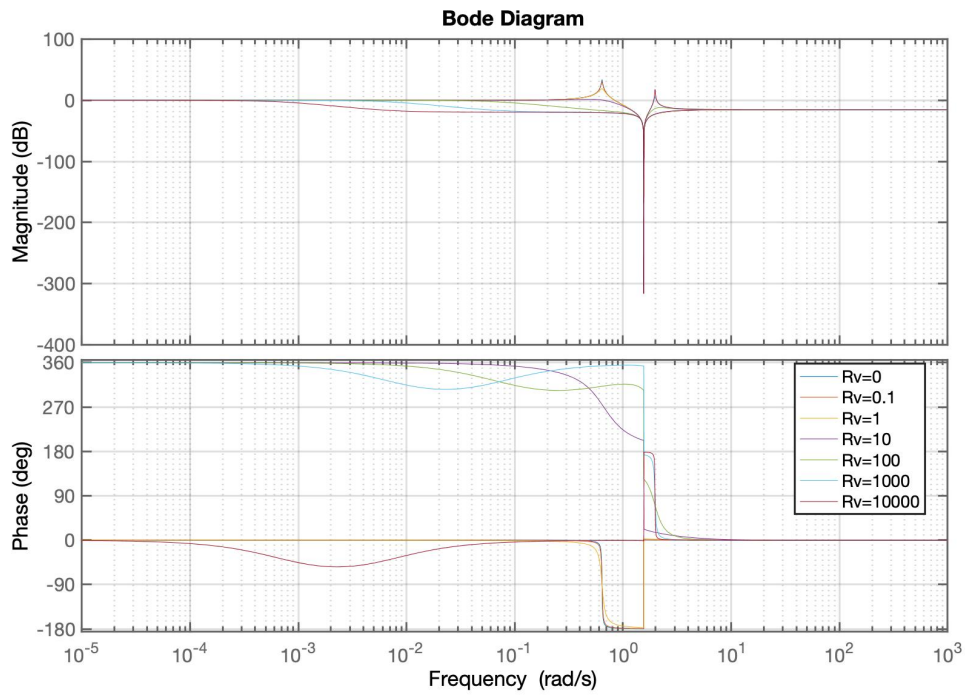


Figure 4.12: Bode Diagram of the global system transfer function using new R_V values

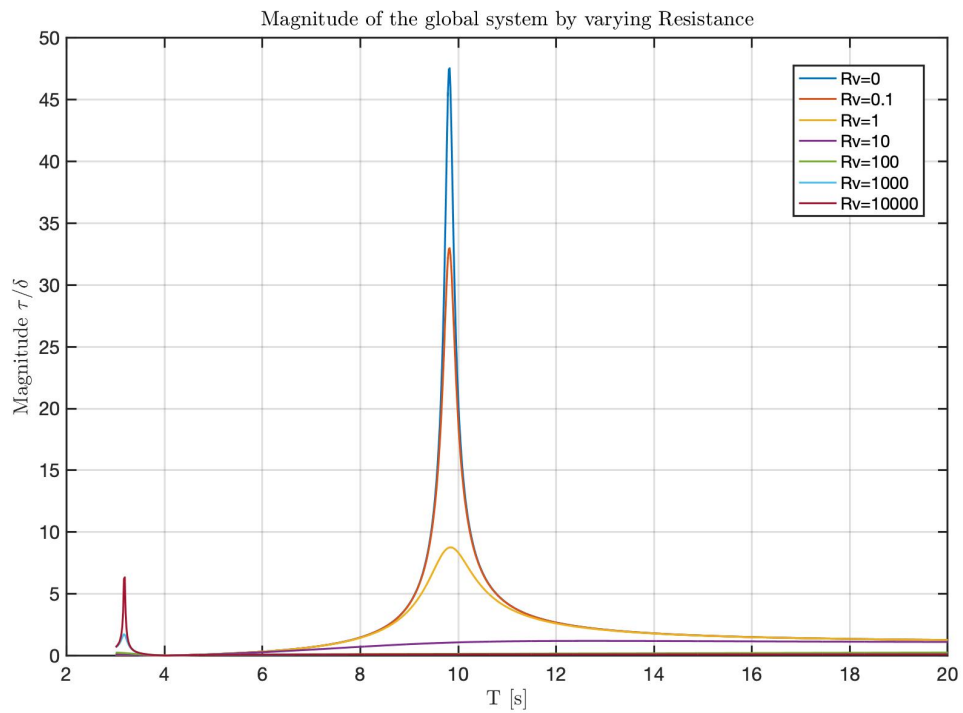


Figure 4.13: : Magnitude of the global system transfer function using new R_V values

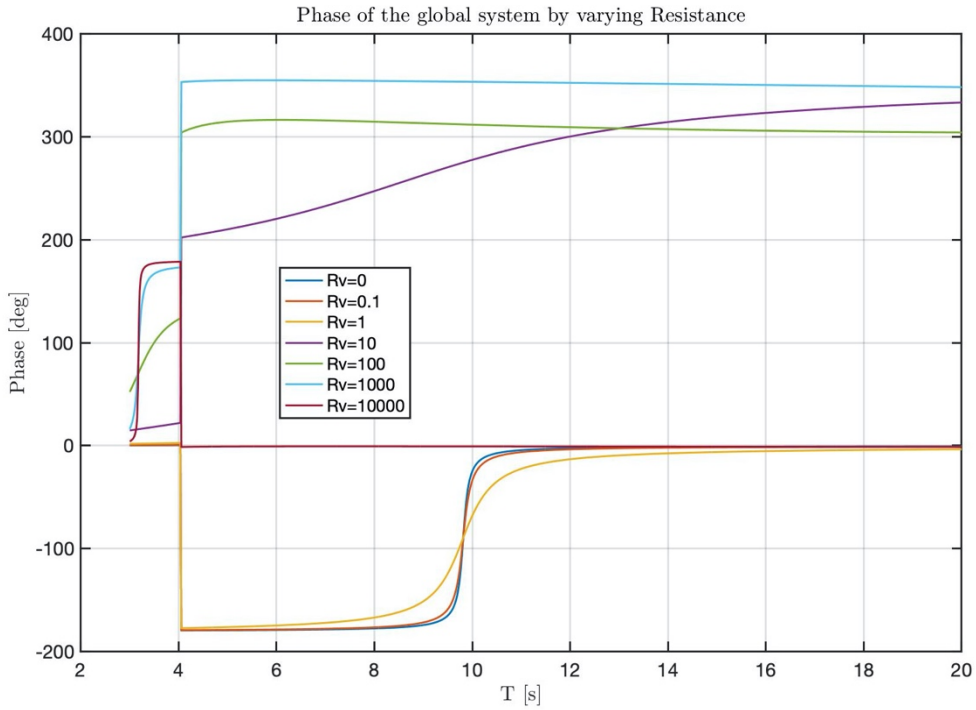


Figure 4.14: : Phase of the global system transfer function using new R_V values

Using the power equation examined in the previous paragraph (see Equation (4.24)), the following graph is obtained for the power extracted through the resistance.

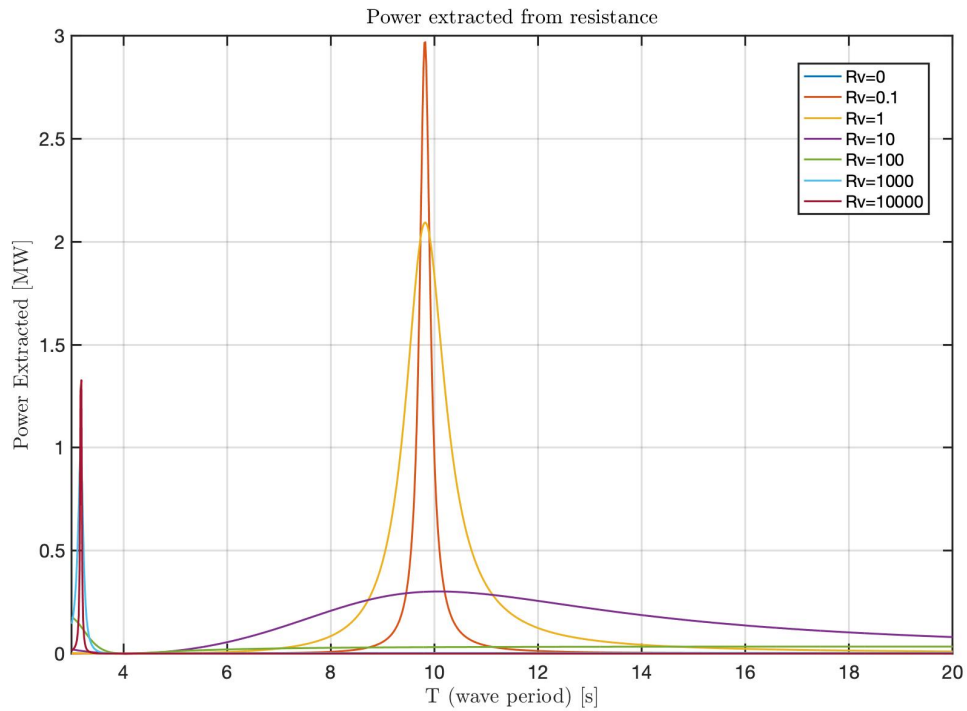


Figure 4.15: Power extracted from resistance using new R_V values

By increasing the value of R_v , it's possible to simulate the case of a closed valve, in this case the air can only compress or expand in its volumes following an isothermal law.

4.4 Initial volume variation

Previously we saw that by simulating a closed valve (with very high resistance values), the air can compress or expand only in its volumes, behaving like a spring. At this point, in addition to the influence of the resistance, the influence of the volume on the resonance frequency is also evaluated. The volume values used in the analysis are equal to $V_0 = [1, 10, 20]V_{0,i}$.

The following figures show the trends of the magnitude, mass flow, power extracted through the resistance and of the pressure variation as the increasing of both the resistance and the initial volume.

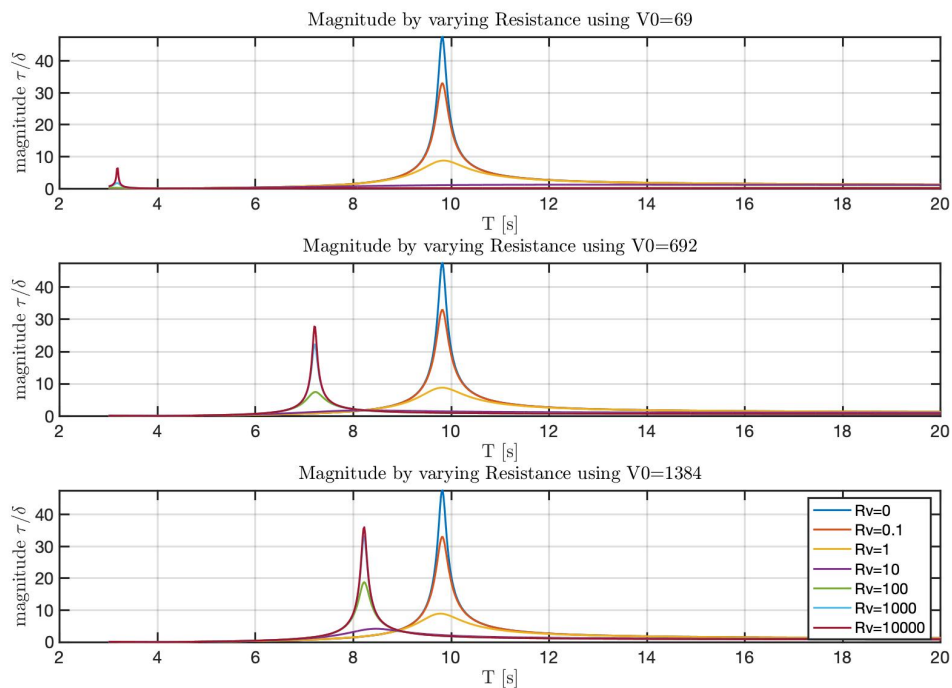


Figure 4.16: Magnitude by varying R_v and V_0

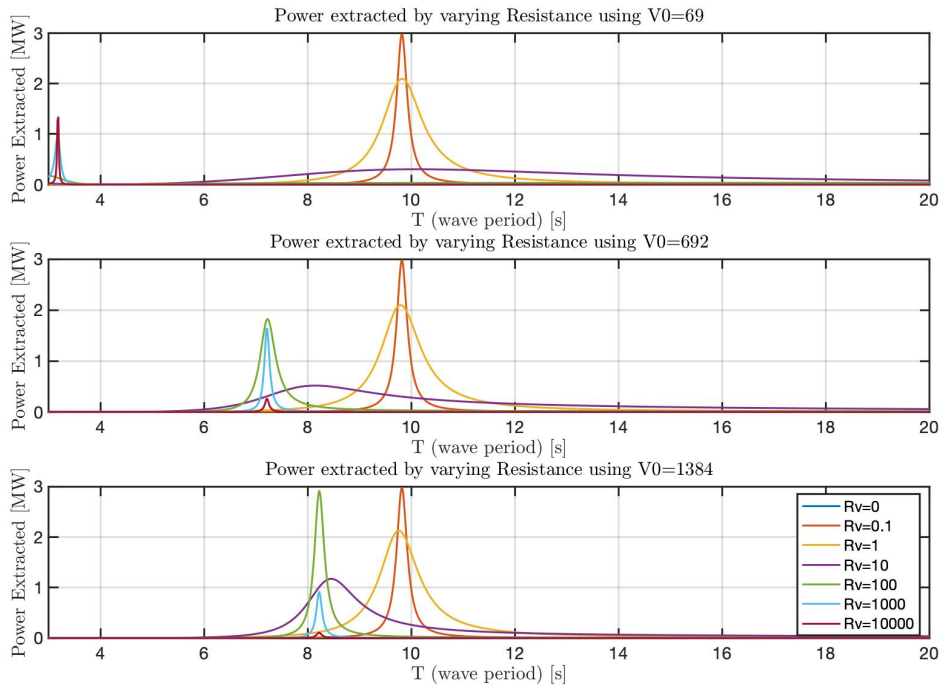


Figure 4.17: Power extracted by varying R_V and V_0

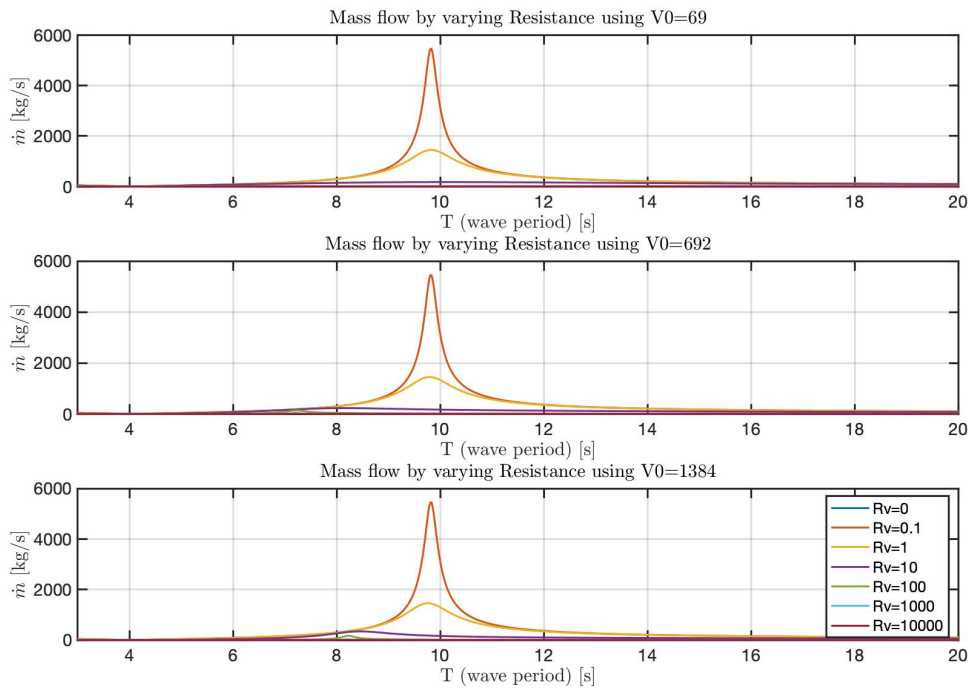


Figure 4.18: Mass flow by varying R_V and V_0

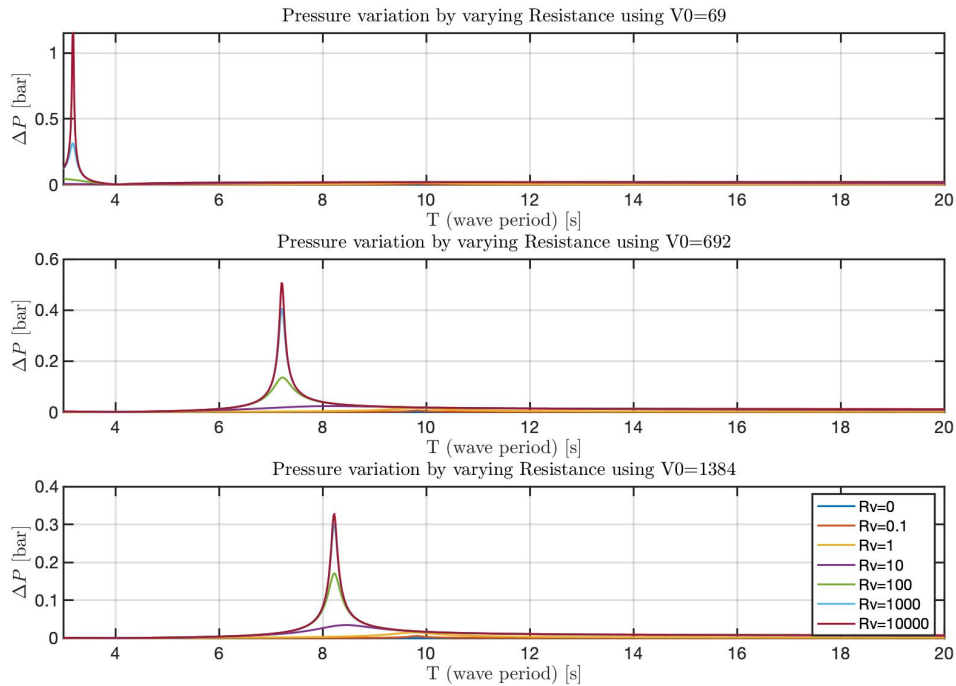


Figure 4.19: Pressure variation by varying R_v and V_0

In this case it's possible to notice that by increasing the resistance value (simulating a closed valve) and increasing the value of the volume of air available, the resonance frequency of the system is shifted.

If the volume of air is very small and the resistance is very high, the stiffness of the system is so high that the resonance frequency is not known because it's at very high frequency.

On the other hand, if we study volumes much larger than the initial value of V_0 with very high values of R_v , we notice the shift in the resonance frequency to a lower frequency.

5. Time Domain

The study performed in the time domain is necessary to evaluate the filling dynamics of the volumes over time.

The system consists of two lateral air chambers of the U-Tank, a tube and a fixed volume where the compressed air (coming out of the U-Tank air chambers) is stored. At the connection point between the fixed volume V_C and the tube, it's assumed the presence of a direction valve, which, depending on the direction of the compressed air flow, supplies the fixed tank to which will be connected a second valve and an extraction turbine.

The system is modelled considering the left and right compression chamber of the U-Tank, the tube (whose losses are schematized with the use of a resistance) and the fixed volume V_C , as shown in the following figure.

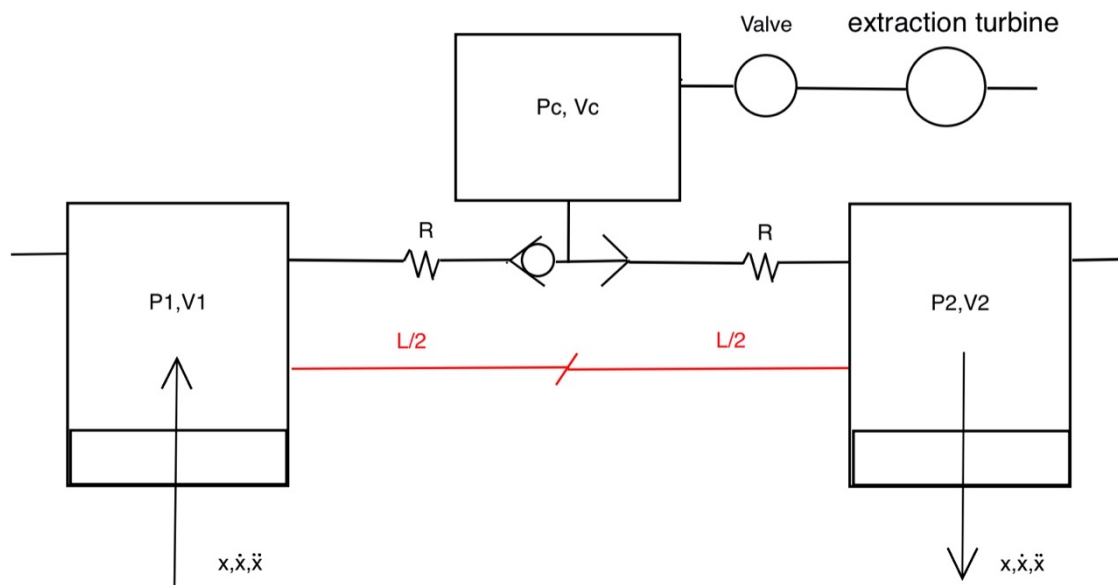


Figure 5.1: Scheme of the analyzed system

On the side of the left and right air chambers of the U-Tank, there are two valves that help the filling process of the chambers at the ambient pressure during the loading phase.

To model the filling dynamics of the U-Tank air chambers and the fixed volume V_C , the following equations are used, which are later modelled also on *Simulink*.

$$\ddot{\tau} = \frac{1}{a_{\tau\tau}} \{ [a_{\tau\delta} \ddot{\delta} + c_{\tau\delta} \dot{\delta}] - Q_r \Delta P - b_{\tau\tau} \dot{\tau} - c_{\tau\tau} \tau \} \quad (5.1)$$

$$x \cong \frac{w}{2} \tau \quad (5.2)$$

$$V_S = V_0 - Ax \quad (5.3)$$

$$V_D = V_0 + Ax \quad (5.4)$$

The Equation (5.1) represents the dynamics of the U-Tank with the influence of the air given by the pressure drop. The single terms of the equation (5.1) are modelled according to Equations from (2.16) to (2.19).

The Equations (5.3) and (5.4) represent the variation of the air volume in the right and left U-Tank chambers. The initial volume V_0 is set equal to 300 [m³] both in the right and left air chamber. This volume variation is a function of the vertical displacement (x) of the water inside the tank. As shown in Equation (5.2), the vertical displacement is function of τ (which is the angle between the water level of the two tanks and it's considered to be small).

In the Figure (5.1), V_1 coincides with the left volume V_S , while V_2 coincides with the right volume V_D . The mass flow out of V_S and V_D is given by the following equation:

$$G = \frac{dM}{dt} = \frac{d(\rho V)}{dt} = \rho \frac{dV}{dt} + V \frac{d\rho}{dt} \quad (5.5)$$

Since the air chambers of the U-Tank are schematized as pneumatic cylinders, it can be written that:

$$\frac{dV}{dt} = A \frac{dx}{dt} \quad (5.6)$$

Then, considering a generic polytropic $pV^n = cost$, it's possible to obtain the density variation as a function of time:

$$\frac{d\rho}{dt} = \frac{\rho_i}{nP_i} \left(\frac{p}{P_i}\right)^{\frac{1-n}{n}} \frac{dp}{dt} \quad (5.7)$$

By substituting the Equations (5.6) and (5.7) into the Equation (5.5), we obtain:

$$G = \rho_i \left(\frac{P}{P_i}\right)^{\frac{1}{n}} A \frac{dx}{dt} + V_s \frac{\rho_i}{nP_i} \left(\frac{P}{P_i}\right)^{\frac{1-n}{n}} \frac{dp}{dt} \quad (5.8)$$

The tube losses are schematized with the use of a resistance, whose value is calculated with the following equation:

$$R = \frac{8\pi\mu L}{S^2} \quad (5.9)$$

Where S is the section of the pipe, L is the length of the pipe and μ is the dynamic viscosity of the air (evaluated at a temperature of 20°C).

S	0.0117	[m ²]
L	4.6	[m]
μ	1.81*10 ⁻⁵	[Pa s]
R	15.829	[Pa s/m]

Table 5-1: Values quantities used for the calculation of resistance R

The resistance given by the valve placed on the intake of the two air chambers of the U-Tank is set equal to 10R.

While the inlet mass flow into the fixed volume V_C is given by:

$$G = V \frac{d\rho}{dt} = V_C \frac{\rho_i}{nP_i} \left(\frac{P}{P_i}\right)^{\frac{1-n}{n}} \frac{dp}{dt} \quad (5.10)$$

At this point, the equations, previously evaluated, have been reconstructed on *Simulink* through the use of a block diagram. The block diagram consists of:

- Dynamics of the U-Tank;
- Volume variation of the left air chamber;

- Volume variation of the right air chamber;
- Dynamic filling of the central fixed volume V_C .

It's possible to obtain the filling dynamics of the chambers over the time by attributing the value of amplitude and frequency to the function δ (pitch angle of the hull).

$$\delta = X \sin(\omega t) \quad (5.11)$$

$$\dot{\delta} = X \omega \cos(\omega t) \quad (5.12)$$

$$\ddot{\delta} = -X \omega^2 \sin(\omega t) \quad (5.13)$$

Where X is the amplitude and $\omega = \frac{2\pi}{T}$ is the frequency. Several simulations were performed for different amplitudes and periods; the values chosen for the amplitude (X) are equal to 5 [deg], 10 [deg] and 20 [deg]; while the period (T) is set equal to 7 [s], the resonance period (9.8236 [s]) and 11 [s].

The following paragraphs show the schemes of the block diagrams created for the verification in the time domain.

5.1 Block Diagrams

5.1.1 Dynamics of the U-Tank

In the following figure is represented the U-Tank dynamics block. The inputs to this block are δ , $\dot{\delta}$, P_{SX} and P_{DX} ; while the outputs are x and \dot{x} .

The value of δ and $\dot{\delta}$ is equal to the Equations (5.11) and (5.13) to which is applied a ramp signal. The value of the pitch angle is assigned to the *Simulink* block through a *From Workspace*, whose structure is given by:

```
VAR_delta = [par.time Par.DELTA];  
VAR_deltad = [par.time Par.DELTA_DOT];  
VAR_deltadd = [par.time Par.DELTA_DDOT];
```

The *par.time* vector is equal to a vector with step 0.1 which contains the time values from 0 to 500 [s]. While *Par.DELTA* and *Par.DELTA_DDOT* contain the ramp signal of δ and

δ from 0 to 200 [s], then the current δ and $\ddot{\delta}$ value calculated with the Equations (5.11) and (5.13). The third and fourth block inputs represent the pressures feedback in the U-Tank air chambers calculated subsequently, which influence the damping of the system.

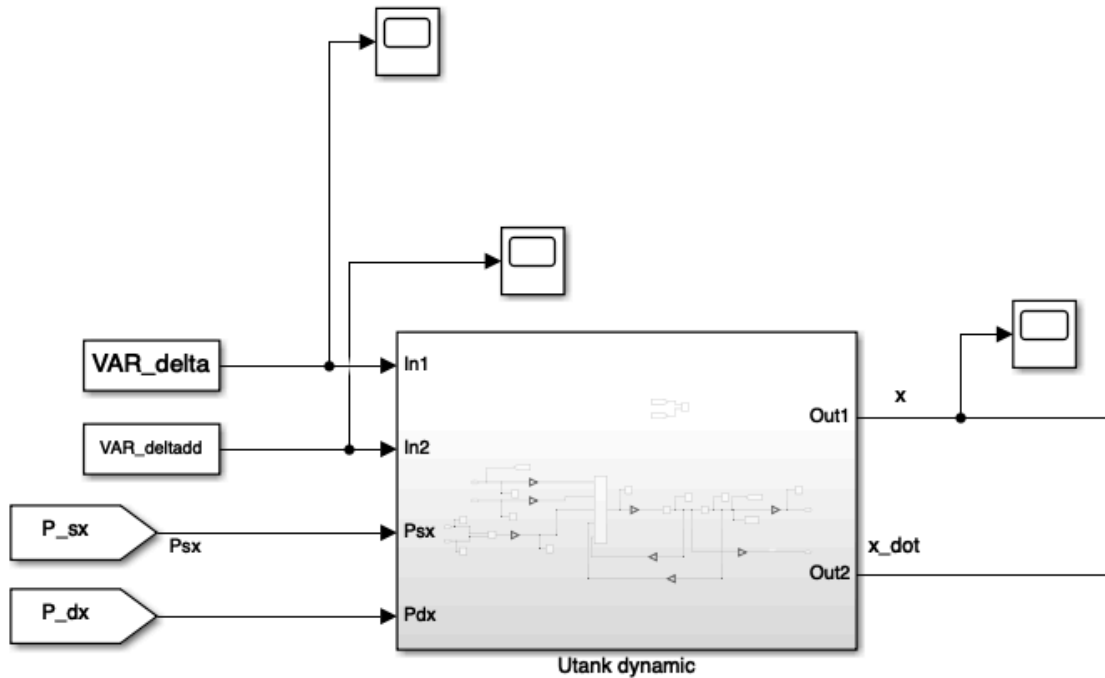


Figure 5.2: U-Tank dynamics block

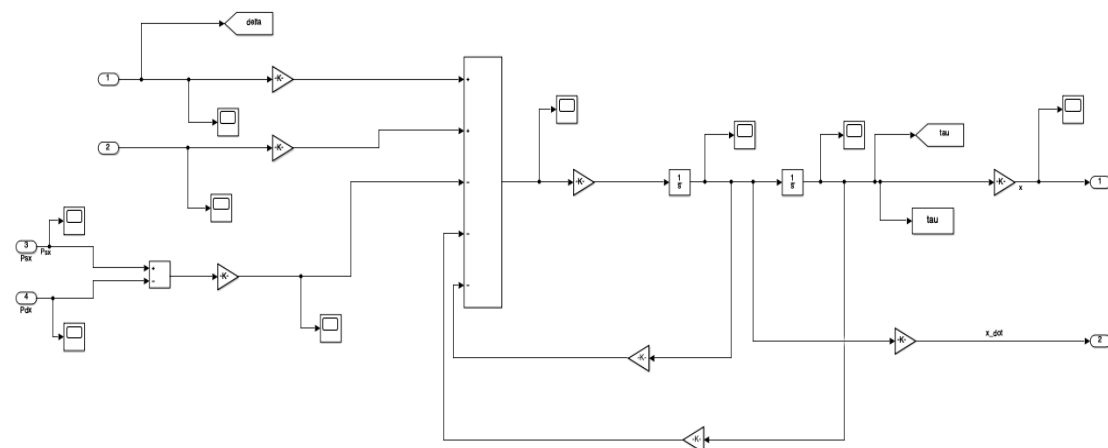


Figure 5.3: Detail of the dynamics U-Tank block diagram

then it's feedback on the block in Figure (5.4)). The output of the block is the pressure inside the air chamber.

In Figure (5.5) is represented the block diagram of the Equation (5.8). To calculate the volume of the left chamber V_s , is used the Equation (5.3), where V_0 is set equal to 300 [m³], A is the area of the air chamber and is equal to 57,918 m².

The detail of the C_1 block diagram is represented in the following figure.

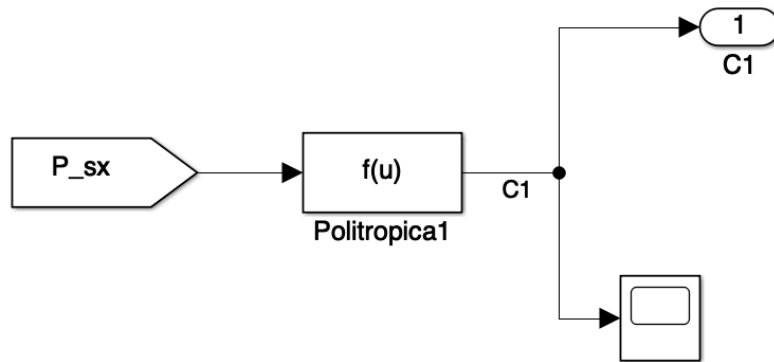


Figure 5.6: Detail of the C1 block diagram left air chamber

Where:

$$f(u) = \rho_0 \left(\frac{P_{sx}}{P_0} \right)^{\frac{1}{n}} \tag{5.14}$$

The polytropic coefficient is set equal to 1.2.

The detail of the C_2 block diagram is represented in the following figure.

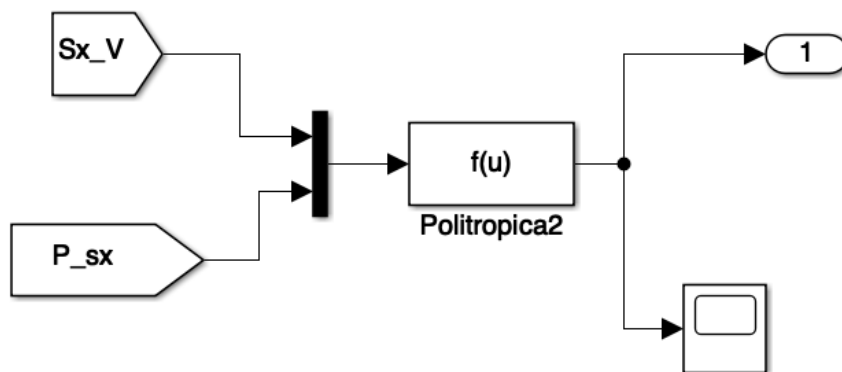


Figure 5.7: Detail of the C2 block diagram left air chamber

5.1.4 Control on the charge and discharge process of the air chamber

At the exit of the volume variation block of the right and left air chamber of the U-Tank there is a control on the charge and discharge process. The equations and the block diagrams used are shown below.

- V_C load from the left chamber

$$P_{SX} > P_C, \dot{x} > 0 \tag{5.16}$$

- Left chamber discharge/intake

$$P_{SX} < P_C, \dot{x} < 0 \tag{6.17}$$

- Left volume pressurization

$$P_{SX} \sim P_C, \dot{x} > 0 \tag{5.18}$$

- V_C load from the right chamber

$$P_{DX} > P_C, \dot{x} < 0 \tag{5.19}$$

- Right chamber discharge/intake

$$P_{DX} < P_C, \dot{x} > 0 \tag{5.20}$$

- Right volume pressurization

$$P_{DX} \sim P_C, \dot{x} < 0 \tag{5.21}$$

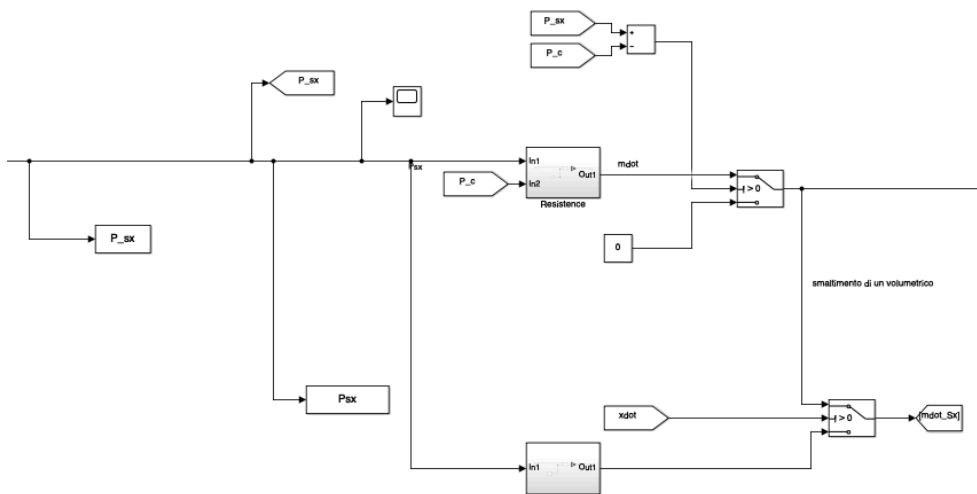


Figure 5.10: Control on the charge and discharge process on the left air chamber

From the block diagram it's possible to see that, on the first line, the pressure difference between the left chamber and the V_C passes over the duct resistance R and returns the mass flow \dot{m}_S ; while, on the second line, the pressure difference between the left chamber and the ambient pressure passes over the discharge/intake resistance (equal to $10R$) and returns another mass flow. The switch on the first line represents the Equations (5.16) and (5.18); while the switch on the second line represents the Equations (5.16) and (5.17).

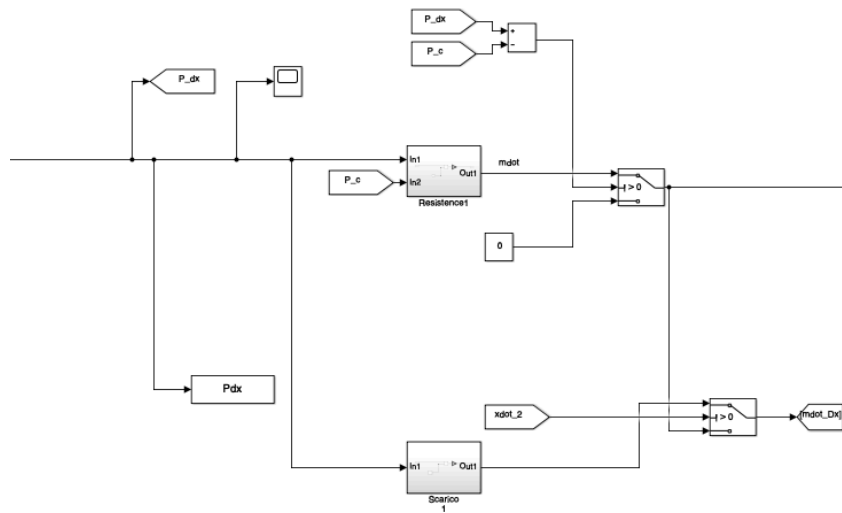


Figure 5.11: Control on the charge and discharge process on the right air chamber

The control on the charge and discharge process on the right air chamber it's the same as described for the left air chamber.

After this control on the right and left air chamber, it's inserted another switch control on the mass flow as a velocity function (\dot{x}).

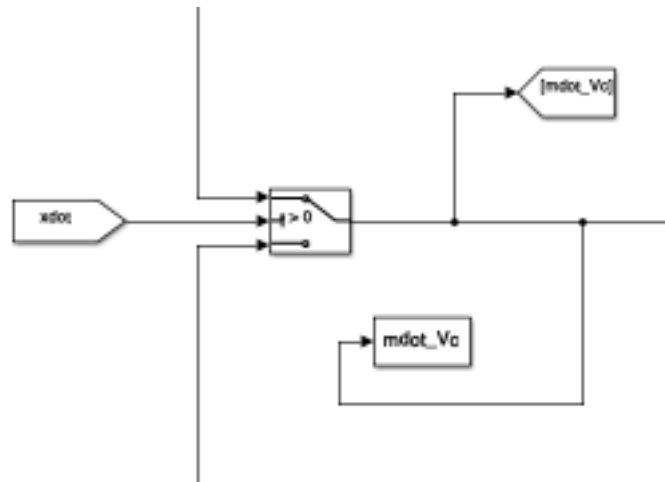


Figure 5.12: Switch control on the mass flow to the fixed volume as a velocity function

If $\dot{x} > 0$ the mass flow extracted from the left air chamber is sent to the fixed volume V_C ; in this case, the water inside the U-Tank acts as a piston and compresses the air in the left chamber, while air is inserted from the outside into the right chamber.

On the contrary, if $\dot{x} < 0$ the mass flow extracted from the right air chamber is sent to the fixed volume V_C ; in this case, the water inside the U-Tank acts as a piston and compresses the air in the right chamber, while air is inserted from the outside into the left chamber.

At this point, the mass flow, which is sent either from the left chamber or from the right chamber, becomes the input of the fixed volume block V_C .

5.1.5 Fixed volume V_C block diagram

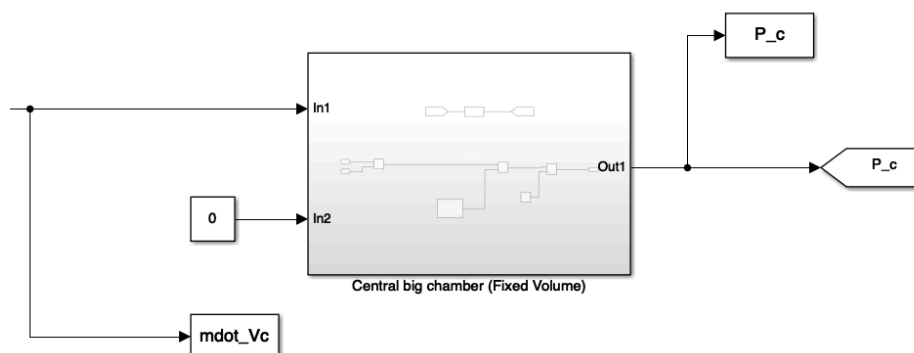


Figure 5.13: Dynamic filling block of the central fixed volume V_C

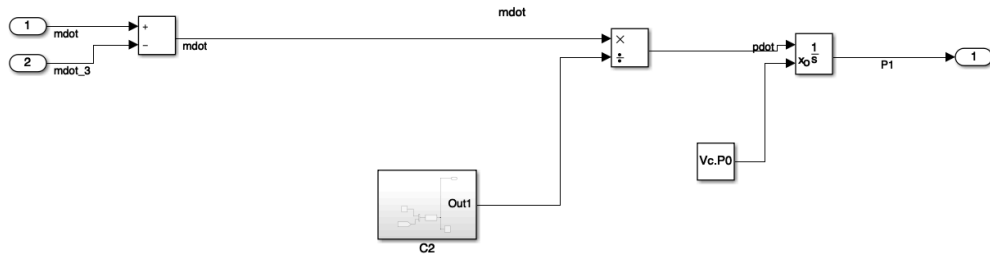


Figure 5.14: Detail of the dynamic filling block of the central fixed volume VC

In Figure (5.13) is represented the block of the central fixed volume V_C . The inputs to this block are the mass flow sent either from the left or right air chamber and the mass flow sucked by the extraction turbine located after the central fixed volume (as shown in the Figure (5.1)). In this first part of simulation, the mass flow sucked by the extraction turbine is set equal to 0 kg/s. The output of the block is the pressure inside the fixed volume.

In Figure (5.14) is represented the detail of this block, which represent the Equation (5.10). The initial volume of the chamber is set to 300 [m³]. In the following figure is represented the detail of the C_2 block diagram.

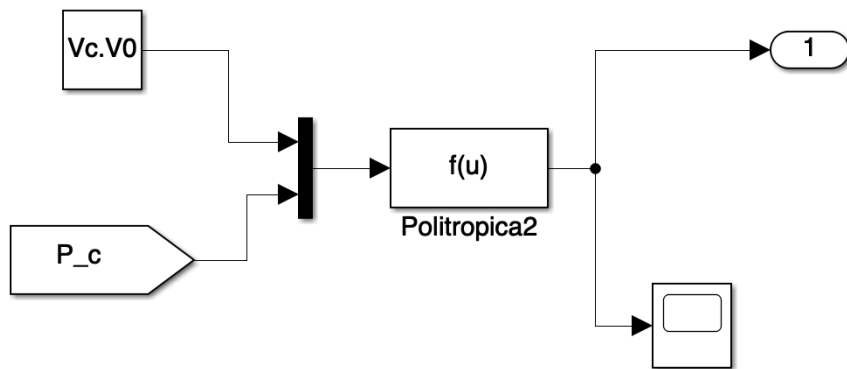


Figure 5.15: Detail of the C_2 block diagram into the central fixed volume VC block

Where:

$$f(u) = \frac{V_C \rho_0}{n P_0} \left(\frac{P_C}{P_0} \right)^{\frac{1-n}{n}} \quad (5.22)$$

5.2 Analysis using different amplitude and period values

After creating the block diagram of the system represented in Figure (5.1), several tests are carried out by varying the amplitude and period of the Equations from (5.11) to (5.13), which represent the δ pitch angle.

5.2.1 Amplitude 5 [deg]

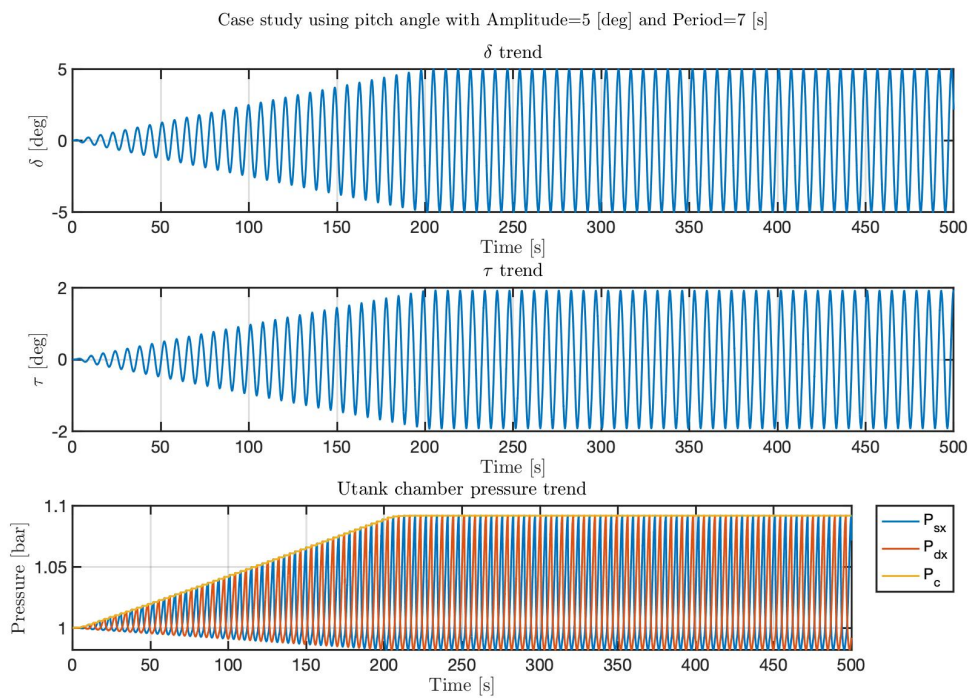


Figure 5.16: δ, τ and pressures trends using $A=5$ [deg] e $T=7$ [s]

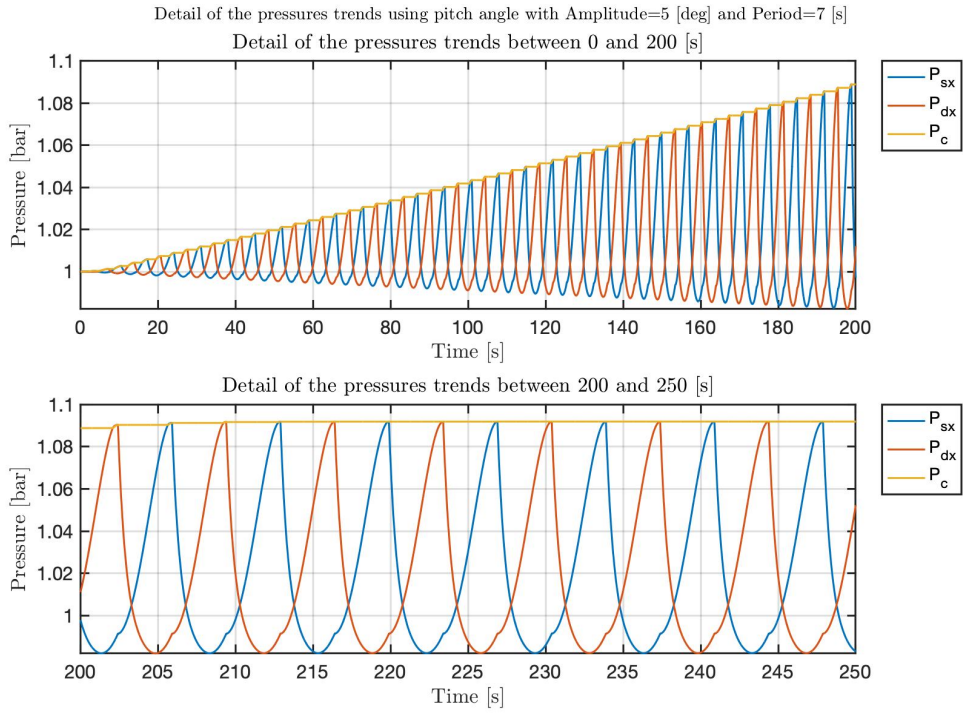


Figure 5.17: Detail of the pressure's trends using pitch angle with Amplitude=5 [deg] and Period=7 [s]

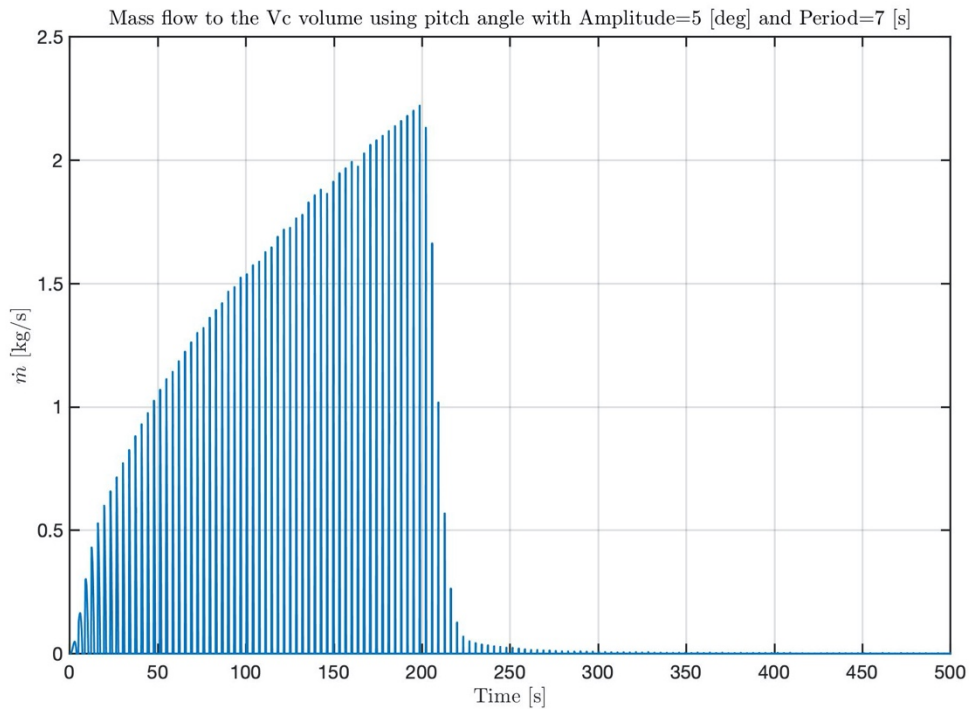


Figure 5.18: Trends of the inlet mass flow to the fixed volume Vc using A=5 [deg] and T=7 [s]

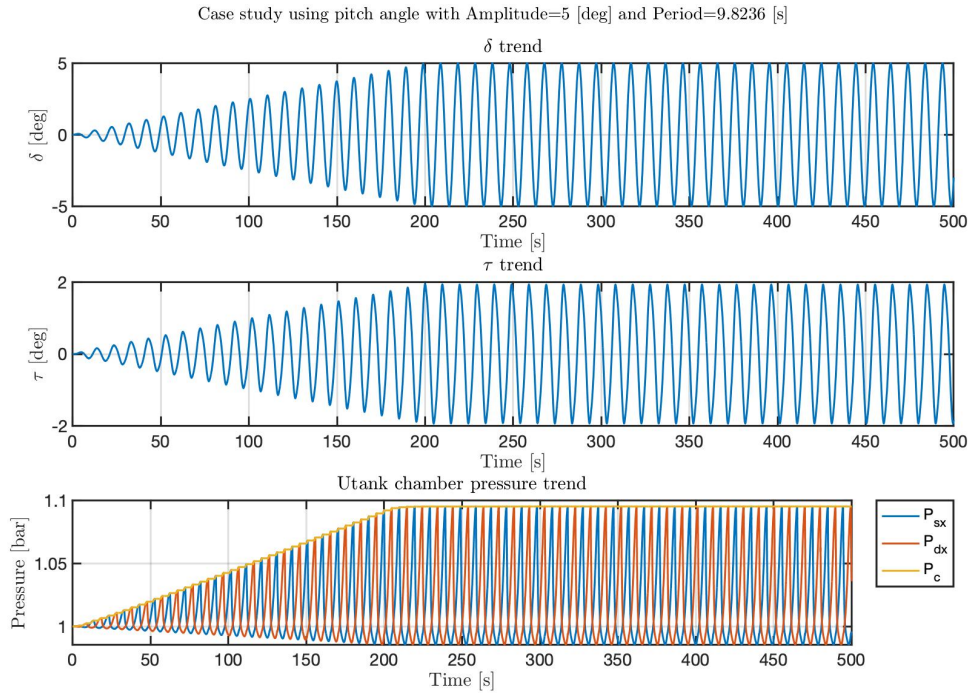


Figure 5.19: δ, τ and pressures trends using $A=5$ [deg] e T of resonance

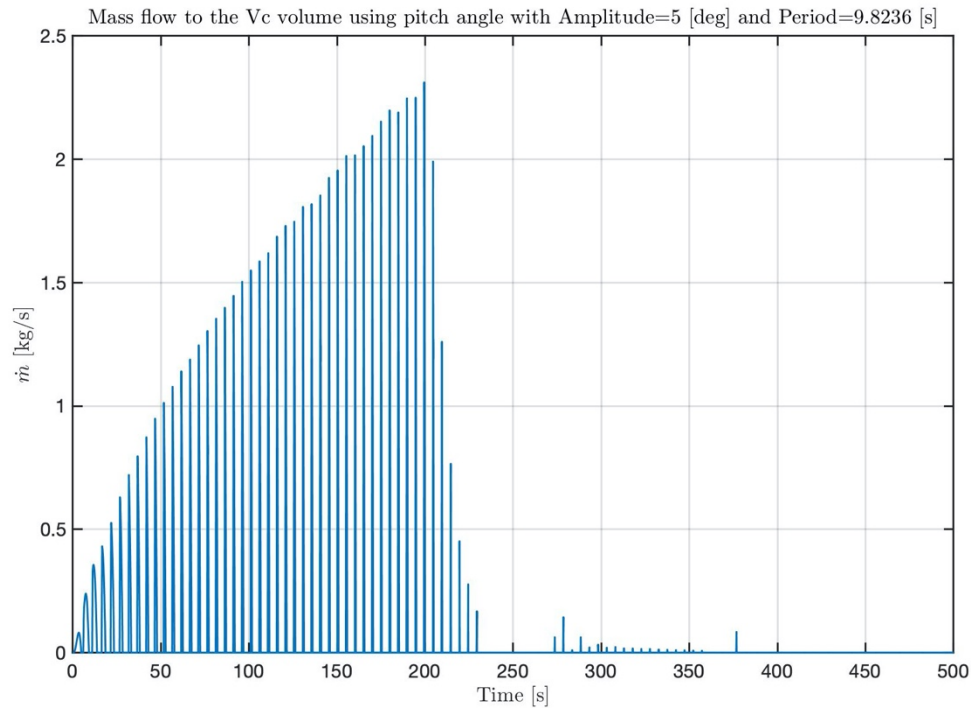


Figure 5.20: Trends of the inlet mass flow to the fixed volume Vc using $A=5$ [deg] and T of resonance

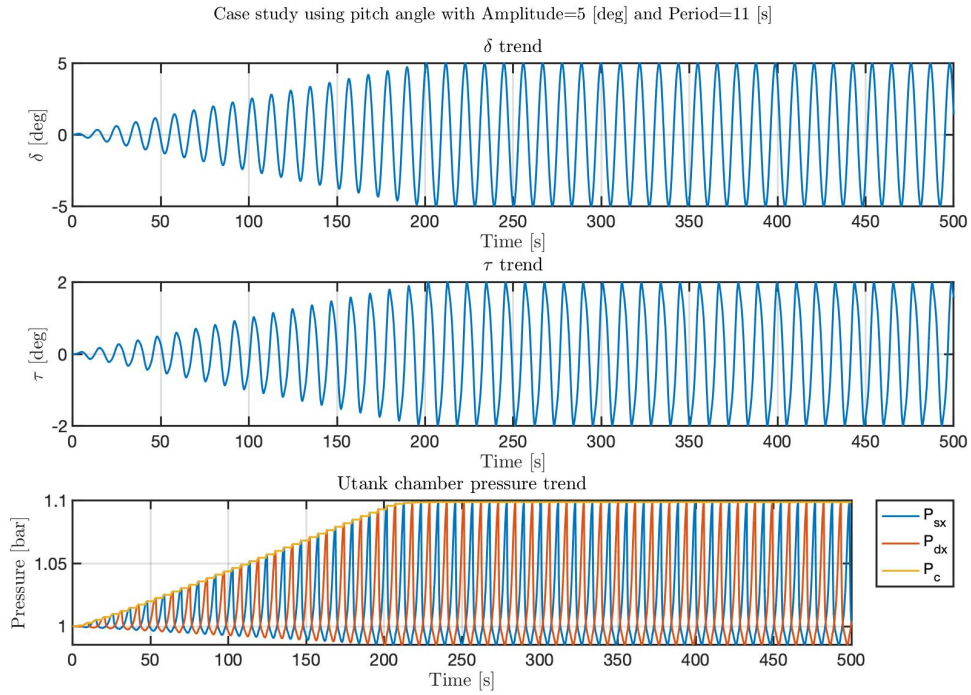


Figure 5.21: : δ, τ and pressures trends using $A=5$ [deg] e $T=11$ [s]

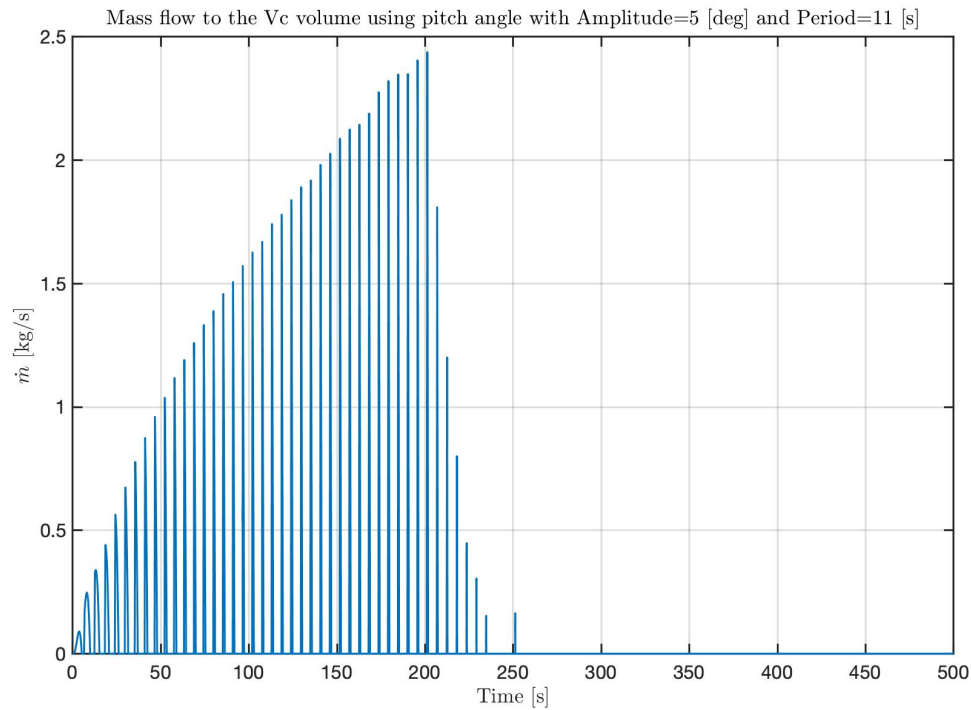


Figure 5.22: Trends of the inlet mass flow to the fixed volume Vc using $A=5$ [deg] and $T=11$ [s]

From the previous Figures it is possible to note that by keeping the amplitude (X) constant and varying the period (T), there is a slight delay of τ with respect to the sinusoidal trend of δ (pitch angle of the hull). This delay in the U-Tank kinematics is due to the influence of the pressure variation in the air chambers.

It's also possible to note that increasing the value of the period (T), increases the value of the maximum pressure reached in the volume V_C without extracting mass flow from the external turbine.

From the Figures (5.18), (5.20) and (5.22), which report the trend of the mass flow, it's possible to notice an increase in the maximum mass flow sent as the period (T) increases.

5.2.2 Amplitude 10 [deg]

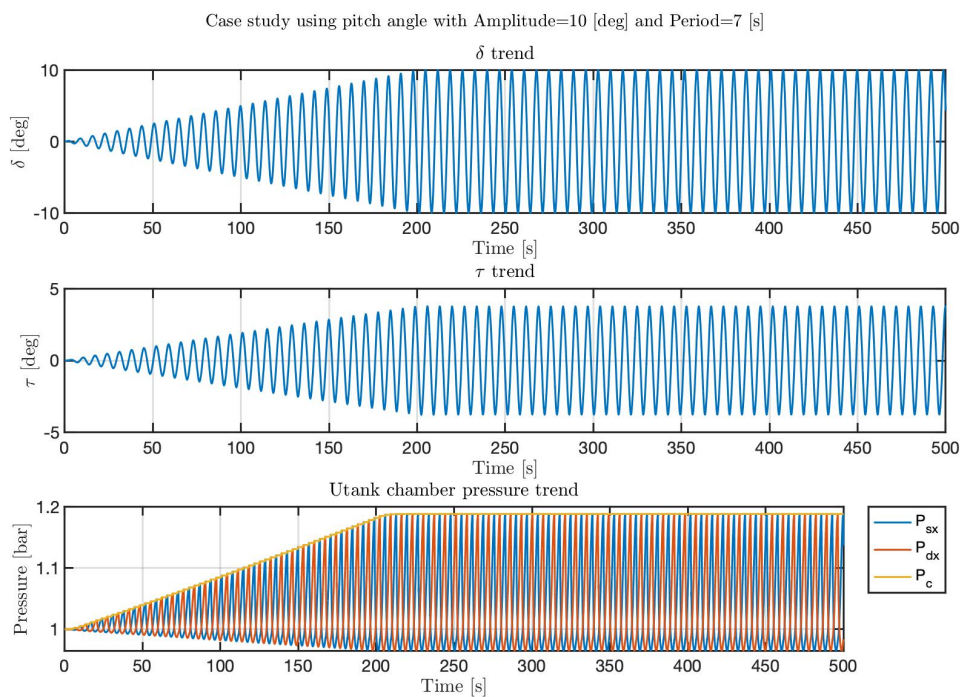


Figure 5.23: δ, τ and pressures trends using $A=10$ [deg] e $T=7$ [s]

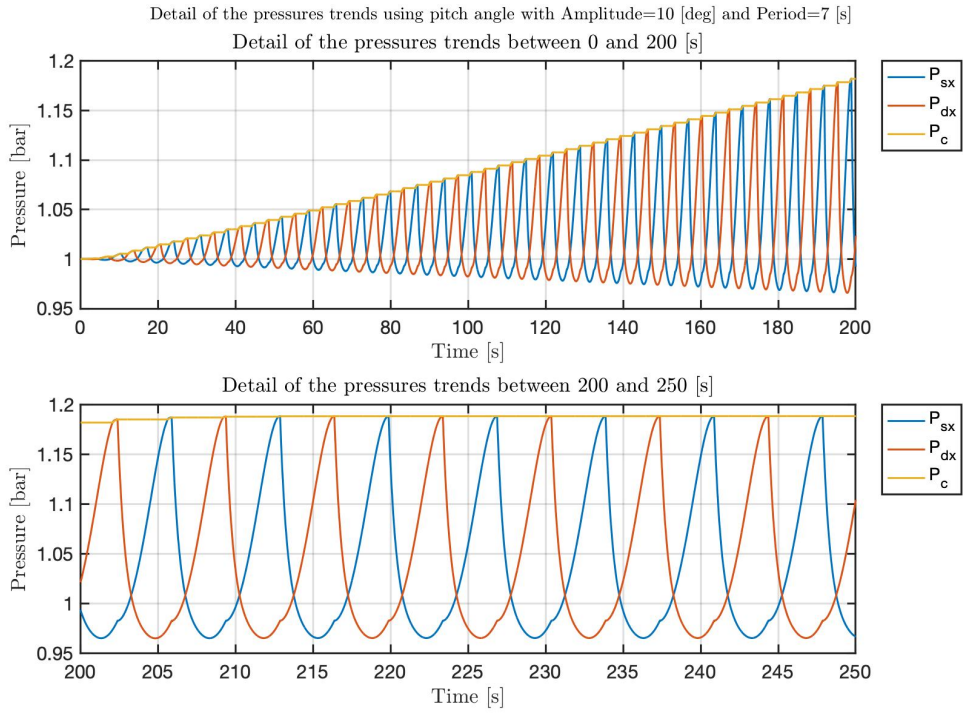


Figure 5.24: Detail of the pressure's trends using pitch angle with Amplitude=10 [deg] and Period=7 [s]

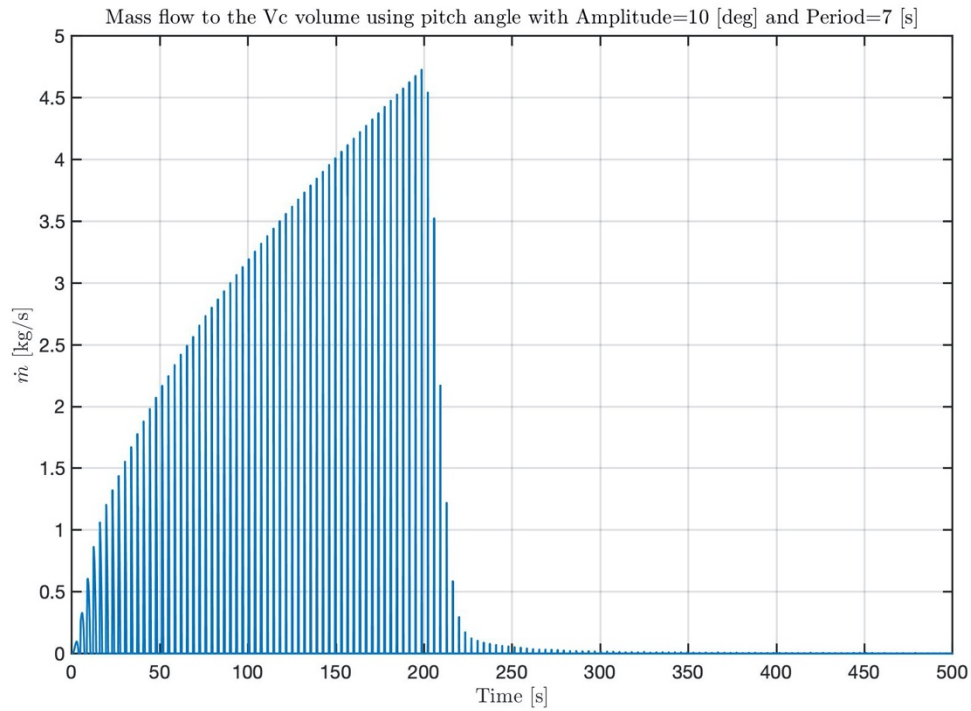


Figure 5.25: Trends of the inlet mass flow to the fixed volume Vc using A=10 [deg] and T=7 [s]

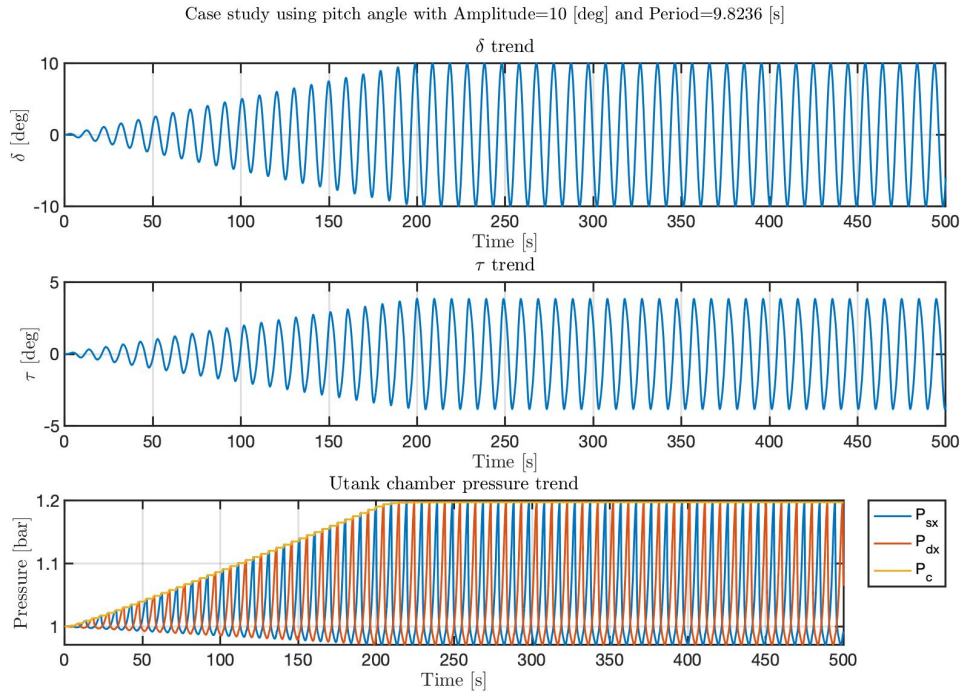


Figure 5.26: δ, τ and pressures trends using $A=10$ [deg] e T of resonance

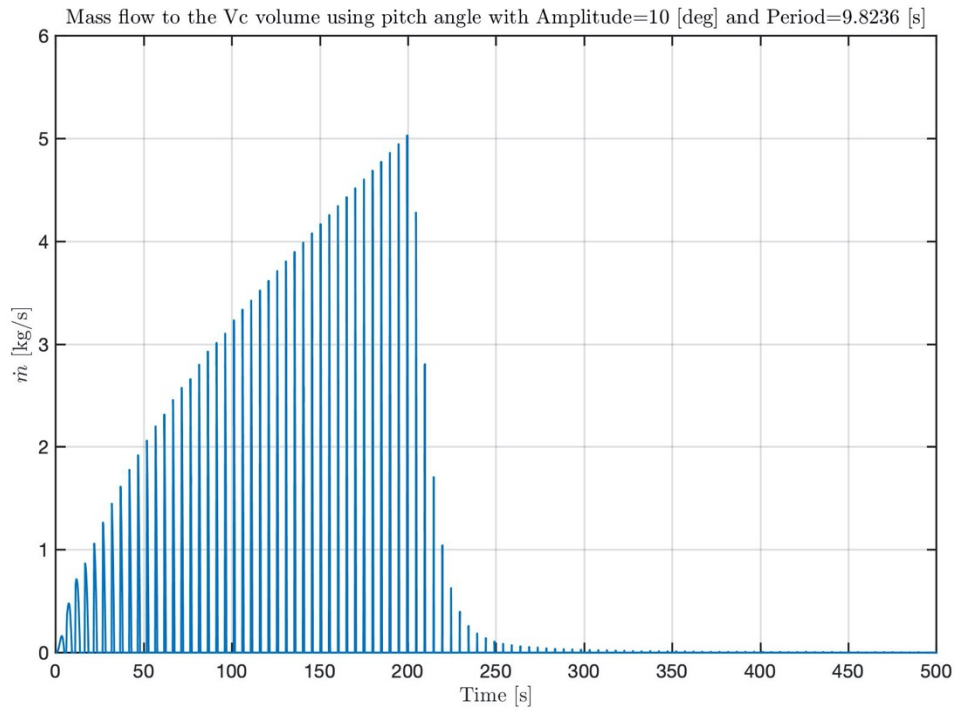


Figure 5.27: Trends of the inlet mass flow to the fixed volume Vc using $A=10$ [deg] and T of resonance

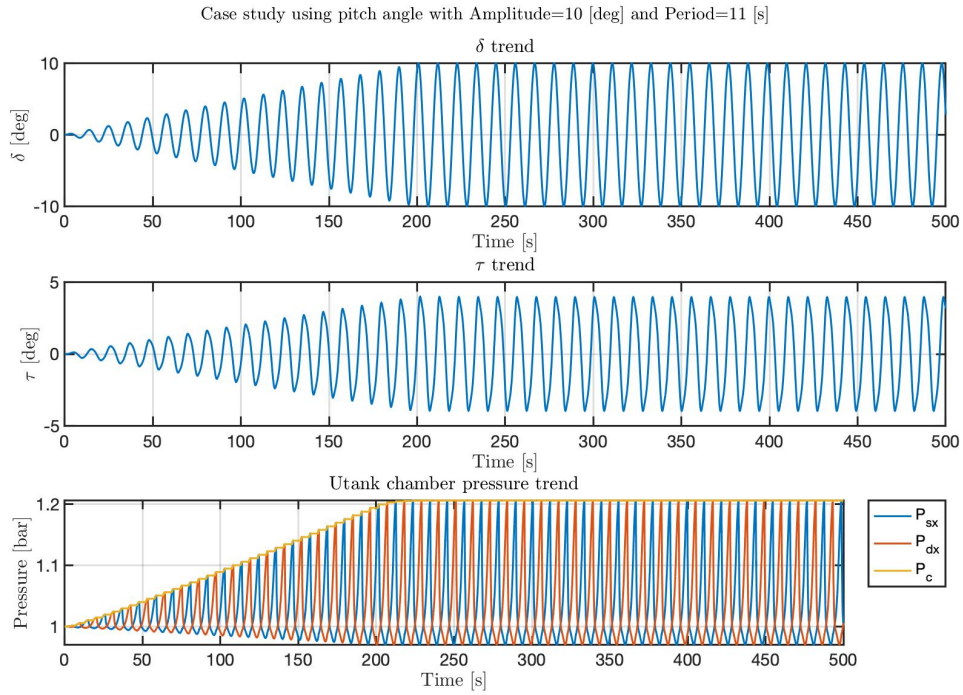


Figure 5.28: δ, τ and pressures trends using $A=10$ [deg] e $T=11$ [s]

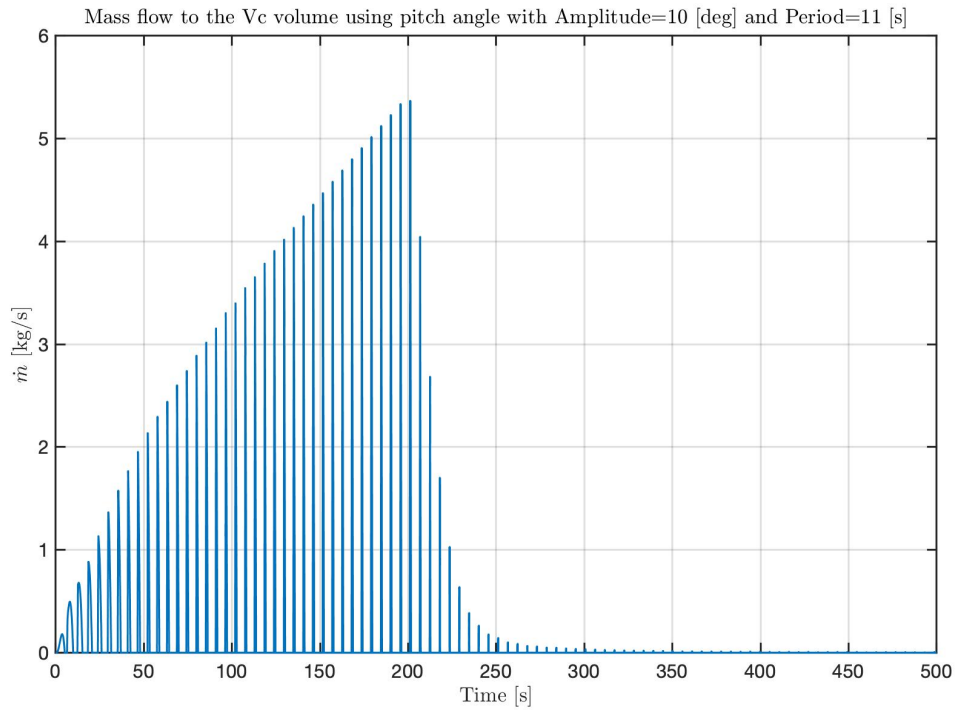


Figure 5.29: Trends of the inlet mass flow to the fixed volume Vc using $A=10$ [deg] and $T=11$ [s]

In the previous Figures it is possible to note that, as in the previous paragraph (5.2.1), by keeping the amplitude (X) constant and varying the period (T), there is a slight delay of τ with respect to the sinusoidal trend of δ (pitch angle of the hull). This delay in the U-Tank kinematics is due to the influence of the pressure variation in the air chambers.

It's also possible to note that increasing the value of the period (T), increases the value of the maximum pressure reached in the volume V_C without extracting mass flow from the external turbine.

From the Figures (5.25), (5.27) and (5.29), which report the trend of the mass flow, it's possible to notice that as the period (T) increases, there is an increase in the maximum mass flow sent.

5.2.3 Amplitude 20 [deg]

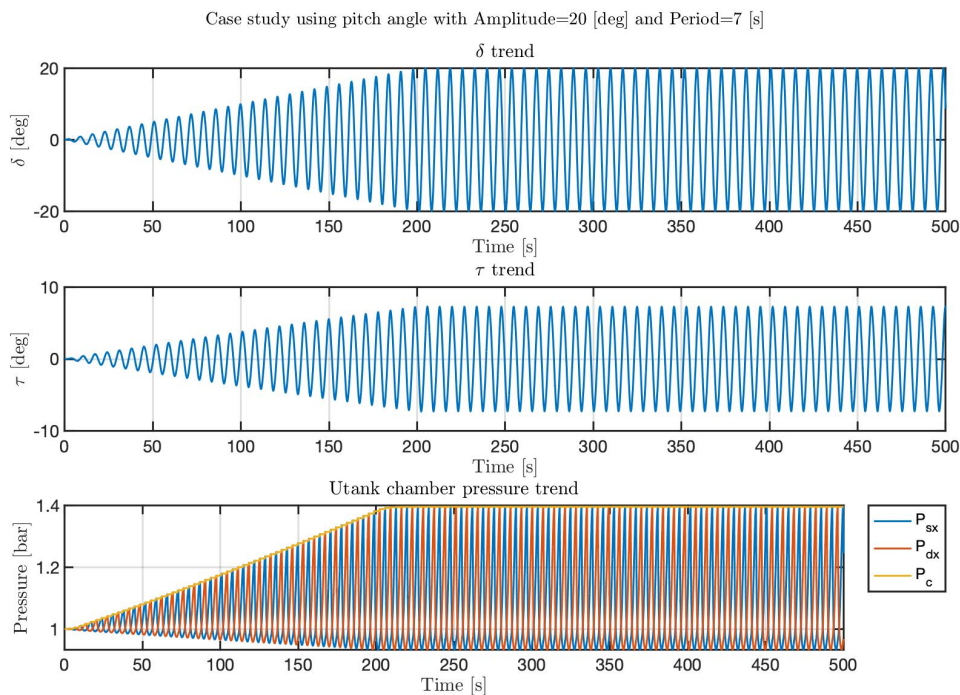


Figure 5.30: δ, τ and pressures trends using $A=20$ [deg] e $T=7$ [s]

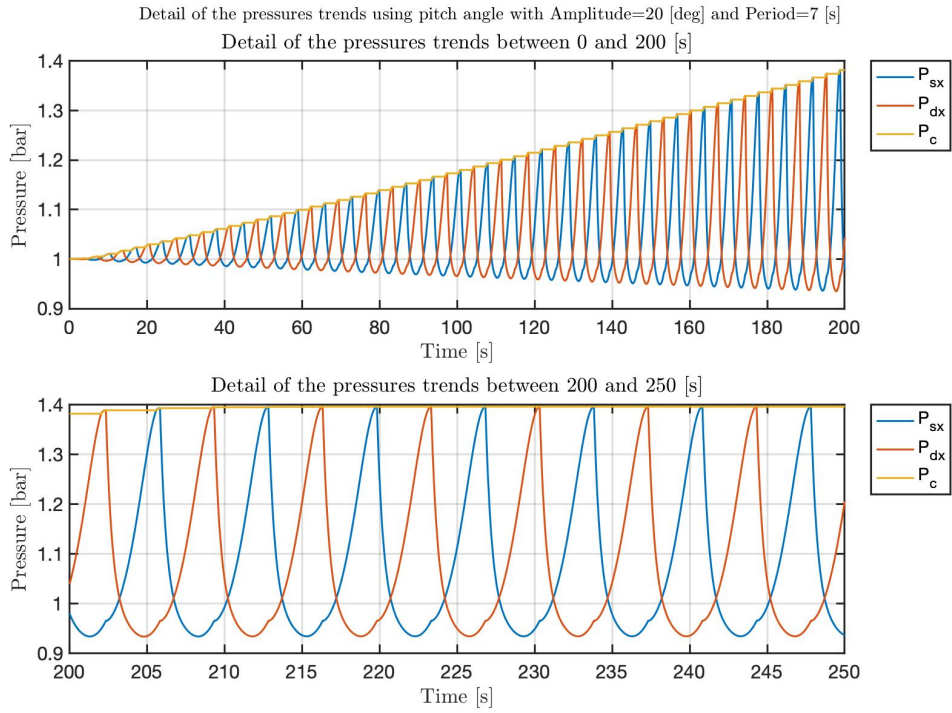


Figure 5.31: Detail of the pressure's trends using pitch angle with Amplitude=20 [deg] and Period=7 [s]

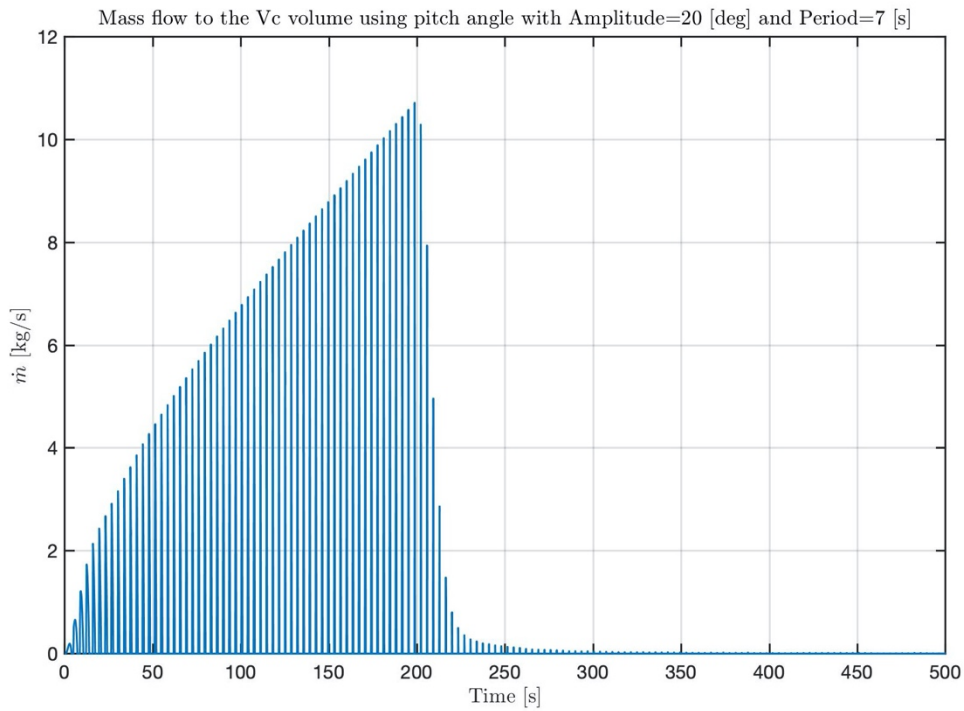


Figure 5.32: Trends of the inlet mass flow to the fixed volume Vc using A=20 [deg] and T=7 [s]

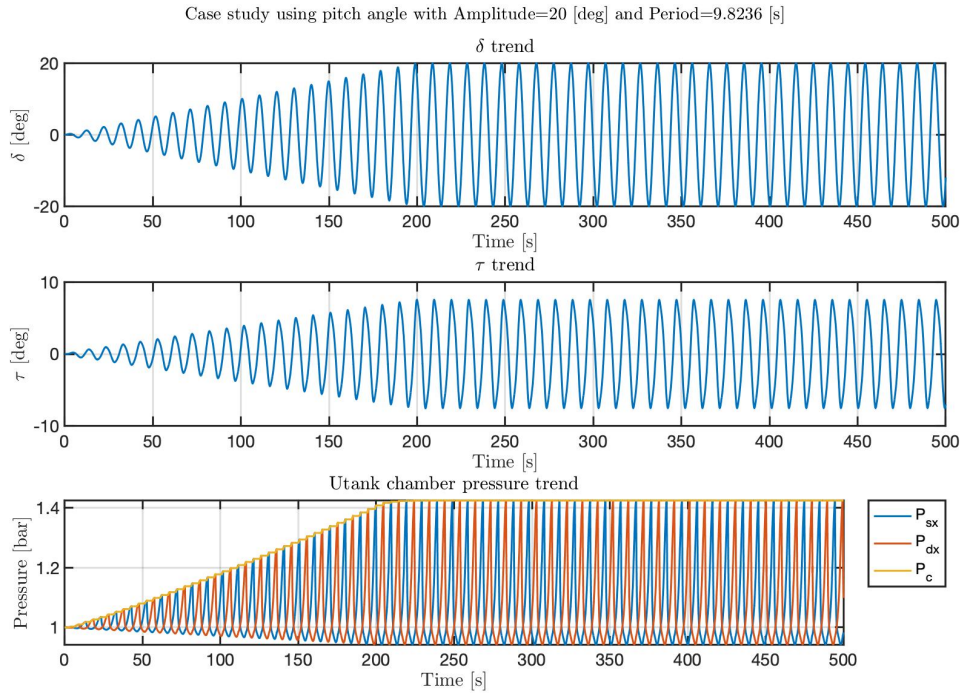


Figure 5.33: δ, τ and pressures trends using $A=20$ [deg] e T of resonance

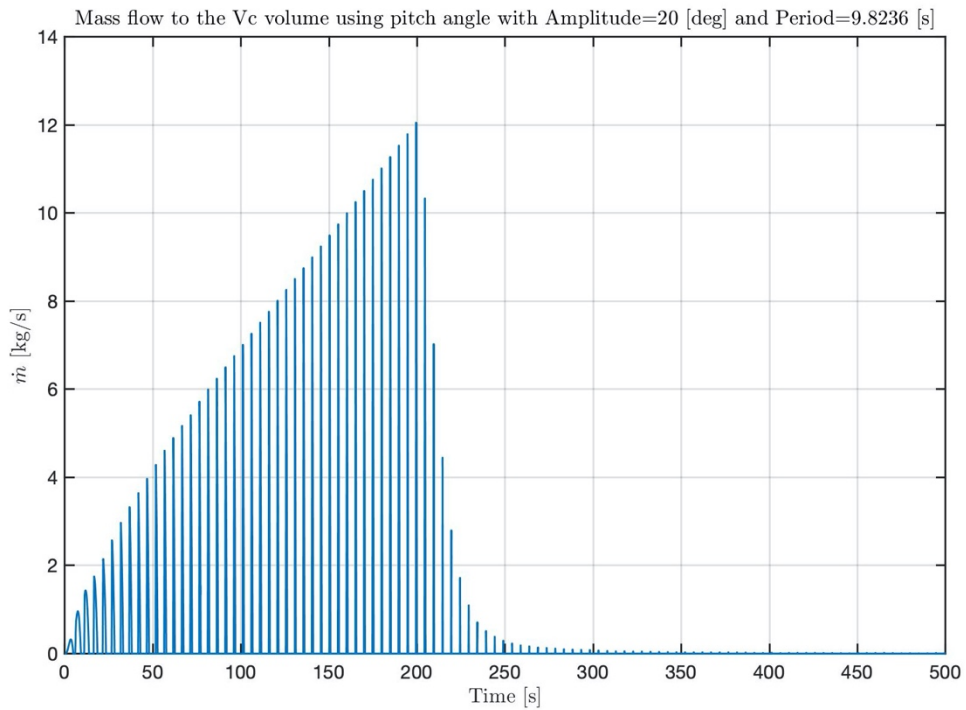


Figure 5.34: Trends of the inlet mass flow to the fixed volume Vc using $A=20$ [deg] and T of resonance

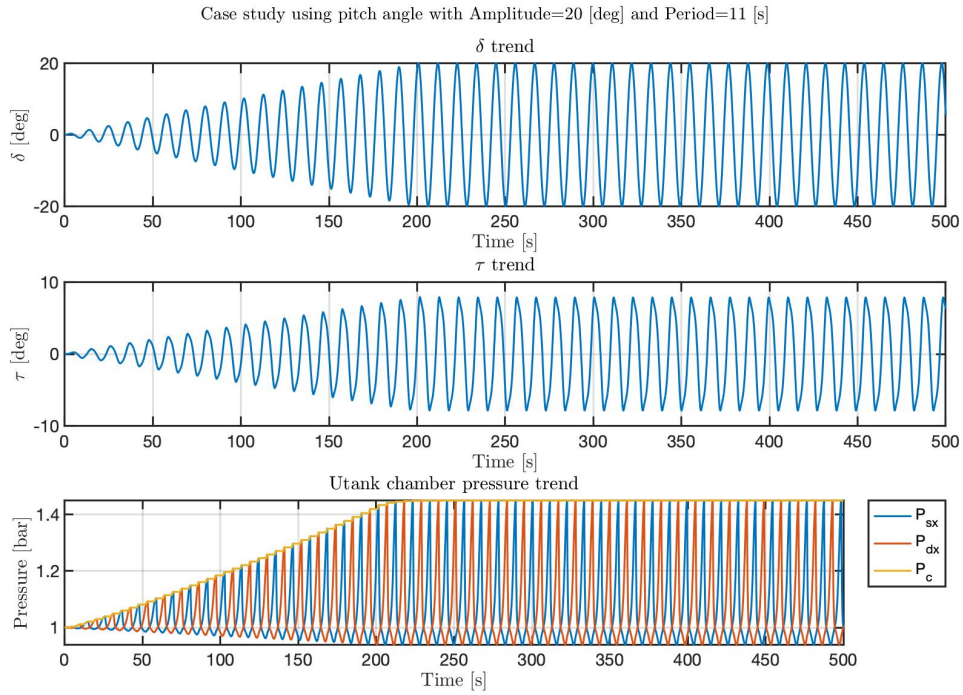


Figure 5.35: δ, τ and pressures trends using $A=20$ [deg] e $T=11$ [s]

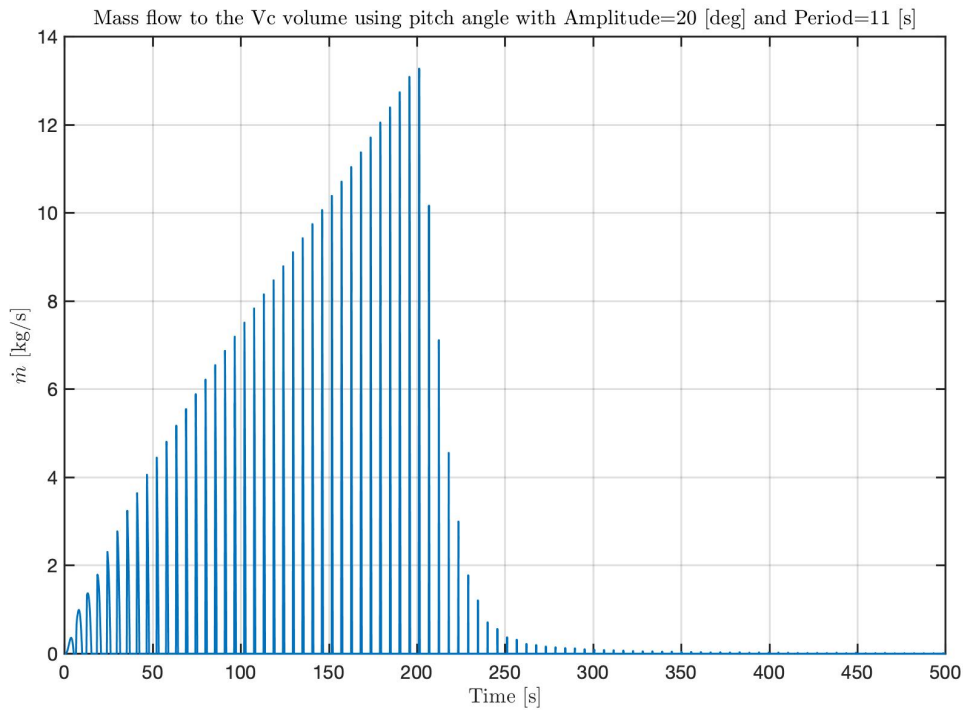


Figure 5.36: Trends of the inlet mass flow to the fixed volume Vc using $A=20$ [deg] and $T=11$ [s]

Also in this case, it's possible to make the same considerations made in the previous paragraphs.

Furthermore, it's possible to see that by increasing the amplitude and the period of the pitch angle with a ramp input for the first 200 [s], there is a gradual increase in the maximum pressure (P_C) reached and a proportional increase in the amplitude of τ (proportional as the amplitude of the pitch angle increases δ).

In τ trends it's possible to note a slight decrease in amplitude from a certain time value onwards, especially for amplitudes of 10 and 20 [deg] and for all 3 period values examined ($T=\{7,9.8236,11\}$ [s]). As a reference, see Figures (5.23), (5.26), (5.28), (5.30), (5.33), (5.35).

For the mass flow, also in this case, the same considerations made for the case with amplitude 5 [deg] and 10 [deg] are valid. It's possible to see how greater flow rates are achieved, increasing the amplitude and period values.

5.3 Air influence comparing linear and non-linear system

In this paragraph the influence of the air on the system is evaluated by comparing the τ amplitude in the case of linear and non-linear systems in the frequency domain.

The linear system is such that the dynamics of the U-Tank is not affected by the effect of the air; therefore, in the τ/δ transfer function there is no feedback of the pressure variation between the air chambers of the U-Tank (see Equation (2.21)).

While, the non-linear system represents the system with the feedback of the pressures and therefore the damping effect of the air. To evaluate the amplitude of τ in the frequency domain, is used firstly the previously described *Simulink* block diagram, from which the value of τ is obtained in the time domain through a *To Workspace* block. Subsequently, the value of the τ amplitude in the time domain and the vector of the time itself, are assigned to a *MATLAB* function created by Sergej Antonello Sirigu et al., which returns the value of frequency and amplitude of τ in the frequency domain. The value of the input δ angle is ramped gradually till 200 [s], then it reaches the nominal value. So, the whole validations are made for a stationary signal in the time range from 400 [s] till to 500 [s].

To do this validation, three values of δ amplitude ($\{1,5,10\}$ [deg]) and a period between 4 and 13 [s] are chosen. Different initial volume value is set (compared to the previous valuation) for the right and left U-Tank air chambers, V_0 is equal to 1000 [m³]; while the V_C value is unchanged and equal to 300 [m³].

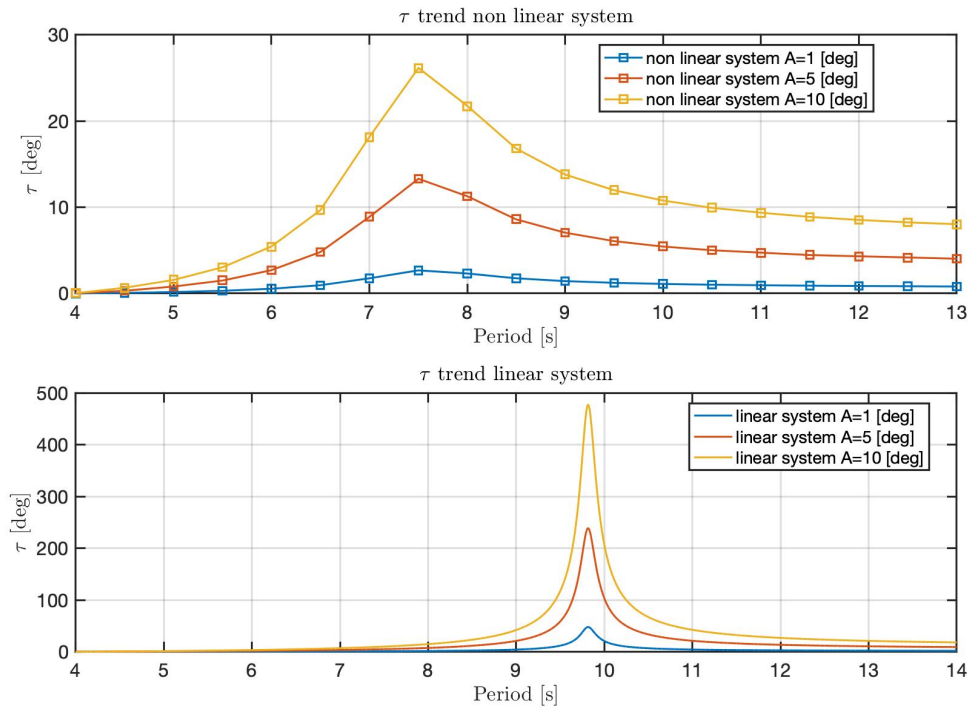


Figure 5.37: influence of air on the linear and non-linear system

The Figure (5.37) shows the damping effect of the air that shifts the resonance peak to higher frequencies and also away from the system's natural frequency. Furthermore, in the non-linear system there is a decrease in the value of the τ amplitude.

In the following figure, is represented the pressure value inside the fixed volume V_C . Also in this case, the analysis is conducted with three different values of δ amplitude and values of the period between 4 and 13 [s]. To evaluate the pressure value within the fixed volume V_C , the function mentioned above in the case of calculating the amplitude of τ in frequency is not used; but the average value of the pressure P_C in the chamber is calculated when the signal is stationary. This mean pressure value is evaluated for each frequency and then it's plot.

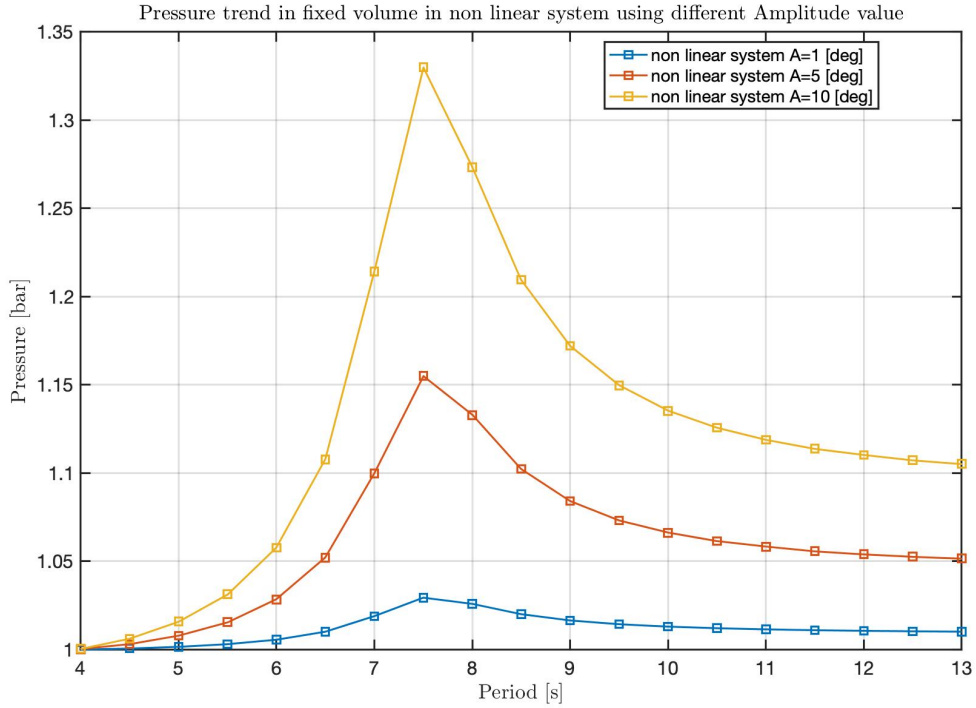


Figure 5.38: Pressure trend in V_c in non-linear system using different amplitude of the pitch angle

After performing these tests with a fixed initial volume of the right and left chamber of the U-Tank and varying the amplitude value of the pitch angle; a further check is carried out by keeping the δ amplitude constant and varying the initial volume of the U-Tank air chambers.

The δ amplitude value is fixed to 10 [deg], the initial volume is set equal to

$$V_0 = \{500, 1000, 1500, 2000, 2500, 3000\} m^3.$$

Also for this validation, in the first test the analysis of the τ amplitude in the frequency domain is carried out using the function to which the vector time and value of τ amplitude in the time domain is assigned and returns the value of frequency and τ amplitude in the frequency domain.

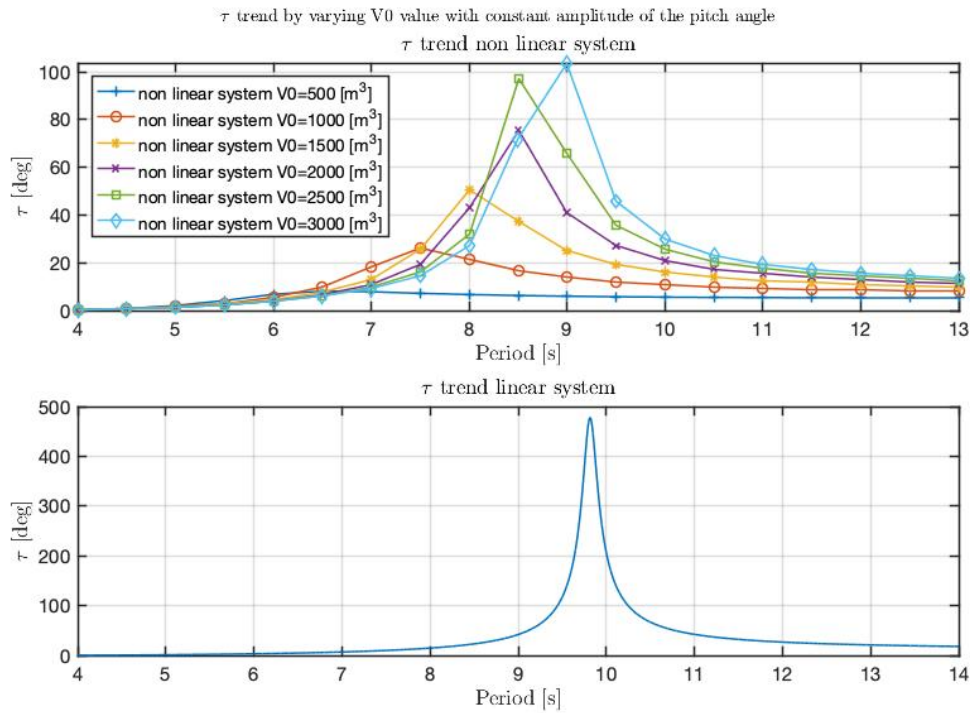


Figure 5.39: influence of air on the linear and non-linear system by varying V_0 value

From figure (5.39), it's possible to see what has already been described in the Paragraph (4.4), i.e. that the effect of air (in the non-linear system) influences the resonance frequency, which is shifted.

By increasing the V_0 value, the resonance frequency is closer to the nominal frequency of the system (at a lower frequency). If the air volume is very small, the resonance frequency is very high, so the stiffness of the system is higher.

In figures (5.39), it's possible to see a gradual increase in the maximum value reached in the τ amplitude. All the maximum values reached, in the τ amplitude, are significantly damped compared to the linear case in which there isn't the action of air.

In the following figure, is represented the pressure value inside the fixed volume V_C when the V_0 value is changed. To evaluate the pressure value within the fixed volume V_C , the function already mentioned is not used; but the average value of the pressure P_C in the chamber is calculated when the signal is stationary. This mean pressure value is evaluated for each frequency and then it's plot.

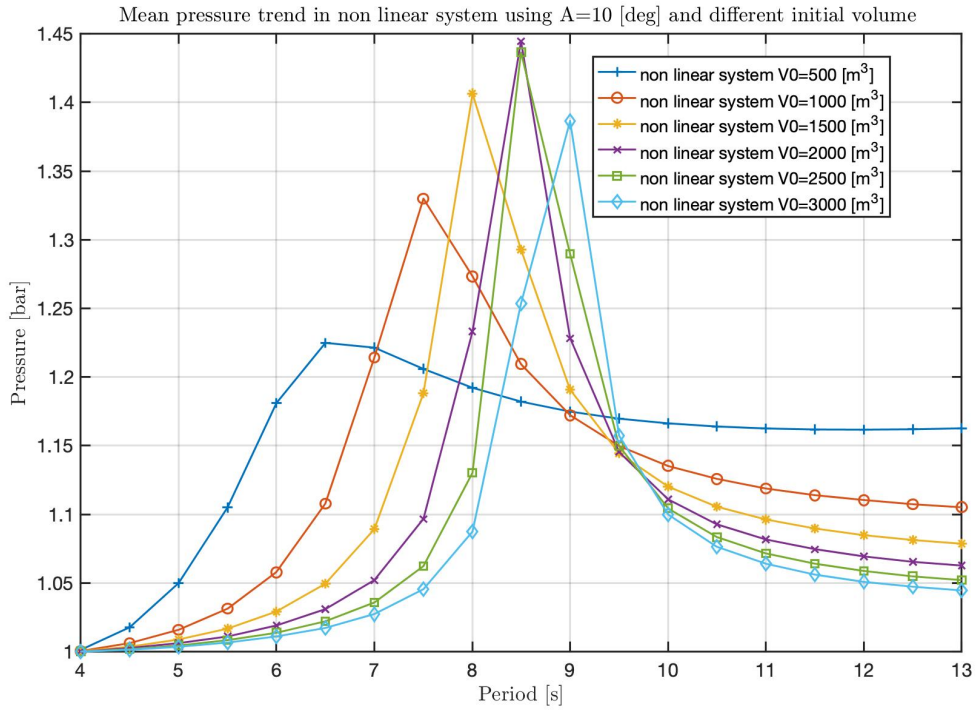


Figure 5.40: Pressure trend in V_c in non-linear system using different V_0 values

In this case, it's possible to notice a gradually increase of the maximum value reached in the mean pressure value till the initial volume value of the air U-Tank chamber is equal to 2000 [m³]; then it suddenly decreases.

6. Power extraction

In this last chapter, the control for the evaluation of gross energy production is analyzed. The system used is a pneumatic PTO with valves and air, which is similar to the hydraulic PTO. According to [22] the pneumatic PTO consists of a pneumatic cylinder, connected through check valves to an accumulator. The accumulator is connected to the motor-generator unit.

The PTO pneumatic system modelled in our case includes:

- The U-Tank, which is a bidirectional flow generator;
- Check valves;
- Constant volume tank (V_C);
- Switch valve;
- Generator unit.

The PTO pneumatic system is represented in the following figure.

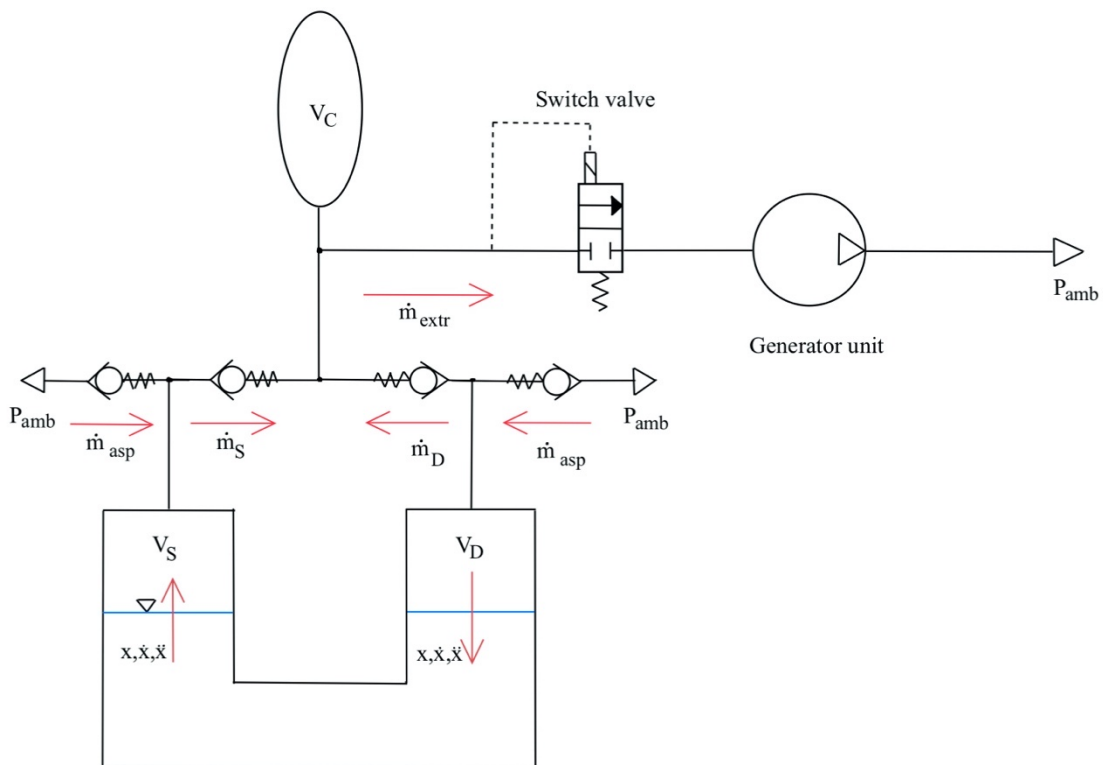


Figure 6.1: The PTO pneumatic system modelled

The air is drawn into the right and left lateral air chamber of the U-Tank through a check valve. The sucked air is subsequently pumped, from the right and left chamber respectively, during the rising movement of the water (which acts as a piston) inside the lateral reservoirs of the U-Tank. The pumped air is then directed to the accumulator through a check valve. The switch valve controls the flow to the generator unit. This switch valve allows the accumulator to be discharged only when the pressure is high enough to allow good power transmission and not to bring the accumulator into depression. The switch valve works in a range of pressures given by the hysteresis function which receives in input the pressure difference between the one inside the accumulator and the ambient pressure (since the suction phase takes place directly from the environment).

The switch valve system described is added to the *Simulink* model reported in Paragraph (5.1.5). The new block diagram created is shown in the following figure and represents the flow rate disposal of the generator unit.

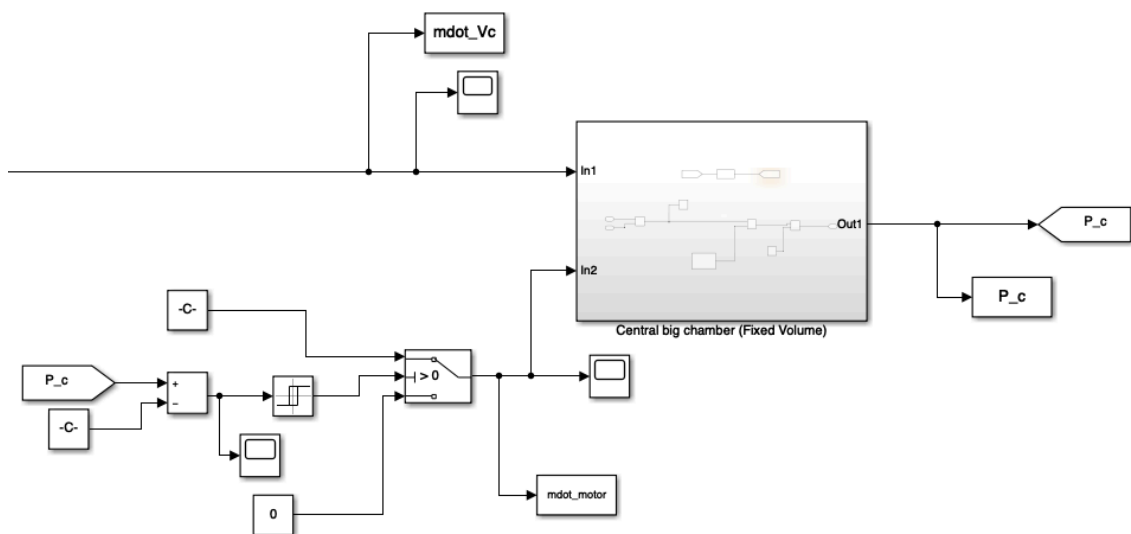


Figure 6.2: Flow rate disposal block of the generator unit

Into the relay block is set a “*Switch on point*” equal to 5000 Pa and a “*Switch off point*” equal to 0 Pa.

The relay block is inserted to have a dead band of inaction, so that the switch doesn't constantly change sign around the equilibrium position. In this dead band of inaction, once the values for the “*switch on point*” and the “*switch off point*” have been set, when the pressure difference (between the accumulator pressure and the ambient pressure) rises

above the "switch on point " value, the switch block disposes of the flow rate value extracted from the generator unit; on the other hand, when the pressure difference drops to 0, the switch block changes contact and disconnects the generator unit, so as to accommodate the filling and pressurizing process of the V_C accumulator.

6.1 Mean Power Extraction

Since the turbine that extracts power is not known, the mass flow rate of air required for the generation of energy is not known. Therefore, the gross power extracted from the system is evaluated with an optimized ideal mass flow range.

A numerical model is developed, where for each period (T) between 4 and 13 [s] and for an amplitude of the pitch angle (δ) equal to 10 [deg], the gross average power value extracted from the stationary system is calculated for each value of mass flow imposed as disposal of the generator.

The equation used for the evaluation of the gross power extraction is the following:

$$P_{gross} = \dot{m}_{extr} \Delta P = \dot{m}_{extr} (P_C - P_{amb}) \quad (6.1)$$

Where \dot{m}_{extr} is the mass flow used by the turbine to produce power, this value is collected from the *To Workspace* "mdot_motor" block placed after the switch in Figure (6.2).

In the following Figure (6.3) is shown the mean gross power extracted for different mass flow values. These mass flow values (\dot{m}_{set}) are set into the constant block of the switch represented in Figure (6.2). The mean gross power value for each period is calculated when the system reaches the steady state, because as input to the *Simulink* model is assigned a ramped value of δ and $\ddot{\delta}$, therefore there is an initial transient period in which the power calculation isn't accurate and similar to optimal working conditions.

From the following figure, it's possible to notice that for each period value till the resonance frequency, there is a different value of \dot{m}_{set} which maximises the mean gross power extracted. The trend of the gross power is calculated by setting an initial volume value of

lateral air chambers of the U-Tank equal to 1000 [m³] and an ambient pressure at suction phase equal to 100000 [Pa].

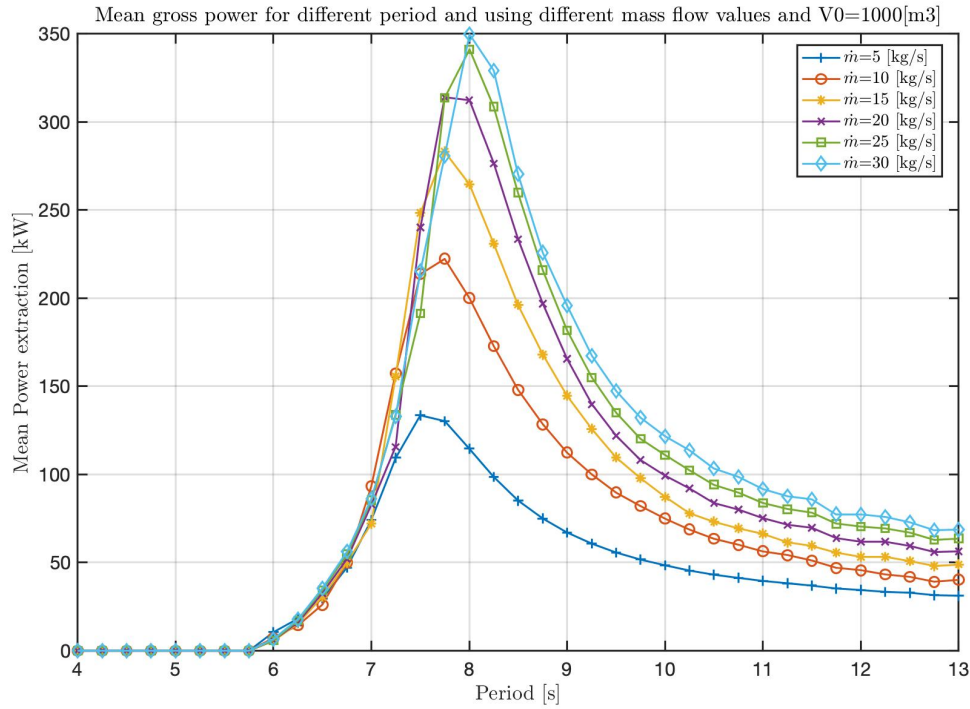


Figure 6.3: Mean gross power for different period and different mass flow values

Thanks to the Figure (6.3), it's possible to say that the U-Tank doesn't work very well for short periods (and high frequencies). In fact, till the resonance (which occurs for shorter period compared to the natural frequency of the system), the \dot{m}_{set} value which maximises the gross power is lower compared to the \dot{m}_{set} value at resonance. At the resonance frequency, there is a lot of movement inside the U-Tank, therefore the maximum value of the mass flow (\dot{m}_{set}) imposed for power extraction is the best, but this optimal mass flow at the resonance doesn't represent the optimal value for each period, especially at lower period.

The *MATLAB* code used to calculate the average gross power is shown below.

```
for i=1:length(Par.period)
    Par.frequency(i)=(2*pi)/Par.period(i); %[rad/s]
    Par.delta=Par.amplitude*sin(Par.frequency(i)*par.time);
    Par.delta_dot=Par.amplitude*Par.frequency(i)*cos(Par.frequency(i)*par.time);
    Par.delta_ddot=-Par.amplitude*(Par.frequency(i)^2)*sin(Par.frequency(i)*par.time);
```

```

Par.DELTA=[Par.delta(1:2001).*par.slope;Par.delta(2002:end)];

Par.DELTA_DOT=[Par.delta_dot(1:2001).*par.slope;Par.delta_dot(2002:end)
]);

Par.DELTA_DDOT=[Par.delta_ddot(1:2001).*par.slope;Par.delta_ddot(2002:
end)];

VAR_delta = [par.time Par.DELTA];
VAR_deltad = [par.time Par.DELTA_DOT];
VAR_deltadd = [par.time Par.DELTA_DDOT];

for j=1:length(motor_mdot)
    out = sim('U_tank_power')
    Gross_power(i,j)=mean(mdots-
tor.Data(45000:end).*(P_c.Data(45000:end)-pressure_out));

end
end

```

Subsequently the trend of τ , mean pressure value inside the accumulator and the mean effective mass flow (\dot{m}_{extr}) are evaluated for the different values of \dot{m}_{set} in frequency domain.

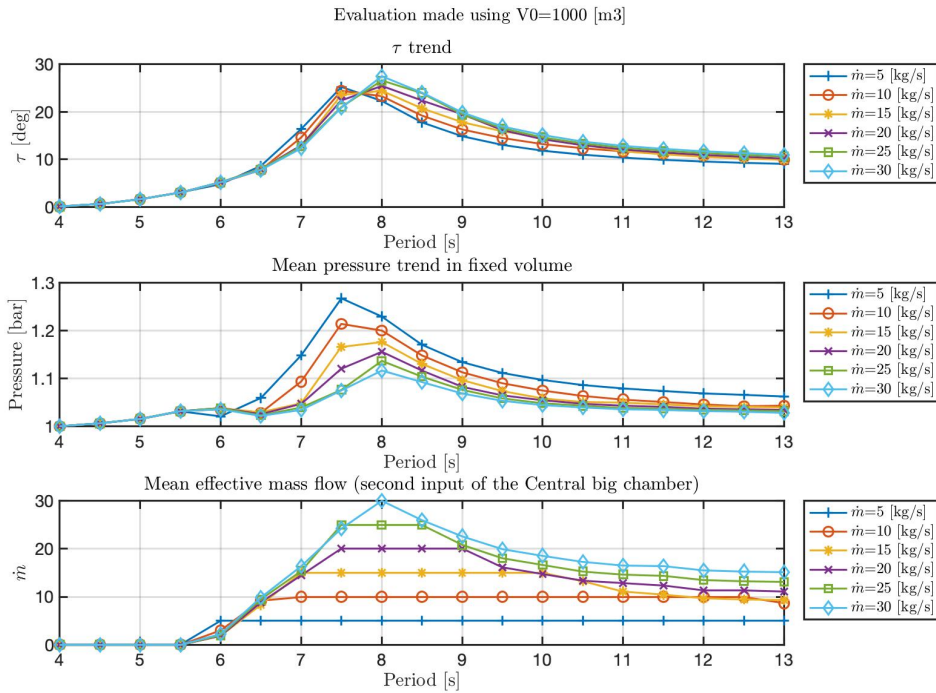


Figure 6.4: τ , mean pressure value, mean mass flow in frequency domain of the PTO pneumatic system

From Figure (6.4) we note how increasing the \dot{m}_{set} value, there is an increasing value of the τ amplitude and the maximum value reached is shifted to higher period (lower frequency). While, for the mean pressure trend inside the accumulator there is a continuous decrease of the maximum value reached as the \dot{m}_{set} value increases. This is due to the greater mass flow rate extracted from the accumulator to meet the flow rate required by the generator unit; this consequently leads to a decrease of the mean pressure value inside the accumulator. Into the last subplot is represented the mean effective mass flow value used as a second input of the central big chamber block represented in Figure (6.2). These values, shown in the last subplot, are the mean value obtained from the *To Workspace* after the switch (see Figure (6.2)) when the system reaches the stationarity for each frequency value.

Then the trend of τ , pressure inside the accumulator, mass flow extracted, and gross power extracted are evaluated for the minimum and maximum value of \dot{m}_{set} at the resonance frequency in time domain.

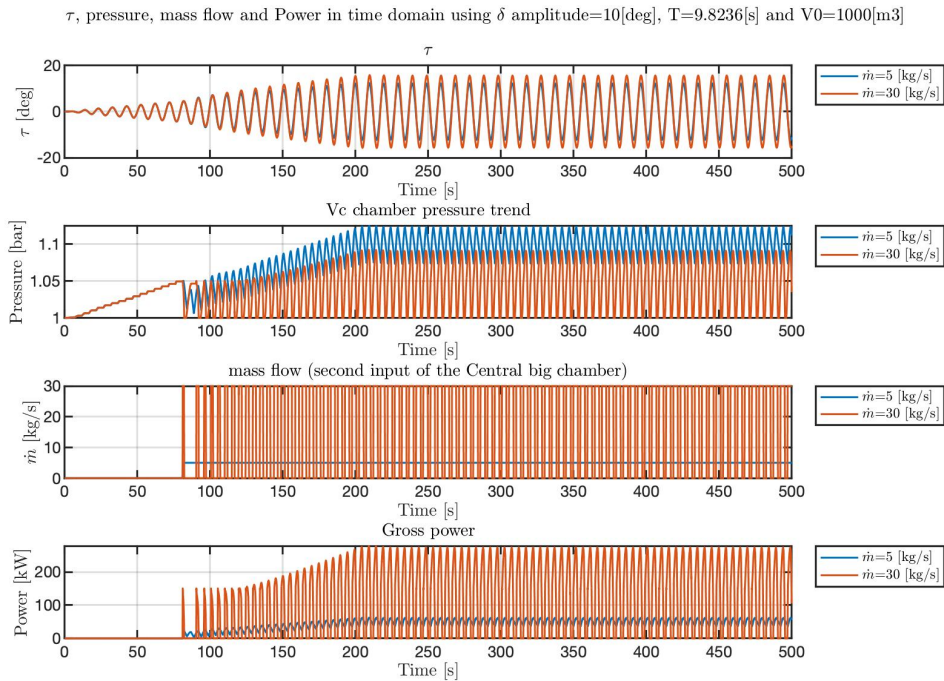


Figure 6.5: τ , pressure inside the accumulator, mass flow extracted and gross power in time domain of the PTO pneumatic system at resonance frequency

Through Figure (6.5) is possible to make a comparison between the minimum and maximum value of \dot{m}_{set} . It's possible to notice that increasing the \dot{m}_{set} value, there is an increase of the τ amplitude and an increase of the gross power extracted following an increase in the \dot{m}_{extr} value and the number of switches made by the switch valve. Because of the increase of the \dot{m}_{extr} value from the generator unit, there is a consequent decrease of the pressure inside the accumulator chamber. The value of the pressure inside the accumulator never drops below the ambient pressure value thanks to the relay block.

All the trends of the quantities shown in the Figure (6.5) are evaluated for a constant pitch angle amplitude equal to 10 [deg] and for a period equal to 9.8236 [s] (which is equal to the natural frequency of the system).

6.2 Variation of the initial air volume

In this paragraph is evaluated the effect of the initial air volume variation. To perform this validation, the initial air volume values of the right and left U-Tank chambers are changed. The new V_0 values are set equal to 125, 250 and 500 [m³]. The following paragraphs shown the results obtained for the mean gross power; for the trend of the τ amplitude, mean pressure inside the accumulator and mean effective mass flow in frequency domain; for the trend of the τ amplitude, pressure inside the accumulator, effective mass flow and gross power in time domain at the resonance frequency of the system.

6.2.1 $V_0=125 \text{ [m}^3\text{]}$

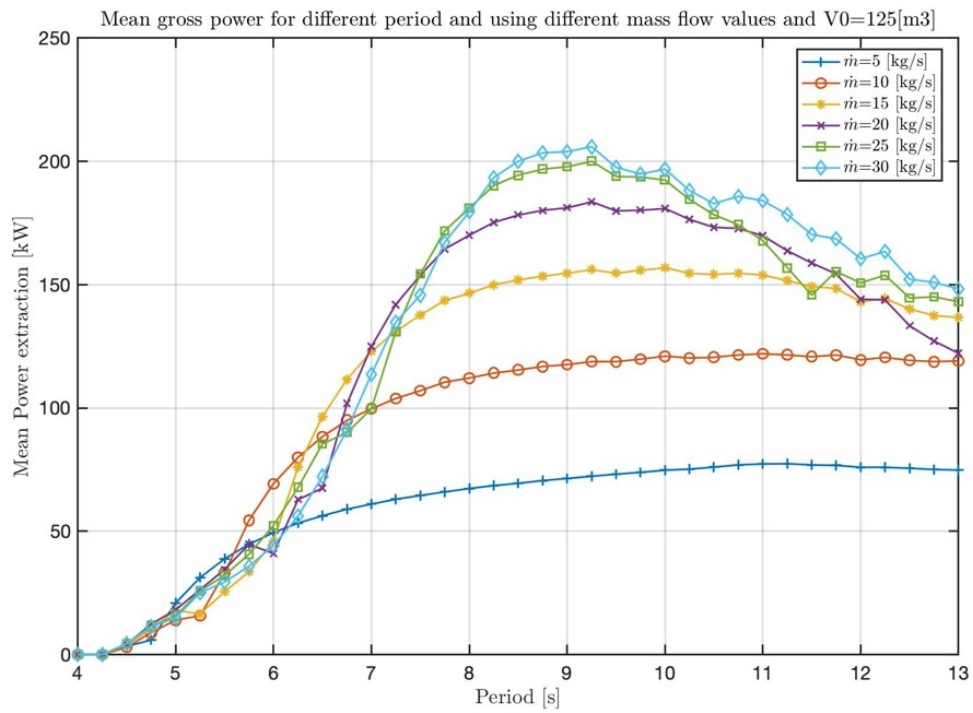


Figure 6.6: Mean gross power for different period and different mass flow values and $V_0=125 \text{ [m}^3\text{]}$

From the Figure (6.6) it's possible to notice that, in comparison to the case with $V_0=1000 \text{ [m}^3\text{]}$ (see Figure (6.3)), the U-Tank system works better at higher frequencies (lower periods). In addition, the maximum mean gross power extracted from the system for each mass flow of set is lower in comparison to the one in Figure (6.3). Then, it's noted that there is no significant decay into the mean gross power trend for frequencies greater than the resonance frequency.

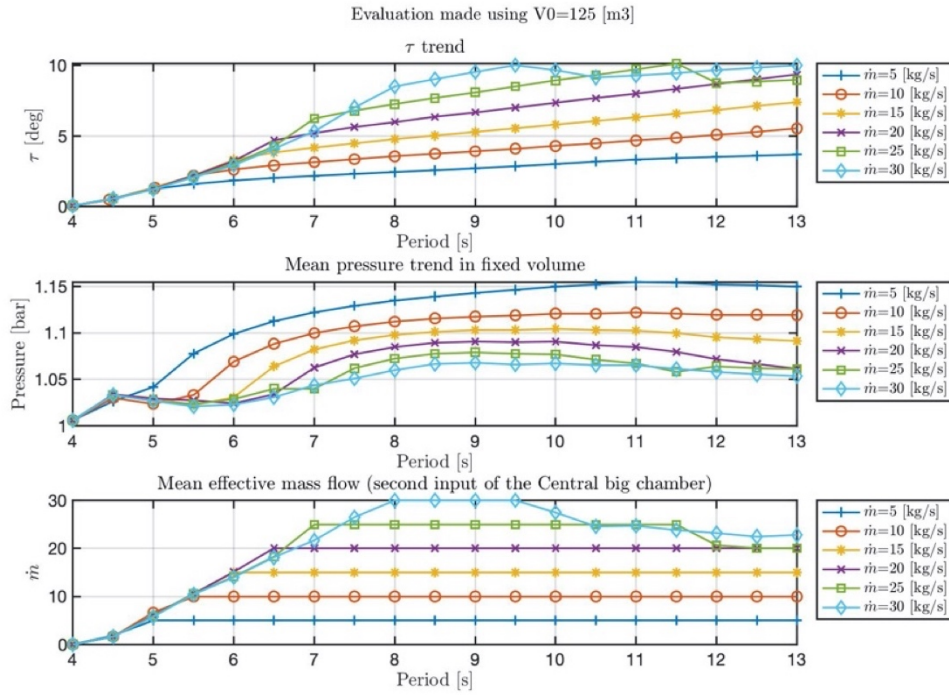


Figure 6.7: τ , mean pressure value, mean mass flow in frequency domain of the PTO pneumatic system for $V_0=125$ [m³]

From Figure (6.7), it's possible to notice that, in the frequency domain, the mean pressure value inside the accumulator is lower in comparison to the previous case using $V_0=1000$ [m³]. Moreover, the amplitude of τ , in this case, is much smaller than in the previous case (see Figure (6.4)).

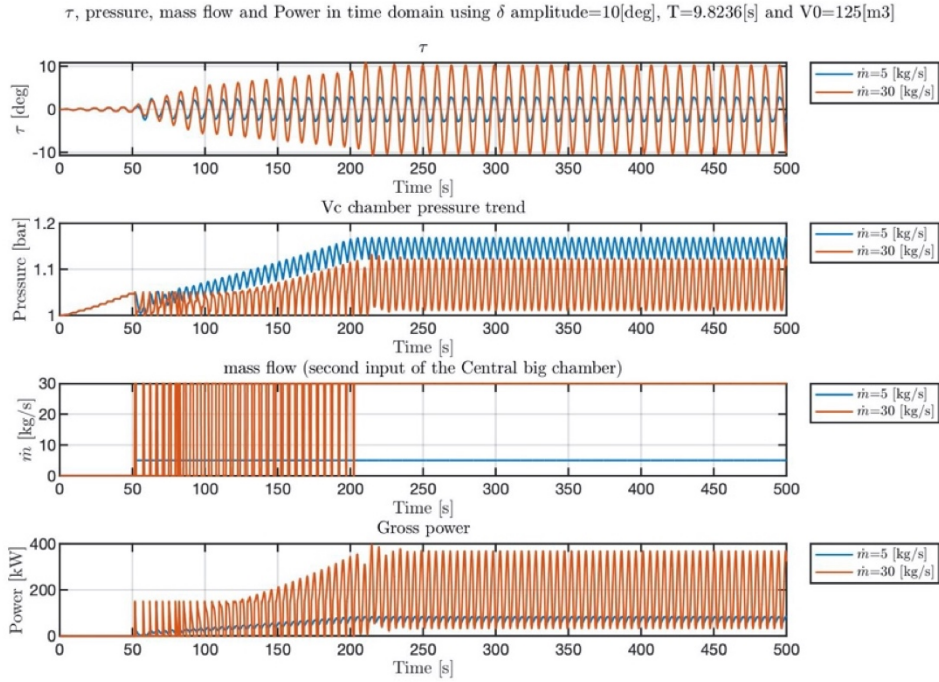


Figure 6.8: τ , pressure inside the accumulator, mass flow extracted and gross power in time domain of the PTO pneumatic system at resonance frequency for $V_0=125$ [m³]

All the trends of the quantities shown in the Figure (6.8) are evaluated for a constant pitch angle amplitude equal to 10 [deg] and for a period equal to 9.8236 [s] (which is equal to the natural frequency of the system).

From Figure (6.8), it's possible to notice that the τ amplitude is really different for the two values of the set mass flow. The τ amplitude value is really small for the mass flow equal to 5 [kg/s]. Moreover, both the τ amplitude values are smaller compared to the relative value shown in Figure (6.5) for the case using $V_0 = 1000$ [m³].

Into the second subplot in Figure (6.8), it's represented the pressure trend. Because of the increase of the \dot{m}_{extr} value from the generator unit, there is a consequent decrease of the pressure inside the accumulator chamber. The value of the pressure inside the accumulator never drops below the ambient pressure value thanks to the relay block. The pressure value reached inside the accumulator is higher in comparison to the pressure value represented in Figure (6.5).

For both the selected flow rates, and in comparison to Figure (6.5), it's possible to say that in this case higher gross powers are reached in the time domain at the resonant frequency.

While, for the effective mass flow, in this case there is a lower number of switches of the switch valve for a set flow rate equal to 30 [kg / s] compared to the case shown in Figure (6.5).

6.2.2 $V_0= 250 \text{ [m}^3\text{]}$

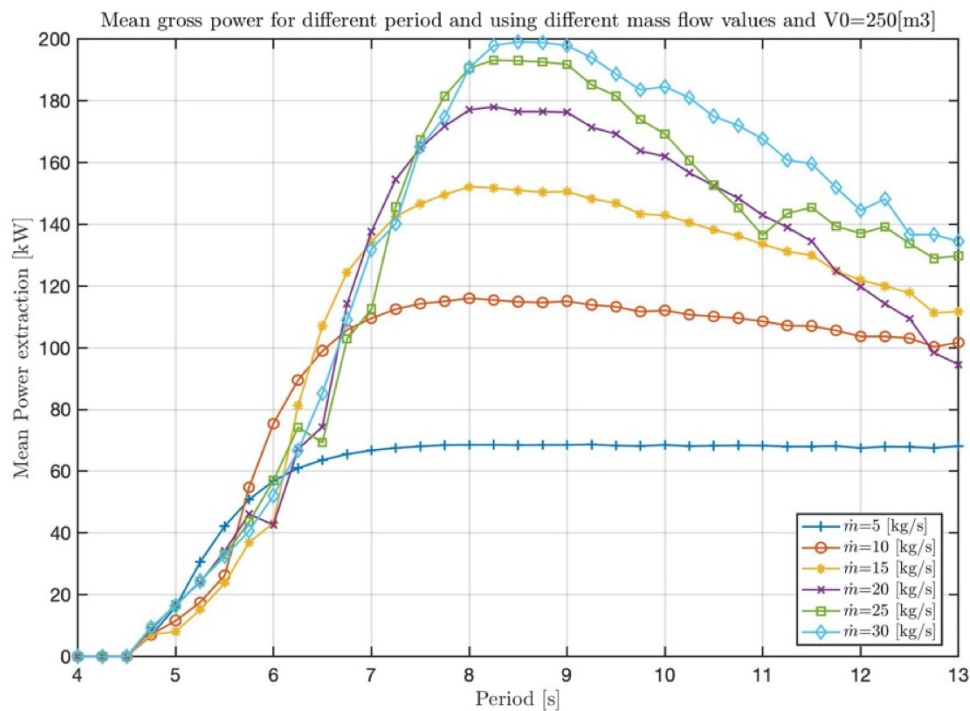


Figure 6.9: Mean gross power for different period and different mass flow values and $V_0=250 \text{ [m}^3\text{]}$

From the Figure (6.9) it's possible to notice that, in comparison to the case using $V_0=1000 \text{ [m}^3\text{]}$ (see Figure (6.3)), the U-Tank system works better at higher frequencies (lower periods). In addition, the maximum mean gross power extracted from the system for each mass flow of set is lower in comparison to the one in Figure (6.3). Then, it's noted that there is no significant decay into the mean gross power trend for frequencies greater than the resonance frequency.

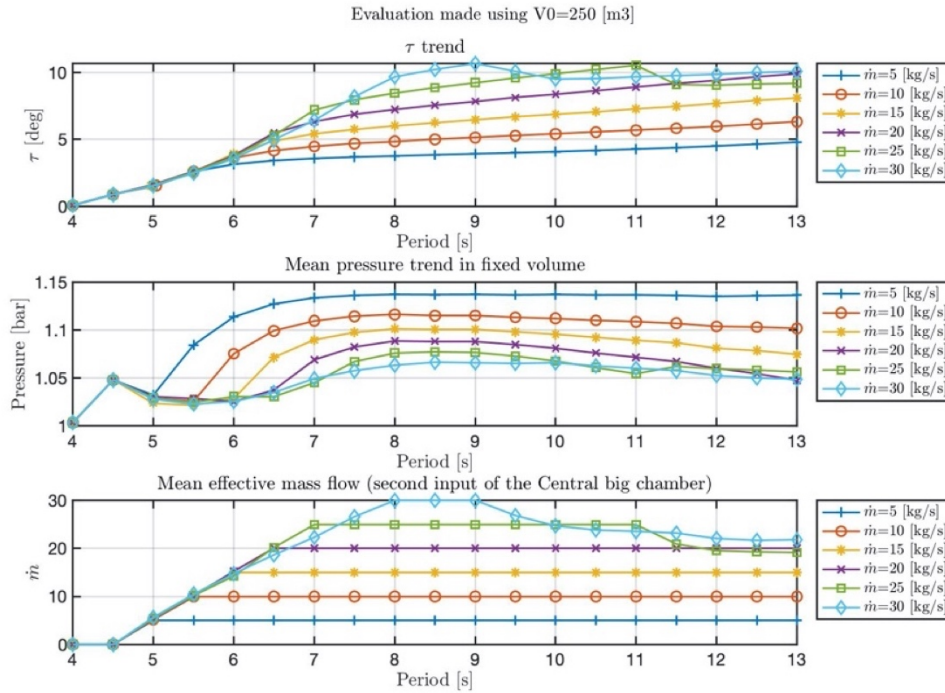


Figure 6.10: τ , mean pressure value, mean mass flow in frequency domain of the PTO pneumatic system for $V_0=250$ [m³]

From Figure (6.10), it's possible to notice that, in the frequency domain, the mean pressure value inside the accumulator is lower in comparison to the case using $V_0=1000$ [m³]. Moreover, the amplitude of τ , in this case, is much smaller than in Figure (6.4).

All the trends of the quantities shown in the following Figure (6.11) are evaluated for a constant pitch angle amplitude equal to 10 [deg] and for a period equal to 9.8236 [s] (which is equal to the natural frequency of the system).

From Figure (6.11), it's possible to notice that the τ amplitude is really different for the two values of the set mass flow. Moreover, both the τ amplitude values are smaller compared to the relative value shown in Figure (6.5) using $V_0 = 1000$ [m³]. The τ amplitude represented for a set mass flow equal to 5 [kg/s] is slightly greater than the one represented in Figure (6.8).

Into the second subplot in Figure (6.11), it's represented the pressure trend. The pressure value reached inside the accumulator are higher in comparison to the pressure value represented in Figure (6.5), but lower in comparison to ones Figure (6.8).

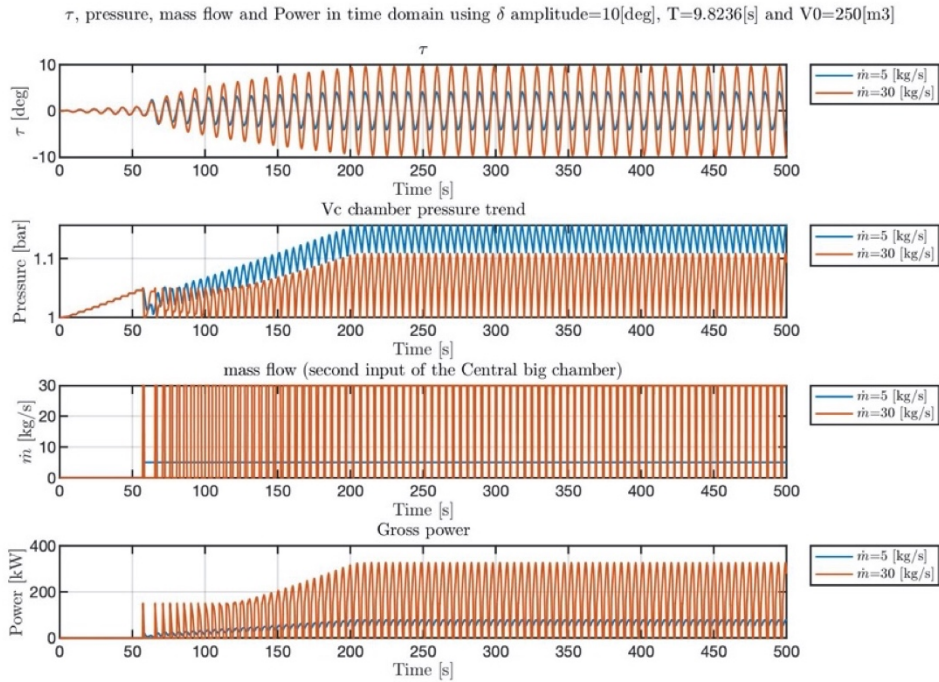


Figure 6.11: τ , pressure inside the accumulator, mass flow extracted and gross power in time domain of the PTO pneumatic system at resonance frequency for $V_0=250$ [m³]

6.2.3 $V_0= 500$ [m³]

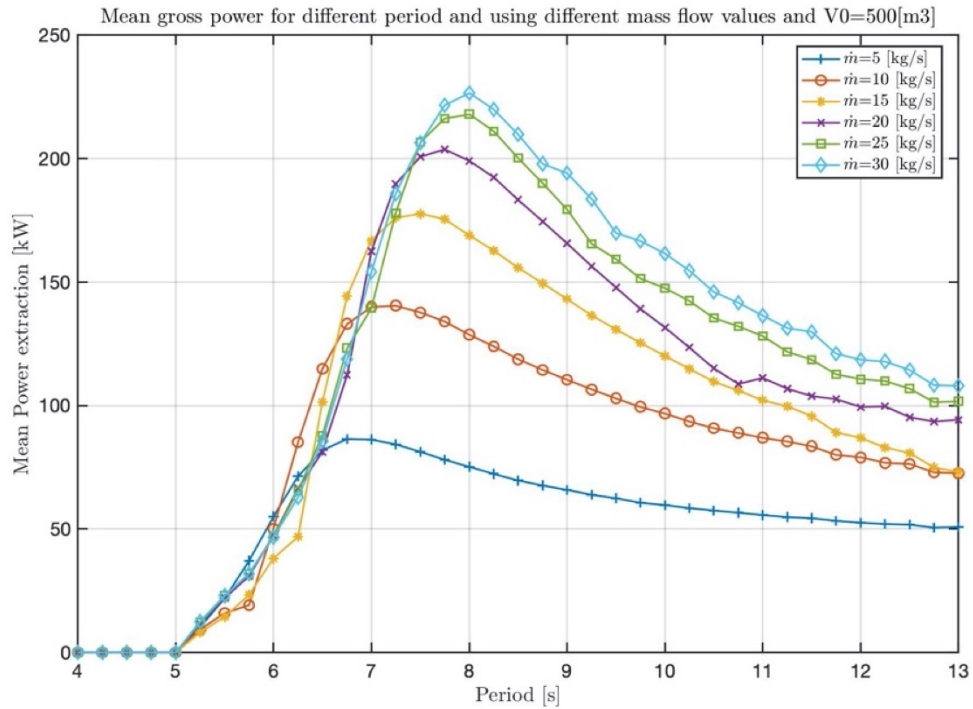


Figure 6.12: Mean gross power for different period and different mass flow values and $V_0=500$ [m³]

From the Figure (6.12) it's possible to notice that, in comparison to the case using $V_0=1000$ [m³] (see Figure (6.3)), the U-Tank system works better at higher frequencies (lower periods). The maximum mean gross power extracted from the system for each mass flow of set is lower in comparison to the one in Figure (6.3). Then, it's noted that starts a decay into the mean gross power trend for frequencies greater than the resonance frequency. For each lower period there is a different value of \dot{m}_{set} which maximises the mean gross power.

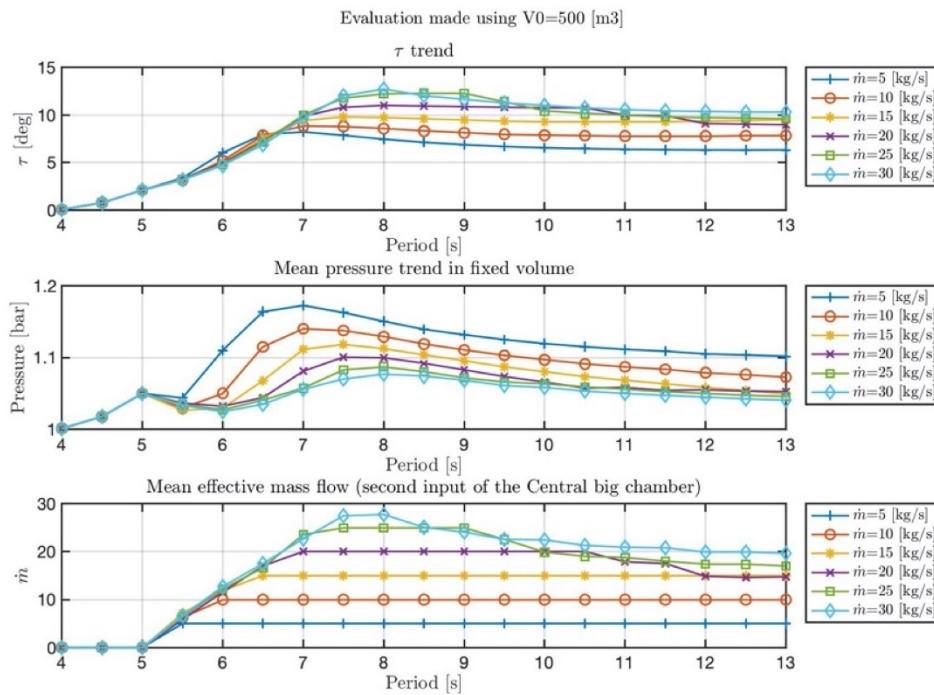


Figure 6.13: τ , mean pressure value, mean mass flow in frequency domain of the PTO pneumatic system for $V_0=500$ [m³]

From Figure (6.13), it's possible to notice that, in the frequency domain, the mean pressure value inside the accumulator is lower in comparison to the case using $V_0=1000$ [m³], but is higher in comparison to the case represented in Figure (6.10). Moreover, the amplitude of τ , in this case, is much smaller than in Figure (6.4), and it's significantly greater than the case represented in figure (6.10) using a $V_0=250$ [m³].

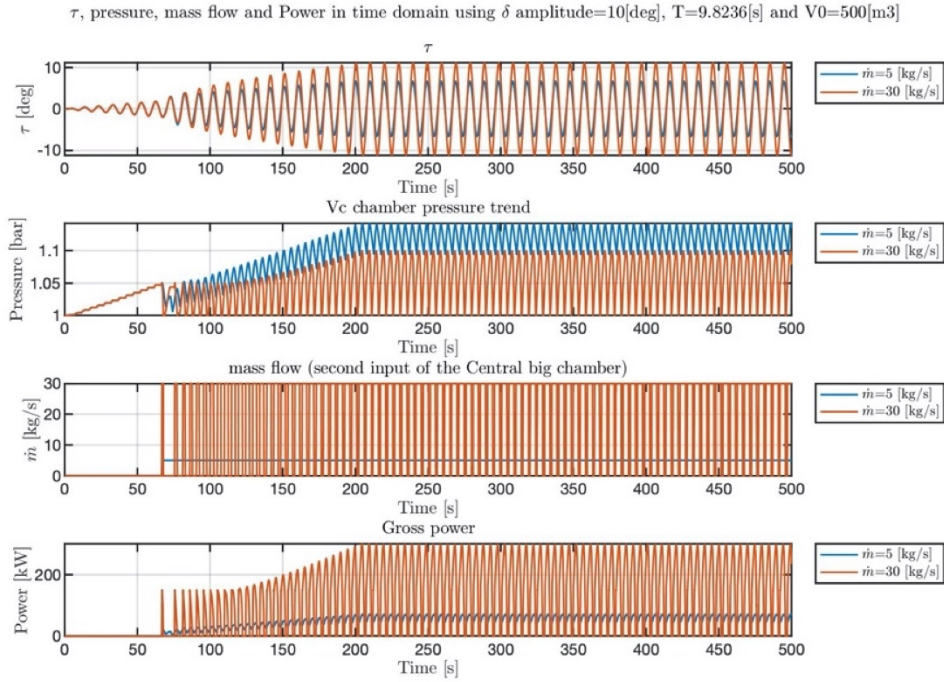


Figure 6.14: τ , pressure inside the accumulator, mass flow extracted and gross power in time domain of the PTO pneumatic system at resonance frequency for $V_0=500$ [m³]

From Figure (6.14), it's possible to notice that the τ amplitude is really different for the two values of the set mass flow. Moreover, both the τ amplitude values are smaller compared to the relative value shown in Figure (6.5) for the case using $V_0 = 1000$ [m³]. The τ amplitude represented for a set mass flow equal to 5 [kg/s] slightly smaller than the one evaluated for a set mass flow equal to 30 [kg/s].

Into the second subplot in Figure (6.14), it's represented the pressure trend. The pressure value reached inside the accumulator are higher in comparison to the pressure value represented in Figure (6.5), but lower in comparison to ones Figure (6.8).

7. Conclusions

The intent of this thesis is to analyze the gross power extraction of the U-Tank technology installed inside an already know IOwec (Inertial Ocean Wave Energy Converter) device for a different sea-state conditions, in frequency and time domain. The IOwec device is able to adapt to the direction and type of wave present in the site where it's installed; therefore, it's a flexible and site-independent device. It's primarily formulated to work in ocean environments, where the types of wave acting are very complex. The integration of the U-Tank technology, allows to obtain the damping of the system (thanks to the motion of the water inside the U-Tank) and the power extraction from the U-Tank (thanks to an energy extraction system placed on the air side duct of the U-Tank). The U-Tank device consist of two lateral rectangular reservoirs connected by a central base duct (partially filled with water) and an upper air side duct (where power is extracted from the compressed air).

To evaluate the behavior of the IOwec system coupled with the U-Tank technology in the regular wave conditions, the following steps are performed:

- **U-Tank Dynamics Model:** A numerical model is developed with the aim of obtaining the transfer function of the system; such that given an input pitch angle (δ), the angle that develops between the two columns of water inside the U-Tank air chamber (τ) is obtained. We need this to evaluate the dynamics of the U-Tank.
- **Evaluation of the damping PTO influence on the system:** Is evaluated the effect of an arbitrary chosen B_{PTO} damping value on the system, without considering the air dynamics. All simulations are carried out in the frequency domain and using different pitch angle values.
- **Influence of the air dynamics:** Is evaluated the influence of air on the entire system. Firstly, the pressure drop through a resistance, located in the air side duct, is evaluated according to the kinematics of the U-Tank; secondly, the influence of air on the entire system made up by the U-Tank coupled with the resistance is evaluated. The analysis is conducted in the frequency domain.
- **Development of the Time Domain Model:** Thanks to the use of the *Simulink* software, the modeling of the entire system is carried out. The time domain model

evaluates the filling dynamics of the U-Tank air chambers and the one of a fixed volume which fills with the air sent from the two air chambers of the U-Tank.

- **Power extraction:** In the last part of the work, is evaluated the gross power extracted from the U-Tank technology installed on an IOwec device. In addition, the effect of the initial volume variation of air inside the lateral chamber of the U-tank on the gross average power extracted is evaluated.

After having developed the numerical model of the U-Tank and its coupling with the float, a study about the damping generated by the PTO (Power Take Off) system in regular wave (without considering the air dynamics) was carried out. The PTO damping has been set equal to a multiplicative coefficient of the hydrodynamic damping coefficient. The validations were carried out for different pitch angles (1 and 5 [deg]) and figures were obtained which show the behavior of the τ angle. The figures obtained show how increasing the pitch angle, there is a consequent increase of the maximum τ value reached; but at the same time, by increasing the PTO damping value, there is a consequent decrease in the maximum τ value at a frequency close to the natural frequency of the system. The mean absorbed power was also calculated for the different PTO damping values set and for the different input pitch angles. The figures obtained from the simulation show how by increasing the input pitch angle value, a higher mean absorbed power is obtained; but on the other hand, by increasing the PTO damping value, there is a decrease in the maximum mean absorbed power. Furthermore, for each frequency value there is a different PTO damping value which maximizes the mean absorbed power.

To evaluate the air effect on the system, firstly was studied the pressure drop through a resistance. R_V is a resistance that can represent the behavior of a valve or an air turbine. It causes a pressure drop between the two U-Tank air reservoirs, influencing the dynamics of the U-Tank. Firstly, the numerical model which evaluate the pressure drop as a function of the kinematics of the U-Tank and resistance was developed. Through the simulations, the trend of the transfer function $\Delta P/\tau$ was obtained. The simulations results show how increasing the resistance, there is a consequent decrease in the cutoff frequency. Secondly, was evaluated the air influence on the whole system. Through the numerical model, the transfer function of the whole system was obtained. Where the τ angle is obtained as a function of the pitch angle and the pressure drop on the resistance. Also in this case, for an increasing resistance value, there is a decreasing of the τ/δ magnitude, so it's possible

to say that increasing the resistance, increase the air damping effect on the whole system. Simulations were also conducted in which in addition to varying the resistance, there is also the variation of the initial air volume in the lateral reservoirs of the U-Tank. From these simulations we note that increasing the value of the volume of air available, the resonance frequency of the system is shifted. When the resistance value is high and the initial air volume is small, the stiffness of the system is so high that the resonance frequency occurs for very high frequency value. On the other hand, for a higher initial volume value and for very high resistance value, the resonance frequency shifts to a lower frequency.

The study performed in the time domain is necessary to evaluate the filling dynamics of the volumes over time. The system was modelled using a *Simulink* block diagram and consists of two lateral air chambers of the U-Tank, a tube and a fixed volume where the compressed air (coming out of the U-Tank air chambers) is stored. The extraction turbine is connected to the fixed storage volume through a valve. Firstly, three different pitch angle and three different period values were set and therefore the filling dynamics of the fixed volume were evaluated. The pressures and flows as well as the trend of the τ angle have been plotted. In τ trends it's possible to note a slight decrease in amplitude from a certain time value onwards, especially for amplitudes of 10 and 20 [deg]. It's also possible to note that increasing the value of the period (T) and the pitch angle value, increases the value of the maximum pressure reached in the volume. Moreover, in mass flow trends it's possible to see how greater flow rates are achieved, increasing the amplitude and period values.

At the end, the air influence on the system was evaluated in frequency domain by comparing linear and non-linear systems. By linear system we mean the one in which the dynamics of the U-Tank is not influenced by the air effect; while, the non-linear system is influenced by the air effect through a pressures feedback that causes the damping effect of the air on the system. Firstly, the τ amplitude was evaluated in the two different systems using three different input amplitude values and when the input signal is stationary. The simulation shows the damping effect of the air that shifts the resonance peak to higher frequencies and away from the system's natural frequency; there is a decrease in the value of the τ amplitude between the linear and non-linear system. The mean pressure value inside the fixed volume was evaluated in the non-linear system for the three different

input amplitude values when the input signal is stationary. Increasing the δ amplitude value, there is an increasing value of the mean pressure inside the fixed volume. Secondly, the τ amplitude trend and the mean pressure inside the fixed volume were evaluated for a fixed δ amplitude value and for a different initial volume inside the U-Tank air chamber. Also for this validation, in the τ amplitude trend it's possible to see that the effect of air (in the non-linear system) influences the resonance frequency, which is shifted. By increasing the V_0 value, the resonance frequency is closer to the nominal frequency of the system (at a lower frequency). If the air volume is very small, the resonance frequency is very high, so the stiffness of the system is higher. The maximum value reached by the τ amplitude gradually increase, but all the maximum values reached by τ amplitude are significantly damped compared to the linear system. Then, was evaluated the mean pressure value within the fixed volume V_C when the V_0 value is changed and the input signal is stationary. Also in this case, it's possible to notice a gradually increase of the maximum value reached in the mean pressure value.

The gross power extracted from the system was evaluated with an optimized ideal mass flow range, because the turbine which extracts power is not known, so the mass flow rate of air required for the generation of energy is not known. To the time domain *Simulink* model was added a switch valve (controlled by a relay block) at the second input of the central big chamber block. This switch valve accommodates the mass flow consumption of the accumulator V_C by the generator unit, when there is a pressure difference on the line such that it doesn't bring the accumulator to vacuum. The mean gross power extracted was evaluated for six different mass flow in the frequency domain. From this evaluation we note that for short periods the U-Tank system doesn't work very well, in fact there is no extraction power. While for a higher period value, till the resonance value, there is a different mass flow of set (\dot{m}_{set}) which maximises the mean gross power extracted. At the resonance frequency, the maximum value of the mass flow (\dot{m}_{set}) imposed for power extraction is the best, but this optimal mass flow at the resonance frequency doesn't represent the optimal value for each period, especially at lower period. Then the trend of τ amplitude, the mean pressure inside the accumulator and the effective mass flow of the generator unit were evaluated. There is an increasing value of the τ amplitude and the maximum value reached is shifted to a lower frequency. While, for the mean pressure trend inside the accumulator there is a continuous decrease in the value as the \dot{m}_{set} value increases. Then the trend of τ , pressure inside the accumulator, mass flow extracted, and

gross power extracted were evaluated for the minimum and maximum value chosen for \dot{m}_{set} at the resonance frequency in time domain. Increasing the \dot{m}_{set} value, there is an increase of the τ amplitude and an increase of the gross power extracted following an increase in the \dot{m}_{extr} value and the number of switch made by the switch valve; so there is a consequent decrease of the pressure inside the accumulator chamber which never drops below the ambient pressure value thanks to the relay block before the switch valve. Then, the mean gross power for different values of the initial air volume of the two lateral reservoirs of the U-Tank is evaluated. So, it's possible to say that increasing the initial air volume value from 125 [m³] till to 1000 [m³], there is a substantial increase in the average gross power extracted, even if the dynamics of the U-Tank worsen for high frequencies. furthermore, there is an increase in the average pressure inside the accumulator. For an initial volume of air in the lateral reservoirs of the U-Tank equal to 1000 [m³], there is a better dynamic behavior of the device in a given frequency class.

In the end, it can be concluded that the integration of the U-Tank device allows the slow tuning of the device with the incoming wave and a good extraction of gross power in the case of a regular wave.

7.1 Further work

At the end of the evaluation of the system in regular wave, it's possible to say that the U-Tank system installed on board an IOwec device (already known) is capable of extracting a significant gross power value. Therefore, further work will be carried out to evaluate the power extraction of the system even in irregular wave.

Further works will be carried out following the steps realized for the regular wave system. After the validation of the system in irregular wave conditions, it will be necessary to choose an extraction turbine which gathers the characteristics outlined during the validation phase of the U-Tank technology system.

Bibliography

- [1] Gunn K. and Stock-Williams C., Quantifying the global wave power resource. *Renewable Energy*, 44, 2012.
- [2] Drew B., Plummer A.R., and Sahinkaya M.N. A review of wave energy converter technology. *Proceedings of the Institution of Mechanical Engineers, Part A: Journal of Power and Energy*, 223, 2009.
- [3] Chozas J.F., Technical and Non-Technical Issues towards the Commercialisation of Wave Energy Converters. PhD thesis, Aalborg University, 2013.
- [4] Folley M., Numerical Modelling of Wave Energy Converters - Single Devices and Arrays, 2016.
- [5] Sirigu A., Development of a resonance-tunable Wave Energy Converter. PhD thesis, Politecnico di Torino, 2019.
- [6] Fonseca N. and Pessoa J., Numerical modeling of a wave energy converter based on U-shaped interior oscillating water column, 2013.
- [7] S. Ribeiro Silva , R.P.F. Gomes and A.F.O. Falcão., Hydrodynamic optimization of the UGEN: Wave energy converter with U-shaped interior oscillating water column, 2016.
- [8] Alternative Energy Tutorials, <https://www.alternative-energy-tutorials.com/wave-energy/wave-energy.html> .
- [9] Soares C., Bhattacharjee J. et al., Review and classification of wave energy converters, 2012.

- [10] Konar T. and Dey Ghosh A., Flow Damping Devices in Tuned Liquid Damper for Structural Vibration Control: A Review, 2020.
- [11] Mattiazzo G., State of the Art and Perspectives of Wave Energy in the Mediterranean Sea: Backstage of ISWEC, 2019.
- [12] Pecher A., Kofoed J.P., Handbook of Ocean Wave Energy, 2017.
- [13] Passione B., Pozzi N. et al., Numerical and experimental analysis of oscillating fluid tanks, 2017.
- [14] Sirigu S.A., Brizzolara S., Bonfanti M., Dafnakis P., Bracco G., and Mattiazzo G., Pitch resonance tuning tanks: A novel technology for more efficient wave energy harvesting. In OCEANS 2018 MTS/IEEE Charleston, Charleston,(SC) USA, 2018.
- [15] G. Vissio., ISWEC toward the sea: Development, Optimization and Testing of the Device Control Architecture. PhD thesis, Politecnico di Torino, 2017.
- [16] Passione B., Hydrodynamic analysis and mooring design of a floating pitching Wave Energy Converter. PhD thesis, Politecnico di Torino, 2018.
- [17] Bracco G., ISWEC: A gyroscopic Wave Energy Converter. PhD thesis, Politecnico di Torino, 2010.
- [18] Bracco G., Cagninei A., Giorcelli E., Mattiazzo M., Poggi D., and Raffero M., Experimental validation of the iswec wave to PTO model. Ocean Engineering, 120:40–51, 2016.
- [19] WaveforEnergy. Deployment of ISWEC full-scale in Pantelleria, 2015, <http://www.waveforenergy.com/news/149-blue-energy-in-pantelleria-deployment-of-the-innovative-iswec-inertial-sea-wave-energy-converter>.
- [20] Sirigu S.A., Bracco G., Bonfanti M., Dafnakis P., and Mattiazzo G., On-board sea state estimation method validation based on measured floater motion. In 11th IFAC Conference on Control Applications in Marine Systems, Robotics, and Vehicles CAMS 2018, Opatija, Croatia, 2018.
- [21] Marine technology news. Deployment of ISWEC scaled-model in Adriatic sea, 2018. <https://www.marinetechologynews.com/news/pilots-energy-converter-587557>.

- [22] M. Liermann et al., Energy efficiency of pneumatic power take-off for wave energy converter, *International Journal of Marine Energy* (2015), <http://dx.doi.org/10.1016/j.ijome.2015.10.002>